

國立交通大學

電子物理學系

博士論文

二維複式結構光子晶體的能隙



Engineering the band gap of a two-dimensional photonic
crystal with hybrid structure

研 究 生: 劉文龍

指 導 教 授: 楊宗哲教授

中 華 民 國 九 十 六 年 六 月



二維複式結構光子晶體的能隙

Engineering the band gap of a two-dimensional photonic crystal with
hybrid structure

研究生: 劉文龍

Student: Wen-Long Liu

指導教授: 楊宗哲

Advisor: Tzong-Jer Yang

國立交通大學

電子物理學系

博士論文



Submitted to Department of Electrophysics
College

National Chiao Tung University

in partial Fulfillment of the Requirements

for the Degree of

Doctor of Philosophy

in

Department of Electrophysics

June 2007

Hsinchu, Taiwan, Republic of China

中華民國九十六年六月



二維複式結構光子晶體的能隙

學生: 劉文龍

指導教授: 楊宗哲

國立交通大學電子物理系博士班

摘 要

光子晶體是一種具有週期性調制介電函數且具有光子能帶及帶隙結構的人工材料, 在光子能隙的頻率波段中電磁波無法在光子晶體內的任何方向傳遞。這種特性具有很多奇特的物理現象及具備應用上的潛力。光子晶體在應用上多數需要具備較寬的光子能隙, 因此, 設計及製造較大寬度能隙的光子晶體是光子晶體研究領域重要課題。再者, 多數研究重心在二維光子晶體上面, 因為它們具有較容易製造以及應用於波導製作方面的諸多優點。因此, 在此論文中, 我們詳細探索多種具有大寬度能隙的二維光子晶體的複式結構, 包括利用在原來晶格中加入額外散射體或移除某部份介質等方式來達成這些目的。

首先, 我們設計了一種可調式光子晶體。此種光子晶體由一組固定方形介質柱套疊另一組具有相同週期可作相對移動的圓形介質柱組成。光子能隙的改變可藉由調整圓柱位置來達成。在此研究中我們主要著重在能隙對各種不同結構參數的敏感度, 尤其是圓柱的位移參數的效應。我們發現: 當圓柱的位移參數在某些範圍內能隙保持不變, 在這範圍內圓柱位置可以不必要求很高的精確度, 這種性質對製造可調式光子晶體有實質上的重要性。其次, 我們研究二維方形晶格中的方形介質柱內挖去部份介質形成空氣圓柱, 空氣圓柱的位置的改變使得介質重新分佈同時改變了能隙的寬度。我們取得某些參數時可得到極大的能隙, 並且在這個條件下能隙邊緣有極平坦的能帶構造, 造成在很寬的 k 空間群速度為零或很小。這種構造可廣範的應用於今在現今光學設計上。最後, 我們詳細研究了二維方形晶格中的方形介質柱四邊中間位置由其它介質細柱連接, 細柱的長度、寬度、位置及介質常數等因素影響能隙的開或合。而且最大的能隙不一定是細柱完全連接起來時才存在, 完全由細柱與方柱之間介電常數的相對關係來決定。又從能帶結構觀點, 我們得到更明確的規律, 能帶寬度與能帶中心位置跟細柱與方柱間介電常數的相關性。這種規律可提供於設計二維光子晶體能隙。



Engineering the band gap of a two-dimensional photonic crystal with hybrid structure

Student: Wen-Long Liu

Advisor: Prof. Tzong-Jer Yang

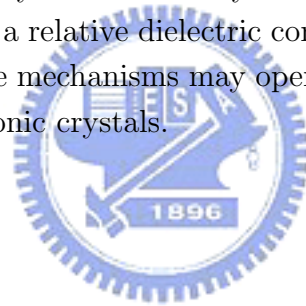
*Department of Electrophysics
National Chiao Tung University*

Abstract

Photonic crystals (PCs) are artificial materials having the periodical modulation of dielectric structures in space and there exhibit photonic band gaps (PBGs) in which the propagation of electromagnetic (EM) waves in any propagating direction and polarization state is inhibited. This feature leads to various peculiar physical phenomena and provides potential applications. Most proposed applications of PCs rely on large PBGs of PCs, therefore, the design and construction of PCs with large PBGs are a major goal in the PC field. Much attention has been devoted two-dimensional (2D) photonic crystals (i.e., structures with periodic dielectric patterns on a plane and translational symmetry in the perpendicular direction), since they are easier to fabricate (particularly in the optical region) and may be employed in waveguide configurations. In this thesis, we developed several procedures to systematically engineer the 2D PCs with large PBGs, which were scribed into the crystal structure by removing partial composited materials or introducing additional scatterers into unit cell of the prototype lattices.

For the first time, we have fabricated a PC with tunable PBGs. The proposed 2D tunable PC structure is realized by inserting a movable circular dielectric rod into a square lattice of square dielectric cylinders in air. The PBGs can be tunable by shifting the position of the circular dielectric rod. In the present work, we mainly concentrate on the subject of sensitivity of the PBGs to the variations of structural parameters of system, especially paying the attention on the effects of the shift s of the position of the circular dielectric rod. We find that there is a region of parameters in which the ratio of the gap width to the midgap is insensitive to the shift of the position of the circular dielectric rod. This property provides the large benefit of relaxing the fabrication tolerance of the tunable PCs. Then, we propose 2D square lattices of square cross-section dielectric rods in air, designed with an air hole drilled into each square rod. By adjusting the shift of the hole position in

the square rod in each unit cell, the dielectric distribution of the square rod will be modified. The PC structure proposed here has a sizable complete PBG and exhibits very gently sloped bands near such gap edge, which resulting in a sharp peak of density of state. In addition, the zero or small group velocities are observed in a broad region of \mathbf{k} -space. This structure can be fabricated with materials widely used today and opens a facinating area for applications in optoelectric devices. Finally, we have investigated in detail the photonic band structures of 2D square lattices of a square dielectric rod connected with another dielectric veins on the middle of each side of dielectric square rod. Properly adjusting the length, width, position and dielectric constant of veins in the unit cell enables the tunable complete PBG generated from the composite structure to be opened and closed. Moreover, it is not necessary for veins to be fully connected to yield the greatest improvement in complete gap size depending on a relative dielectric constant of veins in comparison with those of square rods. These mechanisms may open up a new way for designing photonic band gaps in 2D photonic crystals.



誌 謝

本文得以完成，首先要特別感謝指導老師楊宗哲教授，因為老師悉心指導與鼓勵，使我在光子晶體方面的研究受益匪淺。要不是他的協助與指引此論文是不可能完成的。就學期間承蒙國立交通大學在研究方面及國科會在經費上的支援致上謝忱。同時以感恩的心情謝謝教導過我的老師們，謝謝！

這幾年中有緣與我們研究群的成員結識，曾經在一起討論並且給予我很多建設性的建議與幫助，是一生難忘的記憶，在此致上深深的謝意。特別是：顧本源教授，樂丕剛博士，許永昌博士。趙遠鳳博士給予之協助與討論也致上感謝之意。

其次，也謝謝服務的單位國立沙鹿高工給我這個機會前來進修。

在此，感謝家人隨時的關心，要我多注重身體健康。三個寶貝兒女：貫立，貫維，貫瑩是進修期間最大的精神支柱，謝謝你們。最後，最要感謝妻子張淑綿女士一路無怨無悔的扶持，一輩子感激在心。雖此論文“只可自怡悅，不堪持贈君”，但滿心歡喜地將它獻給妳！

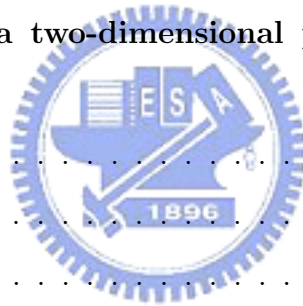


Contents

Abstract in Chinese	i
Abstract in English	iii
Acknowledgement	v
List of Figures	ix
Abbreviation	ix
1 Introduction	1
1.1 Photonic crystals	1
1.2 Photonic crystals as devices and applications	3
1.3 Dissertation outline	4
2 Numerical method for photonic crystals	17
2.1 Two-dimensional plane wave expansion method	17
2.2 Numerical results	20
3 Sensitivity of complete bandgaps to the shift of movable dielectric rod in two-dimensional photonic crystals with complex lattices	27
3.1 Introduction	28
3.2 Structural model and fundamental formulas	29



3.3	Numerical results and analysis	32
3.4	Discussions and summary	35
4	Variation of group velocity and complete bandgaps in two-dimensional photonic crystals with drilling holes into the dielectric rods	49
4.1	Introduction	51
4.2	Theory	52
4.3	Results and discussion	54
4.4	Conclusion	57
5	Photonic band gaps in a two-dimensional photonic crystal with veins	69
5.1	Introduction	69
5.2	Theory	71
5.3	Results and discussion	74
5.4	Conclusion	82
6	Conclusion	99



List of Figures

2.1	Patterns of the structures under consideration: (a) triangular-circles (<i>lattice-scatterers</i>); (b) first Brillouin zone for the triangular structures; (c) square-squares (<i>lattice-scatterers</i>); and (d) first Brillouin zone for the square structures	21
2.2	Calculated photonic band structure for (a) triangular lattice of circular dielectric rods (b) square lattice of square dielectric rods in air for <i>E</i> -polarization (solid lines) and <i>H</i> -polarization (dotted lines) modes. The rods have a dielectric constant of $\varepsilon = 11.4$ and a filling fraction of $f = 0.42$	22
2.3	The gap map for a square lattice of square dielectric rods with the dielectric constant of $\varepsilon = 11.4$ as a function of the filling fraction. . .	23

3.1	Schematic diagram of proposed tunable photonic crystals. The square dielectric cylinders with a side-length of l and dielectric ϵ_a are placed in air with $\epsilon_b = 1.0$ at the four corners of a 2D square lattice with a lattice constant, a , in the xy -plane. Another circular dielectric rod with $\epsilon = \epsilon_a$ and diameter d is inserted into each unit cell, forming composite lattices. We denote $\beta = d/l$ for convenience. This dielectric circular rod is movable. We assume that there is a shift \mathbf{s} of the inserted circular rod with respect to the center of the unit cell, that is $\mathbf{s} = s(\hat{\mathbf{x}} \sin \gamma + \hat{\mathbf{y}} \cos \gamma)$, where γ is the span angle of the displacement vector with respect to the y -axis.	40
3.2	Photonic band structures for two structures : (a) the prototype structure without the inserted circular rod and (b) a TPC with a movable dielectric circular rod in internal of the unit cell. The relevant parameters are chosen as: $\epsilon_a = \epsilon = 11.4$, appropriate for GaAs material; $\epsilon_b = 1.0$ in air. (a) $f = 0.217$, $d/l = 0$ and (b) $f = 0.3$, $d/l = 0.7$, $s = 0$. The solid and dashed curves correspond to the E - and H -polarizations, respectively. The shadow area marks the complete gap region.	41
3.3	Variations of $\Delta\omega/\omega_g$ with the filling fraction f for different values of β : 0.7(solid line), 0.75(dashed line) and 0.8(dotted line). The other parameters are the same as those in Figure 2.2(b).	42
3.4	Same as Figure 2.2(b) except for different values of s : (a) $s = 0.1a$ and (b) $s = 0.25a$. The other parameters are $f = 0.3$, $\beta = 0.7$, and $\gamma = 0^\circ$	43

3.5	Variations of $\Delta\omega/\omega_g$ with the relative shift s for several shifting directions: $\gamma = 0^\circ$ (solid line); $\gamma = 25^\circ$ (dotted line), and $\gamma = 0.45^\circ$ (dashed line). The other parameters are the same as those in Figure 2.2(b).	44
3.6	Variations of $\Delta\omega/\omega_g$ of the complete band gap versus the number N of the plane-waves in the expansion. The parameters are $f = 0.3$, $\beta = 0.7$, $s = 0.1 a$ and $\gamma = 0^\circ$	45
3.7	Variations of $\Delta\omega/\omega_g$ of the complete band gap with s as the number N of the plane-waves in the expansion increases for $\gamma = 0^\circ$ with $f = 0.3$, $\beta = 0.7$. The numbers of plane-waves in the expansions for the H-polarization and the E-polarization are the same.	46
3.8	Gap map of the proposed TPC, as the relative shift s varies for both E - and H -polarizations. The parameters are $f = 0.3$, $\beta = 0.7$, and $\gamma = 0^\circ$. The black area marks the regions of the complete band gaps.	47
4.1	(a) Schematic diagram of proposed photonic crystals. The square dielectric rods with a side-length of l and dielectric ϵ_a are placed in air background with $\epsilon_b = 1.0$ at the center of a 2D square lattice with a lattice constant, a , in the xy -plane. Another circular rod with $\epsilon_b = 1.0$ and diameter d is drilled into square rod in each unit cell. We denote $\beta = d/l$ for convenience. We assume that there is a shift \mathbf{s} of the drilled circular rod with respect to the center of the unit cell, that is $\mathbf{s} = s(\hat{\mathbf{x}} \sin \gamma + \hat{\mathbf{y}} \cos \gamma)$, where γ is the span angle of the displacement vector with respect to the y -axis. (b) the Brillouin zone with symmetry points, Γ , \mathbf{X} , \mathbf{M} , \mathbf{U} , \mathbf{M}' and \mathbf{X}'	61

4.2	Photonic band structures and the corresponding density of states (DOS) for two structures. The parameters in this figure are chosen as $a/l=1.63$, $\beta=0.35$ (corresponding to filling factor $f = 0.34017$). The solid and dotted curves correspond to the E - and H -polarizations, respectively. The shadow area marks the complete gap region.	62
4.2	(con't)	63
4.3	The PBG map as the the relative shift s of the drilled rod for three different directions($\gamma = 0^\circ, 22.5^\circ$, and 45°). The other parameters are as those quoted in Figure ???. The black area denotes the complete band gaps.	64
4.3	(con't)	65
4.3	(con't)	66
4.4	The PBG map as a function of the parameter β for filling factor $f=0.34017$, $s = 0$	67
5.1	Schematic diagram of the proposed photonic crystals. The square dielectric rod with a side-length l and dielectric ϵ_a is placed in air with $\epsilon_b = 1.0$ at the center of a 2D square lattice with a lattice constant, a , in the xy -plane. Another dielectric veins with $\epsilon = \epsilon_v$ and length h and width d is inserted in each unit cell on the middle of each side of dielectric square rod, forming composite lattices. The shift length s of the inserted vein is defined with respect to the edge of the square rod, where δ is the crevice between the edges of the square rod and the vein, thus s is denoted by $s = \delta + h$	86

5.2	Photonic band structures for two structures: the prototype structure without the inserted veins for fixing the side-length of square rod at $l = 0.57a$, $\epsilon_a = 11.4$, appropriate for GaAs material; $\epsilon_b = 1.0$ in air as shown in (a) and three choices of the dielectric constant of veins are demonstrated in (b) $\epsilon_v = 6.0$, (c) $\epsilon_v = 11.4$, (d) $\epsilon_v = 16.0$. The other parameters are the same as those in (a) except for parameters of veins: $\delta=0$, $d = 0.08a$ and h : $0.155a$ (left panel), $0.19a$ (middle panel), $0.215a$ (right panel). The solid and dotted curves correspond to the E - and H -polarizations, respectively. The gray area marks the complete gap region.	87
5.2	(con't)	88
5.2	(con't)	89
5.2	(con't)	90
5.3	The spatial distributions of the electric field intensity $ E^2 $ at the \mathbf{M} point of (a) $H2$ band (or denoted by $H^{(2,M)}$) for $h=0$, (b) $H4$ band ($H^{(4,M)}$) for $h = 0$, and (c) $H2$ band ($H^{(4,M)}$) for $\epsilon_v = 6$ and $h = 0.215a$. Here we mark the states in accordance with their ordering in frequency for the prophase, namely, the initial mode $H^{(n,M)}$ denotes the n th band for the H -polarization mode at \mathbf{M} point. The band center (d) and the band width (e) as functions of h for $H2$ band with $\epsilon_v=6$ (solid line), 11.4 (dotted line), 16 (dashed line) and $E4$ band with $\epsilon_v=16$	91
5.3	(con't)	92
5.3	(con't)	93

5.4 Gap map of the proposed PC, as the vein length h varies for both E - and H -polarizations for (a) $\epsilon_v = 6.0$, (b) $\epsilon_v = 11.4$ and (c) $\epsilon_v = 16.0$, respectively. The parameters are $\epsilon_a = 11.4$, $l = 0.57a$, $\delta=0$ and $d = 0.08a$. The black area denotes the complete band gaps. 94

5.5 The positions of the edge states of the lower complete PBG (CPBG): (a) the evolution of the edge states of the lower complete PBG as a function of vein length, h , for $\epsilon_v = \epsilon_a = 11.4$. The other parameters are: $\epsilon_a = 11.4$, $l = 0.57a$, $\delta=0$ and $d = 0.08a$. The dark region indicates the complete PBG. $H^{(n,\Gamma)}$ ($E^{(n,\Gamma)}$) denote the n th band for the $H(E)$ -polarization modes at Γ point. (b) the evolution of the edge states of the lower complete PBG as functions of the vein refractive index for three different vein lengths ($h = 0.155a$, $0.19a$, and $0.215a$). The vein refractive index of $n=2.45$, 3.376 and 4.0 (i.e., $\epsilon_v=6.0$, 11.4 and 16.0) are indicated by the vertical dotted lines. The dashed-dotted lines represent the curves of $H^{2,M}$ ($H^{3,M}$) or $E^{2,\Gamma}$ modes for different h values 95

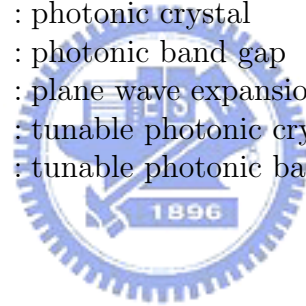
5.5 (con't) 96

5.6 Gap map of the proposed PC, as the vein width d varies for both E - and H -polarizations for (a) $\epsilon_v = 6.0$, (b) $\epsilon_v = 11.4$ and (c) $\epsilon_v = 16.0$, respectively. The parameters are $\epsilon_a = 11.4$, $l = 0.57a$, $\delta = 0$ and $h = h_{max} = 0.215a$ 97

5.7 Variations of $\Delta\omega/\omega_g$ with the shift length s for different vein lengths h : $0.17a$, $0.18a$ and $0.2a$ for (a) $\epsilon_v = 6.0$, (b) $\epsilon_v = 11.4$ and (c) $\epsilon_v = 16.0$. The other parameters are $\epsilon_a = 11.4$, $l = 0.57a$ and $d = 0.08a$ 98

Abbreviation

Abbrev.	Meaning
2D	: two dimension
3D	: density of states
BC	: band center
BW	: band width
CPBG	: complete photonic band gap
DOS	: three dimension
EM	: electromagnetic
FBZ	: first Brillouin zone
FDTD	: finite difference time domain method
LED	: light-emitting diode
PC	: photonic crystal
PBG	: photonic band gap
PWE	: plane wave expansion
TPC	: tunable photonic crystal
TPBG	: tunable photonic band gap





Chapter 1

Introduction

1.1 Photonic crystals

Photonic crystals, which are also known as photonic bandgap (PBG) materials, can be designed with a periodic variation in the dielectric constant in either one, two, or all three spatial directions [1]. Due to the periodical modulation of dielectric structures in space, there may be ranges of frequencies at which no allowed modes exist for electromagnetic (EM) waves in any propagating direction and polarization state. These ranges of frequencies are termed *photonic band gaps*. The dispersion relation (*i.e.*, the frequency–wavevector relation) for EM wave propagation in PBG materials is referred to as the *photonic band structure*. Therefore, the dispersion relations of light in a photonic crystal can be expressed as photonic band structures in a Brillouin zone. The photonic band structure of PBG material depends on lattice type, refractive index contrast, filling factor, and atom configurations, etc. As we know that the first use of the idea of a photonic band structure was probably made by Ohtaka in 1979 [2]. It was, however, that really aroused a widespread interest in this area was in 1987 by Yablonovitch [3]. and John [4]. Then, many groups became attracted to PBG material research as a result of advances in fabrication techniques and the increasing awareness of the potential importance of PBG systems [5–29].

The idea of PCs with band gap is analogous to the electronic band gap due to the spatial periodic potential in natural crystals. Insight into the nature of PBGs can be gained by comparing the equations, that govern propagation of EM waves and electrons. Propagation of EM waves is described by the set of Maxwell's equations:

$$\nabla \times \mathbf{E} = -\frac{\partial \mathbf{B}}{\partial t}. \quad (1.1)$$

$$\nabla \times \mathbf{H} = \sigma \mathbf{E} + \frac{\partial \mathbf{D}}{\partial t}. \quad (1.2)$$

$$\nabla \cdot \mathbf{D} = \rho. \quad (1.3)$$

$$\nabla \cdot \mathbf{B} = 0. \quad (1.4)$$

$$\mathbf{D} = \varepsilon_0 \varepsilon(\mathbf{r}) \mathbf{E}. \quad (1.5)$$

$$\mathbf{B} = \mu_0 \mu \mathbf{H} \quad (1.6)$$

. Here \mathbf{E} and \mathbf{D} are the electric field and displacement vectors, respectively, \mathbf{H} the magnetic field intensity, \mathbf{B} the magnetic flux density, μ_0 the permeability, and ε_0 is the permittivity of vacuum. It can be shown that Maxwell's equations can be transformed into the following expression for harmonic magnetic modes:

$$\left[\nabla \times \frac{1}{\varepsilon(\mathbf{r})} \nabla \right] \times \mathbf{H}_\omega(\mathbf{r}) = \omega^2 \mathbf{H}(\mathbf{r}). \quad (1.7)$$

Electron propagation is described by the Schrodinger equation as follows:

$$\left[-\frac{\hbar^2}{2m} \nabla^2 + V(\mathbf{r}) \right] \psi(\mathbf{r}) = \mathbf{E} \psi(\mathbf{r}). \quad (1.8)$$

where $V(r)$ is the potential, m the mass, and $\psi(r)$ is the wave function of the particle. Eqs. (1.7) and (1.8) look mathematically similar. This allows one to expect significant similarities in the phenomena that they describe. However, because photons are particles without mass or charge, therefore, photon movement does not require additional power and photons do not interact with each other. These

properties seem to be perfectly prepared for problems facing electronic systems and products. In addition, photons propagate in PCs in a manner very similar to electron propagation in semiconductor materials. Thus, by introducing defects into PCs one can create localized photon modes in PBGs just as electron states occur around dopants introduced in semiconductor crystals.

1.2 Photonic crystals as devices and applications

There are both numerous and diverse applications for PBG materials that have been proposed. They are all, however, based on the idea of the modification of the free-space photon dispersion relation from $\omega = ck$, where k is the wavevector, to the more general form $\omega = \omega(k)$. These applications employ either a perfectly periodic PBG material (crystal) or consider a PBG material containing “defects”. In this section I look at photonic crystals as devices and applications in detail. Joannopoulos, et al. [30] first proposed the idea of using PCs with PBG(s) as waveguides for optical interconnection by introducing a line defect (perturbing the crystal along one line). They also indicated that this type of waveguide is useful for compact, low-loss bends because there is no limitation on the bend radius forced by the radiation loss as occurred in dielectric waveguides. Subsequently, waveguiding in a photonic crystal and near 100 percent transmission of electromagnetic waves around sharp 90 degree corners were observed experimentally [31, 32]. Since these studies show that highly efficient transmission of light can be achieved around sharp corners in 2D PBG waveguides. One major limitation to these studies is that the 2D structure used was assumed to be infinite in the dimension perpendicular to the plane of periodicity. Ho, et al. [33] therefore expected leakage of waves in the practical situation of a finite structure. They proposed using high-index slab structures periodically patterned with air cylinders and sandwiched by low-index material for light guiding. It is

reported that the experimental demonstration of highly efficient transmission at a wavelength of around $1.5 \mu\text{m}$ in a high-index-contrast 2D PC slab [34].

Notably, it was also found [33] that there exist significant losses due to the coupling of the guided mode with radiation modes and with the backward guided mode. It is very important that propagation loss be eliminated or at least reduced to an acceptable level, which is practical application rely. So far, many groups have made effort to quantify [35–41] and minimize [42–48] the propagation loss in PC slab waveguides. Several early experiments [49, 50, 51, 52] indicated that low-loss bending is possible to achieve in PC slab waveguides. However, some significant efforts have been made to improve the performance of PC bends in practical applications [53–59]. Researchers also consider photonic integrated circuits using PCs as platforms. Most passive and active devices required by photonic integrated circuits [60–115].

1.3 Dissertation outline

In this dissertation an alternative thesis format is followed, which allows the inclusion of papers published (or submitted/to be submitted) in scholarly journals. Each subsequent chapter consists of a single paper presented exactly the way it was published or submitted. In Chapter 1 we presented an introduction for a brief theoretical background and an extensive review of theoretical and experimental literature in the area of photonic band gap materials. We outlined the different proposed devices and applications that motivated many studies. The goal of this dissertation is to engineer PC dispersion properties for novel applications. This goal will be achieved mainly through target-oriented implementations of the PWE method. To this end, this dissertation is organized as follows. Chapter 2 will introduce numerical techniques, mainly about the PWE method, used in pursuing this dissertation. While general information about this method is briefly introduced for completeness,

most attention will be given as to how to actually implement them to achieve the specific goal in this dissertation. Chapter 3 the PWE method is used to analyze 2D tunable photonic crystals (TPC) with movable components, which consist of a circular dielectric rod inserting into a square lattice of square dielectric cylinders in air. The effect of structural parameters on the band gap is studied first, and then the band gap structures of TPCs can be tuned by adjusting the shift of the position of the circular rod in each unit cell. The convergence and accuracy are also discussed. Chapter 4 two-dimensional square lattices of square cross-section dielectric rods in air, designed with an air hole drilled into each square rod, are studied theoretically. The zero or small group velocities near PBG edge in a broad region of \mathbf{k} -space are studied and discussed. Chapter 5 studies a double-hybrid-rods structure system of 2D PCs of a square lattice with a square dielectric rod connected with dielectric veins on the middle of each side of dielectric square rod. The effect of structural parameters— the length, width, position and dielectric constant of the veins — on the band gap, is studied theoretically. The results are analyzed with the use of the point of view of the band structure. Chapter 6 gives some concluding remarks.



Bibliography

- [1] E. Yablonovitch, J. Phys.: Condens. Matter. **5**, 2443 (1993).
- [2] K. Ohtaka, Phys. Rev. B **19**, 5057 (1979).
- [3] E. Yablonovitch, Phys. Rev. Lett. **58**, 2059 (1987).
- [4] S. John, Phys. Rev. Lett. **58**, 2468 (1987).
- [5] S. L. McCall, P. M. Platzman, R. Dialichaouch, D. Smith, and S. Schultz, Phys. Rev. Lett. **67**, 2017 (1991).
- [6] E. N. Economou and A. Zdetsis, Phys. Rev. B **40**, 1334 (1989).
- [7] E. Yablonovitch and T. J. Gmitter, Phys. Rev. Lett. **63**, 1950 (1989).
- [8] E. Yablonovitch and T. J. Gmitter, J. Opt. Soc. Am **7**, 1792 (1990).
- [9] K. M. Leung and Y. F. Liu, Phys. Rev. B **41**, 10188 (1990).
- [10] R. D. Meade, K. D. Brommer, A. Rappe, and J. D. Joannopoulos, Phys. Rev. B **44**, 13772 (1991).
- [11] K. M. Leung and Y. F. Liu, Phys. Rev. Lett. **65**, 2646 (1990).
- [12] K. M. Ho, C. T. Chan, and C. M. Soukoulis, Phys. Rev. Lett. **65**, 3152 (1990).
- [13] J. Pendry and A. M. Mackinnon, Phys. Rev. Lett. **69**, 2772 (1992).

- [14] K. M. Ho, C. T. Chan, and C. M. Soukoulis, Phys. Rev. Lett. **66**, 393 (1990).
- [15] S. Satpathy, Z. Zhang, and M. R. Salehpour, Phys. Rev. Lett. **64**, 1239 (1990).
- [16] Z. Zhang and S. Satpathy, Phys. Rev. Lett. **65**, 2650 (1990).
- [17] M. Plihal, A. Shambrook, A. A. Maradudin, and P. Sheng, Opt. Commun. **80**, 199 (1991).
- [18] M. Plihal and A. A. Maradudin, Phys. Rev. B **44**, 8565 (1991).
- [19] N. Stefanou, V. Karathanos, and A. Modinos, J. Phys.: Condens. Matter. **4**, 7389 (1992).
- [20] S. Datta, C. T. Chan, K. M. Ho, and C. M. Soukoulis, Phys. Rev. B **46**, 10650 (1992).
- [21] E. Yablonovitch, T. J. Gmitter, R. D. Meade, K. D. Brommer, A.M. Rappe, and J. D. Joannopoulos, Phys. Rev. Lett. **67**, 3380 (1991).
- [22] R. D. Meade, K. D. Brommer, A.M. Rappe, and J. D. Joannopoulos, Appl. Phys. Lett. **61**, 495 (1992)
- [23] E. Yablonovitch, T. J. Gmitter, and K.M. Leung, Phys. Rev. Lett. **67**, 2295 (1991).
- [24] H. S. Sözüer, J. W. Haus, and R. Inguva, Phys. Rev. B **45**, 13962 (1992).
- [25] C. T. Chan, K. M. Ho, and C. M. Soukoulis, Europhys. Lett. **67**, 3380 (1991).
- [26] G. Henderson, T. K. Gaylord, and E. N. Glytsis, Phys. Rev. B **45**, 8404 (1992).
- [27] P. R. Villeneuve and M. Piche, J. Opt. Soc. Am. A **8**, 1296 (1991).

- [28] G. X. Qian, Phys. Rev. B **44**, 11482 (1991).
- [29] P. R. Villeneuve and M. Piche, Phys. Rev. B **46**, 4969 (1992).
- [30] R. D. Meade, A. Devenyi, J. D. Joannopoulos, O. L. Alerhand, D. A. Smith, and K. Kash, J. Appl. Phys. **75**, 4753 (1994).
- [31] A. Mekis, J. C. Chen, I. Kurland, S. Fan, P. R. Villeneuve, and J. D. Joannopoulos, Phys. Rev. Lett. **77**, 3787 (1996).
- [32] S. Y. Lin, E. Chow, V. Hietola, P. R. Villeneuve, and J. D. Joannopoulos, Science **282**, 274 (1998).
- [33] El-Kady, M. M. Sigalas, R. Biswas, and K. M. Ho, J. of lightwave Tech. **17**, 2042 (1999).
- [34] S. Y. Lin, E. Chow, S. G. Johnson, and J. D. Joannopoulos, Opt. Lett. **25**, 1297 (2000).
- [35] M. Qiu, B. Jaskorzynska, M. Swillo, and H. Bensity, Micro. Opt. Tech. Lett. **34**, 387 (2002).
- [36] P. Lalanne and H. Benisty, J. of Appl. Phys. **89**, 1512 (2001).
- [37] Y. Desieres, T. Benyattou, R. Orobtcouk, A. Morand, P. Benech, C. Grillet, C. Seassal, X. Letartre, P. Rojo-Romeo, and P. Viktorovitch, J. of Appl. Phys. **92**, 2227 (2002).
- [38] G. R. Hadley, IEEE Photon. Tech. Lett. **14**, 642 (2002).
- [39] Y. Tanaka, T. Asano, Y. Akahane, B. S. Song, and S. Noda, Appl. Phys. Lett. **82**, 1661 (2003).

- [40] L. C. Andreani and M. Agio, *Appl. Phys. Lett.* **82**, 2011 (2003).
- [41] R. Ferrini, R. Houdre, H. Benisty, M. Qiu, and J. Moosburger, *J. Opt. Soc. Am. B* **20**, 469 (2003).
- [42] C. J. M. Smith, H. Benisty, S. Olivier, M. Rattier, C. Weisbuch, T. F. Krauss, R. M. D. L. Rue, R. Houdre, and U. Oesterle, *Appl. Phys. Lett.* **77**, 2813 (2000).
- [43] B. Temelkuran, E. L. Thomas, J. D. Joannopoulos, and Y. Fink, *Opt. Lett.* **26**, 1370 (2001).
- [44] Y. Ohtera, T. Kawashima, Y. Sakai, T. Sato, I. Yokohama, A. Ozawa, and S. Kawakami, *Opt. Lett.* **27**, 2158 (2002).
- [45] T. Baba, A. Moteg, T. Iwa, N. Fukaya, Y. Watanabe, and A. Sakai, *IEEE J. Quantum Electro.* **38**, 743 (2002).
- [46] M. Notomi, A. Shinya, K. Yamada, J. Takahashi, C. Takahashi, and I. Yokohama, *IEEE J. Quantum Electro.* **38**, 736 (2002).
- [47] M. Mulot, S. Anand, M. Swillo, M. Qiu, B. Jaskorzynska, and A. Talneau, *J. of Vacuum Science & Technology* **21**, 900 (2003).
- [48] S. J. McNab, N. Moll, and Y. A. Vlasov, *Opt. Exp.* **11**, 2927 (2003).
- [49] M. Tokushima, H. Kosaka, A. Tomita, and H. Yamada, *Appl. Phys. Lett.* **76**, 952 (2000).
- [50] M. Loncar, D. Nedeljkovic, T. Doll, J. Vuckovic, A. Scherer, and T. P. Pearsall, *Appl. Phys. Lett.* **77**, 1937 (2000).

- [51] E. Chow, S. Y. Lin, J. R. Wendt, S. G. Johnson, and J. D. Joannopoulos, *Opt. Lett.* **26**, 286 (2001).
- [52] M. Tokushima and H. Yamada, *IEEE J. Quantum Electro.* **38**, 753 (2002).
- [53] S. Olivier, H. Benisty, M. Rattier, C. Weisbuch, M. Qiu, A. Karlsson, C. J. M. Smith, R. Houdre, and U. Oesterle, *Appl. Phys. Lett.* **79**, 2514 (2001).
- [54] S. Olivier, H. Benisty, C. Weisbuch, C. J. M. Smith, T. F. Krauss, R. Houdre, and U. Oesterle, *J. Lightwave Tech.* **20**, 1198 (2002).
- [55] A. Talneau, L. L. Gouezigou, N. Bouadma, M. Kafesaki, C. M. Soukoulis, and M. Agio, *Appl. Phys. Lett.* **80**, 547 (2002).
- [56] M. Loncar, J. Vuckovic, and A. Scherer, *J. Opt. Soc. Am. B* **18**, 1362 (2001).
- [57] A. Sharkawy, D. Pustai, S. Y. Shi, and D. W. Prather, *Opt. Lett.* **28**, 1197 (2003).
- [58] H. Benisty, S. Olivier, C. Weisbuch, M. Agio, M. Kafesaki, C. M. Soukoulis, Min Qiu, M. Swillo, A. Karisson, B. Jaskorzynska, A. Talneau, J. Moosburger, M. Kamp, A. Forchel, R. Ferrini, R. Houdré, and U. Oesterle *IEEE J. Quantum Electro.* **38**, 770 (2002).
- [59] A. Chutinan, M. Okano, and S. Noda, *Appl. Phys. Lett.* **80**, 1698 (2002).
- [60] S. Fan, S. G. Johnson, and J. D. Joannopoulos, *J. Opt. Soc. Am. B* **18**, 162 (2001).
- [61] Y. Akahane, M. Mochizuki, T. Asano, Y. Tanaka, and S. Noda, *Appl. Phys. Lett.* **82**, 1341 (2003).

- [62] M. Qiu, M. Mulot, M. Swillo, S. Anand, B. Jaskorzynska, A. Karlsson, M. Kamp, and A. Frochel, *Appl. Phys. Lett.* **83**, 5121 (2003).
- [63] T. Asano, M. Mochizuki, S. Noda, M. Okano, and M. Imada, *J. Lightwave Tech.* **21**, 1370 (2003).
- [64] M. Li, K. Mori, M. Ishizuka, X. Liu, Y. Sugimoto, N. Ikeda, and K. Asakawa, *Appl. Phys. Lett.* **83**, 216 (2003).
- [65] I. Avrutsky and V. Kochergin, *Appl. Phys. Lett.* **82**, 3590 (2003).
- [66] R. Costa, A. Melloni, and M. Martinelli, *IEEE Photon. Technol. Lett.* **15**, 401 (2003).
- [67] S. Fasquel, X. Melique, O. Vanbesien, and D. Lippens, *Superlattices and Microstructures* **32**, 145 (2002).
- [68] G. Kakarantzas, A. Ortigosa-Blanch, T. A. Birks, P. S. Russell, L. Farr, F. Couny, and B. J. Mangan, *Opt. Lett.* **28**, 158 (2003).
- [69] W. Nakagawa, P. C. Sun, C. H. Chen, and Y. Fainman, *Opt. Lett.* **27**, 191 (2002).
- [70] E. Istrate and E. H. Sargent, *J. Opt. A* **4**, S242 (2002).
- [71] M. Imada, S. Noda, A. Chutinan, M. Mochizuki, and T. Tanaka, *Journal of Lightwave Technology* **20**, 845 (2002).
- [72] A. Chutinan, M. Mochizuki, M. Imada, and S. Noda, *Appl. Phys. Lett.* **79**, 2690 (2001).
- [73] J. A. Oswald, B. I. Wu, K. A. McIntosh, L. J. Mahoney, and S. Verghese, *Appl. Phys. Lett.* **77**, 2098 (2000).

- [74] B. I. Wu, E. Yang, J. A. Kong, J. A. Oswald, K. A. McIntosh, L. Mahoney, and S. Verghese, *Microwave and Optical Technology Letters* **27**, 81 (2000).
- [75] S. H. Fan, P. R. Villeneuve, J. D. Joannopoulos, and H. A. Haus, *Opt. Exp.* **3**, 4 (1998).
- [76] X.-Y. Lei, H. Li, F. Ding, W. Zhang, and N.-B. Ming, *Appl. Phys. Lett.* **71**, 2889 (1997).
- [77] S. H. Fan, P. R. Villeneuve, J. D. Joannopoulos, and H. A. Haus, *Phys. Rev. B* **64**, 245302 (2001).
- [78] E. A. Camargo, H. M. H. Chong, and R. M. Rue, *Opt. Exp.* **12**, 588 (2004).
- [79] M. F. Uanik, S. Fan, and M. Soljagic, *Appl. Phys. Lett.* **83**, 2739 (2003).
- [80] R. Ozaki, M. Ozaki, and K. Yoshino, *Jpn. J. Appl. Phys.* **42**, L669 (2003).
- [81] A. Forchel, *Nature Materials* **2**, 13 (2003).
- [82] L. X. Chen and D. Kim, *Opt. Commun.* **218**, 19 (2003).
- [83] F. Cuesta, A. Griol, A. Martinez, and J. Marti, *Elect. Lett.* **39**, 455 (2003).
- [84] J. E. Sharping, M. Fiorentino, P. Kumar, and R. S. Windeler, *IEEE Photon. Techno. Lett.* **14**, 77 (2002).
- [85] L. H. Peng, Y. C. Shih, S. M. Tsan, and C. C. Hsu, *Appl. Phys. Lett.* **81**, 5210 (2002).
- [86] P. Mach, P. Wiltzius, M. Megens, D. A. Weitz, K. H. Lin, T. C. Lubensky, and A. G. Yodh, *Europhys. Lett.* **58**, 679 (2002).
- [87] S. Lan and H. Ishikawa, *Opt. Lett.* **27**, 1259 (2002).

- [88] C. S. Kee, M. Y. Jang, I. Park, H. Lim, J. E. Kim, H. Y. Park, and J. I. Lee, *Appl. Phys. Lett.* **80**, 1520 (2002).
- [89] P. M. Johnson, A. F. Koenderink, and W. L. Vos, *Phys. Rev. B* **66**, 081102 (2002).
- [90] A. Sharkawy, S. Y. Shi, D. W. Prather, and R. A. Soef, *Opt. Exp.* **10**, 1048 (2002).
- [91] M. Soljacic, M. Ibanescu, S. G. Johnson, Y. Fink, and J. D. Joannopoulos, *Phys. Rev. E* **66**, 055601 (2002).
- [92] M. Florescu and S. John, *Phys. Rev. A* **64**, 033801 (2001).
- [93] A. Hache and M. Bourgeois, *Appl. Phys. Lett.* **77**, 4089 (2000).
- [94] J. Danglot, O. Vanbesien, and D. Lippens, *IEEE Micro. Guided Wave Lett.* **9**, 274 (1999).
- [95] P. Tran, *Opt. Lett.* **21**, 1138 (1996).
- [96] H. B. Lin, R. J. Tonucci, and A. J. Campillo, *Opt. Lett.* **23**, 94 (1998).
- [97] I. Abdulhalim, *J. Opt. A* **2**, 19 (2000).
- [98] N. Susa, *Jpn. J. Appl. Phys.* **39**, 6288 (2000).
- [99] S. Hava, J. Ivri, and M. Auslender, *J. Opt. A* **3**, S190 (2001).
- [100] H. L. Guo, H. Y. Chen, P. G. Ni, Q. Zhang, B. Y. Cheng, and D. Z. Zhang, *Appl. Phys. Lett.* **82**, 373 (2003).
- [101] M. F. Yanik, S. Fan, M. Soljacic, and J. D. Joannopoulos, *Opt. Lett.* **28**, 2506 (2003).

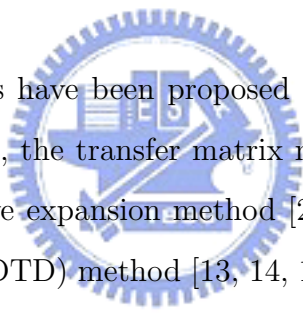
- [102] K. G. Hougaard, J. Broeng, and A. Bjarkev, *Electron. Lett.* **39**, 599 (2003).
- [103] T. V. Andersen, J. Thogersen, S. R. Keiding, and J. J. Larsen, *Appl. Phys. B* **76**, 639 (2003).
- [104] M. Bayindir, B. Temelkuran, and E. Ozbay, *Appl. Phys. Lett.* **77**, 3902 (2000).
- [105] P. Halevi, A. A. Krokhin, and J. Arriaga, *Appl. Phys. Lett.* **75**, 2725 (1999).
- [106] S. Y. Lin, E. Chow, J. Bur, S. G. Johnson, and J. D. Joannopoulos, *Opt. Lett.* **27**, 1400 (2002).
- [107] Y. Sugimoto, N. Ikeda, N. Carlsson, K. Asakawa, N. Kawai, and K. Inoue, *Opt. Lett.* **27**, 388 (2002).
- [108] Y. Ohtera, T. Sato, T. Kawashima, T. Tamamura, and S. Kawakami, *Electro. Lett.* **35**, 1271 (1999).
- [109] M. D. B. Charlton, M. E. Zoorob, G. J. Parker, M. C. Netti, J. J. Baumberg, S. J. Cox, and H. Kemhadjian, *Mat. Sci. & Eng. B* **74**, 17 (2000).
- [110] M. Bayindir, E. Ozbay, B. Temelkuran, M. M. Sigalas, C. M. Soukoulis, R. Biswas, and K. M. Ho, *Phys. Rev. B* **63**, 081107 (2001).
- [111] S. Kim, G. P. Nordin, J. Cai, and J. Jiang, *Opt. Lett.* **28**, 2384 (2003).
- [112] R. Wison, T. J. Karle, I. Moerman, and T. F. Krauss, *J. of Opt. A* **5**, S76 (2003).
- [113] A. Martinez, F. Cuesta, A. Friol, D. Mira, J. Garcia, P. Sanchis, R. Llorente, and J. Marti, *Appl. Phys. Lett.* **83**, 3033 (2003).
- [114] K. B. Chung and J. S. Yoon, *Opt. and Quant. Electron.* **35**, 959 (2003).

- [115] S. Lan, K. Kanamoto, T. Yang, S. Nishikawa, Y. Sugimoto, N. Ikeda, H. Nakamura, K. Asakawa, and H. Ishikawa, Phys. Rev. B **67**, 115208 (2003).



Chapter 2

Numerical method for photonic crystals



Several numerical methods have been proposed for the research of photonic band gap materials, for example, the transfer matrix method [1, 2, 3, 4], scattering matrix method [5], plane wave expansion method [23, 7, 25, 9, 10, 11, 12], and finite difference time domain (FDTD) method [13, 14, 15], etc. Generally, the plane wave expansion method is a frequency domain method, and it can be used for photonic bandgap analysis of infinite and uniform crystals. Analysis of defect modes can also be achieved using the plane wave expansion method under the so-called “super-cell approximation”. The FDTD method is a very powerful tool to study the dynamics of PBG devices, though it usually needs a large amount of computer resources and a long computation time. The transfer matrix method and scattering matrix method can be used to obtain the transmission or reflection spectrum for finite photonic crystals.

2.1 Two-dimensional plane wave expansion method

The plane wave expansion method is a very useful technique to solve periodic electromagnetic problems such as 1D, 2D and 3D periodic problems. It can yield the

band structure, equifrequency contours, the spatial field profile, the energy velocity of a propagating wave etc. However, for 3D problems, a significant number of plane waves (which require impractical computational costs) are demanded to ensure numerical accuracy.

This method relies on the solution of Maxwell's equations, under periodic (Bloch) boundary conditions. In the following we develop the details of plane wave expansion method for the E - and H -polarization cases. In a periodic and dielectric medium where the dielectric constant $\varepsilon(\mathbf{r})$ is position dependent, Maxwell's equations (in Gaussian units) [23, 19] for EM waves can be written as

$$\nabla \times \mathbf{E} = i \frac{\omega}{c} \mathbf{H} \quad (2.1)$$

$$\nabla \times \mathbf{H} = -i \frac{\omega}{c} \mathbf{D} \quad (2.2)$$

$$\nabla \cdot \mathbf{H} = 0 \quad (2.3)$$

$$\nabla \cdot \mathbf{D} = 0 \quad (2.4)$$

The electric displacement vector \mathbf{D} is related to the electric field \mathbf{E} as

$$\mathbf{D}(\mathbf{r}) = \varepsilon(\mathbf{r})\mathbf{E}(\mathbf{r}). \quad (2.5)$$

We adopt the method of Ho, Chan, and Soukoulis [23] to solve photonic band structures of such a periodic structure. In this way, Maxwell's equations can be further simplified to an equation satisfied by the magnetic field \mathbf{H} as

$$[\nabla \times \varepsilon^{-1}(\mathbf{r})\nabla] \times \mathbf{H} = \frac{\omega^2}{c^2} \mathbf{H} \quad (2.6)$$

where $\varepsilon^{-1}(\mathbf{r})$ is the inverse of $\varepsilon(\mathbf{r})$. Since $\varepsilon(\mathbf{r})$ is periodic, we can use Bloch's theorem to expand the \mathbf{H} field in terms of plane waves,

$$\mathbf{H}(\mathbf{r}) = \sum_{\mathbf{G}} \sum_{\lambda=1}^2 H_{\mathbf{G},\lambda} \hat{\mathbf{e}}_{\lambda} e^{i(\mathbf{k}+\mathbf{G})\cdot\mathbf{r}}, \quad (2.7)$$

where \mathbf{k} is a wave vector in the Brillouin zone of the lattice, \mathbf{G} is a reciprocal-lattice vector, and $\hat{\mathbf{e}}_1, \hat{\mathbf{e}}_2$ are orthogonal unit vectors that are both perpendicular to wave vector $\mathbf{k} + \mathbf{G}$ because of the transverse character of magnetic field \mathbf{H} (i.e., $\nabla \cdot \mathbf{H} = 0$) and $H_{\mathbf{G},\lambda}$ is the Fourier expansion component of the magnetic fields. The dielectric constant can also be expanded into its Fourier form as

$$\varepsilon(\mathbf{r}) = \sum_{\mathbf{G}} \varepsilon(\mathbf{g}) e^{i\mathbf{G}\cdot\mathbf{r}}, \quad (2.8)$$

where the Fourier transform coefficient $\varepsilon(\mathbf{G})$ can be obtained either analytically or numerically. The Fourier coefficient $\varepsilon(\mathbf{G})$ is given by

$$\varepsilon(\mathbf{G}) = \frac{1}{A_{cell}} \int_{cell} \varepsilon(\mathbf{r}) e^{-i\mathbf{G}\cdot\mathbf{r}} d\mathbf{r}, \quad (2.9)$$

where the integration is performed over the unit cell. The analysis of Eq. 2.6 can be reduced to solving two standard eigenvalue equations, each describing a particular wave polarization. They are given as follows:

$$\sum_{\mathbf{G}'} A(\mathbf{k} + \mathbf{G}, \mathbf{k} + \mathbf{G}') H(\mathbf{G}') = \frac{\omega^2}{c^2} H(\mathbf{G}) \quad (2.10)$$

with

$$A(\mathbf{K}, \mathbf{K}') = \begin{cases} |\mathbf{K}| |\mathbf{K}'| \varepsilon^{-1}(\mathbf{K} - \mathbf{K}') & \text{for the E-polarization state,} \\ \mathbf{K} \cdot \mathbf{K}' \varepsilon^{-1}(\mathbf{K} - \mathbf{K}') & \text{for the H-polarization state,} \end{cases} \quad (2.11)$$

where $\mathbf{K} = \mathbf{k} + \mathbf{G}$, $\mathbf{K}' = \mathbf{k} + \mathbf{G}'$. $\varepsilon^{-1}(\mathbf{K} - \mathbf{K}') = \varepsilon^{-1}(\mathbf{G} - \mathbf{G}')$ can be computed from solving the following equation

$$\sum_{\mathbf{G}''} \varepsilon^{-1}(\mathbf{G} - \mathbf{G}'') \varepsilon(\mathbf{G}'' - \mathbf{G}') = \delta_{\mathbf{G}\mathbf{G}'}. \quad (2.12)$$

To numerically solve eigenvalue Eq. 2.10 the matrix $\mathbf{A}(\mathbf{K}, \mathbf{K}')$ needs to be truncated. Convergence issues apply related to the truncation of this matrix. Ho et al. [18],

proposed to use for $\varepsilon^{-1}(\mathbf{G} - \mathbf{G}')$, the inverse of the matrix that corresponds to the expansion of the dielectric function $\varepsilon(\mathbf{r})$ instead. This method, known as Ho's method, was shown to have faster convergence [18, 19]. In our band structure calculations in Chapters 2–6 we used Ho's method. Note that the matrix elements $\varepsilon^{-1}(\mathbf{G} - \mathbf{G}')$ depend on the shape of the scatterers under consideration. $\varepsilon(\mathbf{G})$ is evaluated by

$$\varepsilon(\mathbf{G}) = \begin{cases} f\varepsilon_a + (1-f)\varepsilon_b & \text{for } \mathbf{G} = 0, \\ (\varepsilon_a - \varepsilon_b)S(\mathbf{G}) & \text{for } \mathbf{G} \neq 0, \end{cases} \quad (2.13)$$

Here, the filling factor f is the ratio of the areas A_{scat} of dielectric scatterers over the area of the unit cell A_{cell} . ε_a is the dielectric constant of the scatterers that are embedded in a material with dielectric constant ε_b . In fact, for the cases of circular and square scatterers, the structural factor $S(\mathbf{G})$ is then given by

$$S(\mathbf{G}) = \begin{cases} \left(\frac{l^2}{A_{cell}}\right) Sinc\left(\frac{G_x l}{2}\right) Sinc\left(\frac{G_y l}{2}\right) & \text{for square scatterers,} \\ \frac{2\pi R^2}{A_{cell}} \frac{J_1(GR)}{GR} & \text{for circular scatterers,} \end{cases} \quad (2.14)$$

where $Sinc(x) = \sin x/x$ and $J_1(x)$ is the Bessel function of the first kind, and $G = |\mathbf{G}|$. We denote l for the side-length of square scatterers, R for the radius of circular scatterers.

2.2 Numerical results

The patterns of 2D structures under consideration are depicted in Figure 2.1, as follows: (a) basic triangular lattice of circular dielectric rods in air, (b) the first Brillouin zone for the triangular structures, (c) basic square lattice of square dielectric rods in air and (d) the first Brillouin zone for the square structures. The bands for both H - and E -polarization modes were calculated. When the triangular lattices were considered, the Γ , \mathbf{J} , and \mathbf{X} points in the Brillouin zone were included

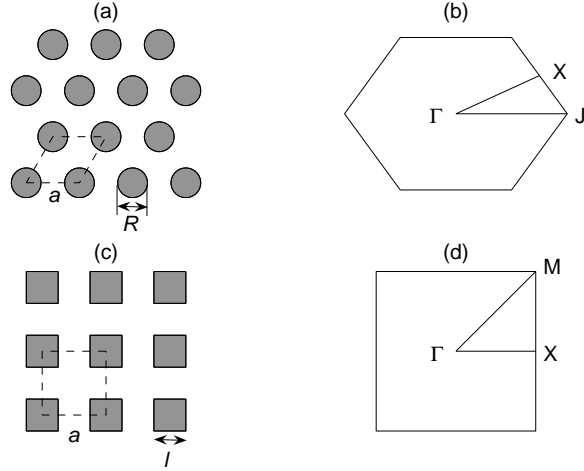


Figure 2.1: Patterns of the structures under consideration: (a) triangular-circles (*lattice-scatterers*); (b) first Brillouin zone for the triangular structures; (c) square-squares (*lattice-scatterers*); and (d) first Brillouin zone for the square structures

in calculated and the photonic bands were traced along the Γ -**J**-**X**- Γ path. For the square lattices of square rods, the calculations were performed along the Γ -**X**-**M**- Γ path.

We design elements for a particular wavelength of light: $\lambda = 1.5\mu m$, the wavelength of light which is often used in telecommunication [20]. It is known that the gallium arsenide (GaAs) has been widely used in optoelectronics. For light with a wavelength between $\lambda = 1.0\mu m$ and $\lambda = 10.0\mu m$, GaAs has a dielectric constant of 11.4. 361 plane waves in the Fourier expansion are used to calculate PBGs for the $E(H)$ -polarization. We discuss 2D PBG structures fabricated from isotropic material. We first examine 2D PBG structures consisting of dielectric cylinders in air. The circular rods are arranged in triangular lattice. The photonic properties have been studied and shown to exhibit band gaps for each of the two polarization modes [21]. However, there is some discrepancy about whether a complete band gap is present. Our simulations demonstrate that band gaps in the two polarization

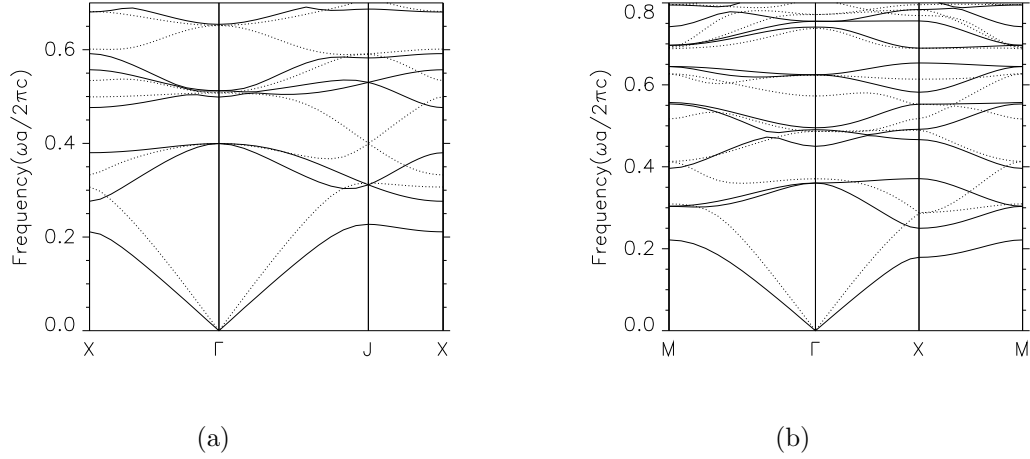


Figure 2.2: Calculated photonic band structure for (a) triangular lattice of circular dielectric rods (b) square lattice of square dielectric rods in air for E -polarization (solid lines) and H -polarization (dotted lines) modes. The rods have a dielectric constant of $\varepsilon = 11.4$ and a filling fraction of $f = 0.42$.

modes do not overlap with each other, resulting in the absence of the complete band gap. This can be clearly seen from Figure 2.2 (a), which displays the band structures of two polarization modes for a triangular lattice of circular dielectric rods in air. The rods have a dielectric constant of $\varepsilon = 11.4$ and a filling fraction of $f = 0.42$. Three band gaps open for the E -polarization mode (plotted in solid lines), *i.e.* the 1-2 band gap, 3-4 band gap and 6-7 band gap. For the H -polarization mode (plotted in dotted lines) a band gap is opened between 1-2 bands. However, the H 1-2 band gap lies between the E 1-2 and 3-4 band gaps, thus no complete band gap is present. Simulations at other filling fractions also show that no complete band gap is opened as the higher edge of the H 1-2 band gap always coincides with the lower edge of the E 3-4 band gap at high dielectric constant. This can be attributed to the degeneracy between the H 2 band and E 3, 4 bands, as shown in Figure 2.2 (a).

Figure 2.2 (b) depicts the photonic band structure for a square lattice of square

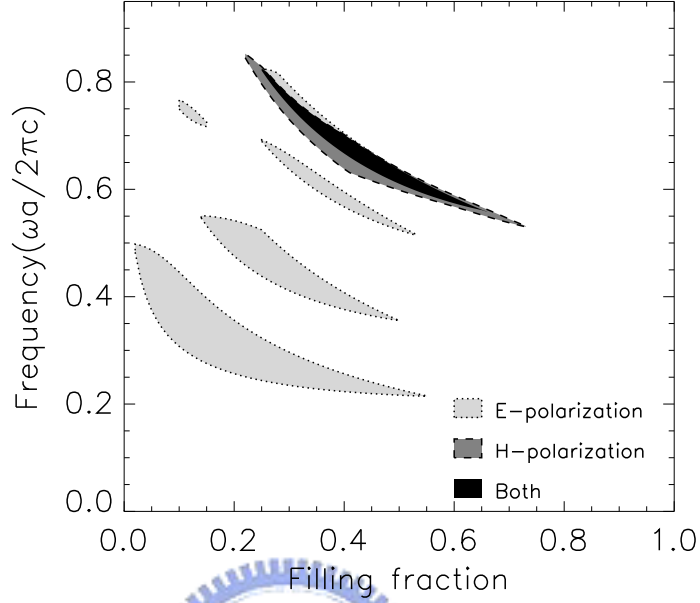


Figure 2.3: The gap map for a square lattice of square dielectric rods with the dielectric constant of $\varepsilon = 11.4$ as a function of the filling fraction.

dielectric rods in air. The filling fraction of the dielectric rods $f = (l/a)^2 = 0.42$, where l is the width of the square dielectric rods and a the lattice constant. An complete PBG occurs where E 8-9 and H 6-7 gaps overlap.

Figure 2.3 shows the gap map for a square lattice of square dielectric rods with the dielectric constant 11.4 as a function of the filling fraction of the square dielectric rods. The complete PBG is represented in black region. We only consider the bands below the tenth band for both E - and H -polarizations. The complete PBG starts near f is about 0.25 ($l/a = 0.5$) and ends at about 0.66 ($l/a = 0.8124$). The gap size reaches it maximum value at $f = 0.42$, which corresponds to $l/a = 0.648$. We should note here that H 6-7 gap is the only band gap appearing below the tenth band of H -polarization. Therefore, the only one complete PBG exists due to the overlap of E 8-9 and H 6-7 gaps in this frequency region.



Bibliography

- [1] J. B. Pendry and P. M. Bell, in *Photonic band gaps and localizations*, Ed. by C.M. Soukoulis, (Plenum Press, NY., 1993).
- [2] K. Busch, C. T. Chan, and C. M. Soukoulis, in *Photonic band gaps and localizations*, Ed. by C.M. Soukoulis, (Plenum Press, NY., 1993).
- [3] J. B. Pendry and A. MacKinnon Phys. Rev. Lett. **69**, 2772 (1992).
- [4] J. B. Pendry, J. Mod. Opt. **41**, 209 (1994).
- [5] J. Yonekura, J. Lightwave Technol. **17**, 1500 (1999).
- [6] K. M. Ho, C. T. Chan, and C. M. Soukoulis, Phys. Rev. Lett. **65**, 3152 (1990).
- [7] S. Satpathy, Z. Zhang, and M. Salehpourv, Phys. Rev. Lett. **64**, 1239 (1990).
- [8] K. M. Leung and Y. F. Liu, Phys. Rev. Lett. **65**, 2646 (1990).
- [9] H. S. Sozuer, J. W. Haus, and R. Inguva, Phys. Rev. B **45**, 13962 (1992).
- [10] R. D. Meade, D. Brommer, A. M. Rappe, J. D. Joannopoulos, and O. L. Alerhand, Phys. Rev. B **48**, 8434 (1993).
- [11] K. M. Leung, in *Photonic band gaps and localizations*, Ed. by C.M. Soukoulis, (Plenum Press, NY., 1993).

- [12] E. Yablonovitch, T. J. Gmitter, and K. M. Leung, Phys. Rev. B **67**, 2295 (1991).
- [13] K. S. Yee, IEEE Trans. Antennas Propagat. **14**, 302 (1996).
- [14] K. S. Kunz and R. J. Luebbers, *The Finite Difference Time Domain Method for Electromagnetics* (CRC, Boca Raton, 1993).
- [15] A. Mekis, S. Fan, and J. D. Joannopoulos, IEEE Microwave & Guided wave letters, **9**, 502 (1999).
- [16] F. Brechet, J. Marcou. D. Pagnoux, Opt. Fiber Technol. **6**, 181 (2000).
- [17] A. Figotin and Y.A. Godin, J. Comp. Phys. **136**, 585 (1997).
- [18] K. M. Ho, C. T. Chan, and C. M. Soukoulis, in *Photonic band gaps and localizations*, Ed. by C.M. Soukoulis, (Plenum Press, NY., 1993).
- [19] P. R. Villeneuve and. M. Piche, Prog. Quantum Electron. **18**, 153 (1994).
- [20] J. D. Joannopoulos, R. D. Meade, and J. N. Winn, *Photonic Crystals– Molding the Flow of Light* (Princeton University Press, 1995).
- [21] 15 M. Plihal, A.A. Maradudin, Phys. Rev. B **44**, 8565 (1991).

Chapter 3

Sensitivity of complete bandgaps to the shift of movable dielectric rod in two-dimensional photonic crystals with complex lattices



A paper published in the Journal of Physics: Condensed Matter¹

Wen-Long Liu, Tzong-Jer Yang and Ben-Yuan Gu

Two-dimensional tunable photonic crystals (TPC) with movable components are proposed, which consist of a circular dielectric rod inserting into a square lattice of square dielectric cylinders in air. The band gap structures of TPCs can be tuned by adjusting the shift of the position of the circular rod in each unit cell. Band gap structures are calculated with the use of plane-wave expansion method for various structural parameters, such as different filling fractions, ratio of the radius of the circular rod to the side-length of the square cylinder, different shifts or shifting orientations of the circular rod, etc. We find that there is a region of parameters in which the ratio of the gap width to the midgap is insensitive to the shift of the position of the circular dielectric rod. It is anticipated that the proposed TPC

¹J. Phys.: Condens. Matter. **16**, 4557 (2004).

may become a favorable candidate of the PCs owing to the benefit of facilitating fabrication, allowing a large tolerance.

3.1 Introduction

During the past decade, novel properties and means of fabricating periodically modulated dielectric structures have attracted much attention. One of the important characteristics of such materials — the so-called photonic crystals (PCs) — is that they exhibit photonic band gaps (PBGs) in which the propagation of electromagnetic (EM) waves in any propagating direction and polarization state is inhibited [1, 2, 3, 4, 5, 6]. This feature leads to various peculiar physical phenomena [3] and provides potential applications [6, 5, 4, 11].

Most proposed applications of PCs rely on large PBGs of PCs, therefore, the design and construction of PCs with large PBGs are a major goal in the PC field [6, 5, 4, 11]. Various methods have been proposed and implemented, for instance, introducing additional scatterers into unit cell of the prototype lattices to lift the degeneracy of the photonic bands at high symmetric points in the first Brillouin zone (FBZ) [12], rotating the lattices [7], employing anisotropic dielectric materials [8], rotating the non-circular rods [9, 10, 17, 18], modifying the distribution of permittivity in the unit cell [12, 17, 13], etc. Other design schemes with the use of various materials and mechanisms have also been developed [22, 23, 24, 25, 26, 27, 28].

In view of practical applications, a PC with tunable PBGs (TPBGs) is favorable because of tunability of the operation frequency in optical or microwave devices, thus, recently, TPCs have received much attention. Various materials have been suggested to the realization of the TPCs, including liquid crystals [29, 30, 31], metals and semiconductors [32, 33, 34, 35], ferrites [36], piezoelectric materials [37] and other optical materials [38, 39], etc.

Motivated by these works, in this article we propose alternative scheme of the construction of TPCs. The proposed two-dimensional TPC structure is realized by inserting a movable circular dielectric rod into a square lattice of square dielectric cylinders in air. The PBGs can be tunable by shifting the position of the circular dielectric rod. Indeed, several similar researches have been reported[7, 9, 10, 17, 18]. Their studies dominantly focused on the studies of the effects of rotating the 2D lattices or scatterers on PBGs. However, in the present work, we mainly concentrate on the subject of sensitivity of the ratio $\Delta\omega/\omega_g$ (where $\Delta\omega$ is the width of the complete band gap and ω_g is the midgap) to the variations of structural parameters of system, especially paying the attention on the effects of the shift s of the position of the circular dielectric rod. The band structures of the TPCs are calculated with the use of the plane-wave expansion method. Numerical simulations show that there is a range of parameters in which the variations of $\Delta\omega/\omega_g$ is insensitive to the changes of s . Thus, it concludes that the proposed TPCs may become a favorable candidate of the PCs owing to the facilitated fabrication with an allowance of large tolerance.

The rest of this paper is organized as follows. Section II briefly describes the model structures and the fundamental formulas used in calculations. Section III presents the numerical results and the analysis. Finally, Section IV discusses and summarizes the main findings.

3.2 Structural model and fundamental formulas

The schematic diagram of the proposed TPC structure is displayed in Figure 2.1. The square dielectric cylinders with a side-length of l and dielectric ϵ_a are placed in air with $\epsilon_b = 1.0$ at the four corners of a 2D square lattice with a lattice constant, a , in the xy -plane. Another circular dielectric rod with $\epsilon = \epsilon_a$ and diameter d

is inserted into each unit cell, forming composite lattices. We denote $\beta = d/l$ for convenience.

The electromagnetic (EM) fields with the E/H -polarization (in-pane magnetic/electric fields) in the 2D PC are governed by the Maxwell's equations

$$\left\{ \nabla \times \frac{1}{\epsilon(\mathbf{r})} \nabla \times \right\} \mathbf{H}(\mathbf{r}) = \frac{\omega^2}{c^2} \mathbf{H}(\mathbf{r}), \quad (3.1)$$

where $\mathbf{H}(\mathbf{r})$ denotes the magnetic fields; ω the angular frequency; c the speed of light in vacuum, and $\epsilon(\mathbf{r})$ the periodically modulated dielectric function. The magnetic fields and the dielectric function can be expanded in terms of Fourier series as

$$\mathbf{H}(\mathbf{r}) = \sum_{\mathbf{G}} \sum_{\lambda=1}^2 h_{\mathbf{G},\lambda} \hat{\mathbf{e}}_{\lambda} e^{i(\mathbf{k}+\mathbf{G})\cdot\mathbf{r}}, \quad (3.2)$$

$$\epsilon(\mathbf{r}) = \sum_{\mathbf{G}} \epsilon(\mathbf{G}) e^{i\mathbf{G}\cdot\mathbf{r}}, \quad (3.3)$$

where \mathbf{k} is the Bloch wave vector in the FBZ, and \mathbf{G} the 2D reciprocal lattice vector. The polarization unit vectors $\hat{\mathbf{e}}_{\lambda}$ with $\lambda = 1, 2$ are perpendicular to $(\mathbf{k}+\mathbf{G})$ and $h_{\mathbf{G},\lambda}$ is the Fourier expansion component of the magnetic fields. The Fourier coefficient $\epsilon(\mathbf{G})$ is given by

$$\epsilon(\mathbf{G}) = \frac{1}{A_{cell}} \int_{cell} \epsilon(\mathbf{r}) e^{-i\mathbf{G}\cdot\mathbf{r}} d\mathbf{r}, \quad (3.4)$$

where the integration is performed over the unit cell. Here, the filling fraction f , which is the ratio of the areas A_{scat} of dielectric scatterers in a unit cell to the area A_{cell} of a unit cell of square lattice, is as

$$f = \frac{l^2}{a^2} \left(1 + \frac{\pi\beta^2}{4} \right). \quad (3.5)$$

For the proposed TPC, $\epsilon(\mathbf{G})$ is evaluated by

$$\epsilon(\mathbf{G}) = \begin{cases} f\epsilon_a + (1-f)\epsilon_b & \text{for } \mathbf{G} = 0, \\ (\epsilon_a - \epsilon_b)S(\mathbf{G}) & \text{for } \mathbf{G} \neq 0, \end{cases} \quad (3.6)$$

We assume that there is a shift \mathbf{s} of the inserted circular rod with respect to the center of the unit cell, that is $\mathbf{s} = s(\hat{\mathbf{x}} \sin \gamma + \hat{\mathbf{y}} \cos \gamma)$, where γ is the span angle of the displacement vector with respect to the y -axis. The structural factor $S(\mathbf{G})$ is then given by [40]

$$S(\mathbf{G}) = e^{-i\mathbf{G} \cdot (\hat{\mathbf{x}} + \hat{\mathbf{y}})a/2} S_1(\mathbf{G}) + e^{-i\mathbf{G} \cdot \mathbf{s}} S_2(\mathbf{G}), \quad (3.7)$$

where

$$S_1(\mathbf{G}) = \left(\frac{l^2}{a^2}\right) \text{Sinc}\left(\frac{G_x L}{2}\right) \text{Sinc}\left(\frac{G_y L}{2}\right) \quad (3.8)$$

with $\text{Sinc}(x) = \sin x/x$ and

$$S_2(\mathbf{G}) = \left(\frac{l^2}{a^2}\right) \frac{\pi \beta^2 J_1(Ga)}{2 Ga}, \quad (3.9)$$

where $J_1(x)$ is the Bessel function of the first kind, and $G = |\mathbf{G}|$.

The band structures are then determined from solving the following equation

$$\sum_{\mathbf{G}'} A(\mathbf{k} + \mathbf{G}, \mathbf{k} + \mathbf{G}') H(\mathbf{G}') = \omega^2 H(\mathbf{G}) \quad (3.10)$$

with

$$A(\mathbf{K}, \mathbf{K}') = \begin{cases} |\mathbf{K}| |\mathbf{K}'| \epsilon^{-1}(\mathbf{K} - \mathbf{K}') & \text{for the E-polarization state,} \\ \mathbf{K} \cdot \mathbf{K}' \epsilon^{-1}(\mathbf{K} - \mathbf{K}') & \text{for the H-polarization state,} \end{cases} \quad (3.11)$$

where $\mathbf{K} = \mathbf{k} + \mathbf{G}$, $\mathbf{K}' = \mathbf{k} + \mathbf{G}'$. $\epsilon^{-1}(\mathbf{K} - \mathbf{K}') = \epsilon^{-1}(\mathbf{G} - \mathbf{G}')$ can be computed from solving the following equation

$$\sum_{\mathbf{G}''} \epsilon^{-1}(\mathbf{G} - \mathbf{G}'') \epsilon(\mathbf{G}'' - \mathbf{G}') = \delta_{\mathbf{G}\mathbf{G}'}. \quad (3.12)$$

3.3 Numerical results and analysis

The following parameters are used in the calculations: $\epsilon_a = \epsilon = 11.4$ appropriate for gallium arsenide (GaAs) at wavelength $\lambda \approx 1.5\mu m$ and $\epsilon_b = 1.0$ in air. 1521 plane waves in the Fourier expansion are used to calculate PBGs for the $E(H)$ -polarization. First, the PBG structures of the prototype square lattices just with square cylinders are calculated, as shown in Figure 2.2(a), fixed the filling fraction $f = 0.217$. The solid (dashed) curves correspond to the $E(H)$ -polarization. Hereafter, we always adopt these line styles in the same manner to plot the photonic band structures except for the special statement made. It is clearly seen that there are two large PBGs (solid curves) for the E-polarization: $\omega_{g1} = 0.3(2\pi c/a)$ and $\omega_{g2} = 0.5(2\pi c/a)$; however, no PBG is survival for the H-polarization. Thus, the complete PBG is now absent in the prototype PC. In contrast, when a circular GaAs rod is introduced into each unit cell, the calculated band structures are demonstrated in Figure 2.2(b). It is evident that a complete PBG now is generated, as indicated by the gray region. The parameters are $f = 0.3$, $\beta = 0.7$, and $s = 0$. This PBG becomes a complete one when E_9 and H_6 are overlapped with each other, where E_i (H_i) denotes the band gap appearing between the i th and $(i+1)$ th bands for the $E(H)$ -polarization. Notably, introducing an extra circular rod into each unit cell substantially lowers the band frequencies and generates new bands for the E -polarization. These results can be interpreted by considering the effects of scattering and interference of light waves to be significantly modified and enhanced when introducing the extra scatterer into each unit cell [12, 17, 13]. For the H -polarization bands, the introduction of the extra scatterer should lead to the lowering of the frequency of the higher index bands but small modification of the profile of the lower index bands.

The effects of the filling fraction f on the dispersion spectrum are revealed by

the plot of the dependence of the $\Delta\omega/\omega_g$ as a function of f for different β 's : $\beta = 0.7, 0.75$ and 0.8 , fixed $s = 0$, as depicted in Figure 2.3. $\epsilon_a = \epsilon = 11.4$ and $\epsilon_b = 1.0$ are chosen. From $f = (1 + \pi\beta^2/4)(l/a)^2$ and given f as well as β , one can easily evaluate l/a . Notably, the $\Delta\omega/\omega_g$ is taken the largest of all the complete PBGs at a given f and specified β . In the calculations, only the first ten-bands are considered for both E - and H - polarizations. Apparently, all of the curves exhibit a Gaussian-like broad bump with a right-wing; the nonzero $\Delta\omega/\omega_g$ spans only a finite range, $f = [0.2, 0.6]$. As β is increased, the peak position in curve is shifted toward larger f regime, while the right-wing falls rapidly. The largest peak value of $\Delta\omega/\omega_g$ is 0.0649, corresponding to $f = 0.29$ and $\beta = 0.7$ (solid curve). As β is altered, this peak value and the profile of $\Delta\omega/\omega_g$ are changed gradually; for instance, $(\Delta\omega/\omega_g)_{max}$ are 0.0649, 0.063 and 0.0589, at $f = 0.29, 0.33, 0.32$ and $\beta = 0.7, 0.75, 0.8$, respectively. The dependence of $(\Delta\omega/\omega_g)$ on f is also calculated at other values of β : the corresponding curves exhibit significantly deformation. The decline trend of the right-wing is quite fast and its extension is remarkably shortened as β is increased. This broad bump profile manifests the large freedom in the choice of the structural parameters, which provide the benefit of the facilitated construction of the TPCs with a large allowance of tolerance.

The influences of the shift s of the dielectric circular rod on the PBGs is now investigated. The sample is the same as that in Figure 2.2(b), except that s is changed. Figure 2.4 depicts the calculated band structures for two values of s — (a) $s = 0.1a$, (b) $s = 0.25a$. The other parameters are $f = 0.3$, $\beta = 0.7$, $\epsilon_a = \epsilon = 11.4$ and $\epsilon_b = 1.0$, at fixed $\gamma = 0^\circ$. The shift of the inserted circular rod leads to lower the symmetry of structures and lift the degeneracy at the high symmetric points in the FBZ, therefore, the complete PBG can be produced. Figure 2.4 demonstrates the existence of a complete PBG with $\omega_g = 0.77805(2\pi c/a)$ and

$\Delta\omega = 0.0509(2\pi c/a)$, which covers the overlapping region of the E_9 and H_7 bands. When s is increased to $0.25a$, the complete gap remains, but the midgap is slightly changed: $\omega_g = 0.78795(2\pi c/a)$; however, the gap width is reduced substantially to $\Delta\omega = 0.0311(2\pi c/a)$, as shown in Figure 4(b). The increase of s significantly shifts the top of the E_9 band upwards, but the bottom of the H_7 band almost remains unchanged, consequently, the gap is narrowed remarkably.

We now study the influences of the the direction of the displacement of the inserted dielectric circular rod on $\Delta\omega/\omega_g$. The following parameters are chosen: $f = 0.3$, $\beta = 0.7$; the other parameters are as those in Figure 2.4. The variations of $\Delta\omega/\omega_g$ with s are shown in Figure 2.5 for three different shifting directions of $\gamma = 0^\circ, 25^\circ$ and 45° . Notably, for a given γ , the varying region of s is limited, i.e., only from zero to a certain value at which the outermost edge of the internal dielectric circular rod just touches the outermost edge of the square dielectric cylinder at the lattice or the boundary of the unit cell of the lattice. All the curves in Figure 2.5 exhibit a plateau profile at around $\Delta\omega/\omega_g = 0.07$ at the beginning of curves, and then decline monotonically to zero at a certain s , depending on γ . Subsequently, the curves, except for the solid one with $\gamma = 0^\circ$, oscillate with s , as shown in Figure 2.5. Importantly, these plateaus in curves have only a small positive slope near the beginning. This plateau spans a finite region of about $s = [0, 0.1]a$, thus, it can greatly relax the tolerance in the fabrication of TPCs.

The convergence of the calculated results with the increase of the number of plane-waves in the expansion must be confirmed with the robustness and reliability of the obtained results.

The variations of $\Delta\omega/\omega_g$ of the complete band gap as a function of the number N of the plane-waves in the expansion are depicted in Figure 2.6. The following parameters are used: $f = 0.3$, $\beta = 0.7$, $s = 0.1a$ and $\gamma = 0^\circ$. Clearly, the curve

tends a saturation value of about 0.068 as N increases. The relative error defined by $[(\Delta\omega/\omega_g)(\text{at } N=2500) - (\Delta\omega/\omega_g)(\text{at } N=1521)]/0.5[(\Delta\omega/\omega_g)(\text{at } N=2500) + (\Delta\omega/\omega_g)(\text{at } N=1521)]$ is 0.016. In the calculation herein, $N = 1521$ is used. Therefore, these results are reliable.

To confirm the existence of the plateau, we study the $(\Delta\omega/\omega_g) - s$ dependence for several N , are displayed in Figure 2.7. The relative errors defined by $[(\Delta\omega/\omega_g)(\text{at } N=3249) - (\Delta\omega/\omega_g)(\text{at } N=1521)]/0.5[(\Delta\omega/\omega_g)(\text{at } N=3249) + (\Delta\omega/\omega_g)(\text{at } N=1521)]$ are 0.023, 0.0221, 0.0217, 0.0219, 0.0239 and 0.0243 for $s = 0.0, 0.02, 0.04, 0.06, 0.08$ and 0.1 , respectively. This implies that the existence of the plateau is believable.

An additional plot in Figure 2.8 provides more information on the TPCs. The PBG map as the relative shift s of the inserted rod is presented. The parameters are chosen as : $f = 0.3, \beta = 0.7$ and $\gamma = 0^\circ$. Only the first ten-bands are involved in this map for both E - and H -polarizations. Notably, all the gap widths for the E -polarization gradually shrink as s increases. The E_1 and E_4 band gaps are in the range $s = [0, 0.5]a$, while the gap width of the E_1 band is quite small and almost unobservable. The gaps of the E_2 and E_9 bands span a short region of s less than $0.4a$. For the H -polarization modes, the gap region for the H_2 and H_6 bands covers only a narrow range of s and the gap width is narrower than that in the E -polarization case. Only one complete PBG appears between H_7 and E_9 , and is marked by the black area in Figure 2.8. It starts with near $s=0$ and ends at about $0.31a$. The complete PBG is centered near $\omega a/2\pi c=0.775$ with $\Delta\omega/\omega_g = 0.0646$ when $s = 0$.

3.4 Discussions and summary

The tunable PCs containing a movable dielectric circular rod in each unit cell are proposed. Such TPCs can be fabricated by separately building two 2D PCs, one

PC consists of dielectric circular rods located at internal of a square lattice, and the other PC consists of dielectric square cylinders located at four corners of a square lattice with the identical lattice constant, a . They are then combined into a final interpenetrating structure. Properly adjusting the position of the dielectric circular rod in the unit cell enables the tunable *complete* PBG generated from the composite structure to be opened and closed. Additionally, when the relative shift s of the circular rod is under $0.1a$, the ratio of the gap-width to the midgap almost remains unchanged or varies a little. This property provides the large benefit of relaxing the fabrication tolerance of the TPCs. The TPCs can be easily fabricated and operated in the micro-wave region because a is in the order of microwave wavelengths — several mm or cm.

In summary, the properties of the proposed TPCs are systematically investigated. When the filling fraction f and the ratio of the diameter of the dielectric circular rod to the side-length of the dielectric square cylinder, $\beta = d/l$, are suitably chosen, a range of relative shift of the circular rod, exists in which the gapwidth-midgap ratio $\Delta\omega/\omega_g$ is insensitive to changes of s , regardless of the direction of \mathbf{s} . Such insensitivity provides large advantage for practical fabrication of TPC, allowing large tolerance. The proposed TPCs is anticipated to be encouraged in applications to new microwave devices. Its acoustic counterpart [10] can also be created and used as tunable acoustic crystals.

Acknowledgments

The authors would like to thank the National Science Council of the Republic of China, Taiwan (Contract No. NSC 90-2112-M-009-028) and the Electrophysics Department, National Chiao Tung University, Taiwan, for their support. Dr. Young-Chung Hsue and Dr. Pi-Gang Luan are appreciated for their useful discussions.

Bibliography

- [1] E. Yablonovitch, Phys. Rev. Lett. **58**, 2059 (1987).
- [2] S. John, Phys. Rev. Lett. **58**, 2486 (1987).
- [3] M. Pilhal and A. A. Maradudin, Phys. Rev. B **44**, 8565 (1991).
- [4] P. R. Villeneuve and M. Piché, Phys. Rev. B **46**, 4973 (1992).
- [5] C. S. Kee, J. E. Kim and H. Y. Park, Phys. Rev. B **56**, R6291 (1997).
- [6] M. Agio and L. C. Andreani, Phys. Rev. B **61**, 15519 (2000).
- [7] S. John, Nature **390**, 661 (1997).
- [8] *Photonic Band Gaps and Localization*, edited by C. M. Soukoulis (Plenum, New York, 1993).
- [9] J. D. Joannopoulos, R. D. Meade, and J. N. Winn, *Photonic Crystals– Molding the Flow of Light* (Princeton University Press, 1995).
- [10] K. Sakoda, *Optical Properties of Photonic Crystals* (Springer-Verlag, 2001).
- [11] E. Yablonovitch, Sci. Am. Vol.**285**, No.6, 34 (2001).
- [12] C. M. Anderson and K. P. Giapis, Phys. Rev. Lett. **77**, 2949 (1996).
- [13] C. M. Anderson and K. P. Giapis, Phys. Rev. B **56**, 7313 (1997).

- [14] Z. Y. Li, B. Y. Gu, and G. Z. Yang, Phys. Rev. Lett. **81**, 2574 (1998); Eur. Phys. J. B **11**, 65 (1999).
- [15] X. H. Wang, B.Y. Gu, Z. Y. Li, and G. Z. Yang, Phys. Rev. B **60**, 11417 (1999).
- [16] C. Goffaux and J. P. Vigneron, Phys. Rev. B **64**, 075118 (2001).
- [17] R. Z. Wang, X. H. Wang, B. Y. Gu, and G. Z. Yang, J. Appl. Phys. **90**, 4307 (2001).
- [18] N. Susa, J. Appl. Phys. **91**, 3501 (2002).
- [19] R. D. Meade, A. M. Rappe, K. D. Brommer, and J. D. Joannopoulos, J. Opt. Soc. Am. B **10**, 328 (1993).
- [20] Min Qiu and Sailing He, J. Opt. Soc. Am. B **17**, 1027 (2000).
- [21] X. D. Zhang, Z. Q. Zhang, L. M. Li, C. Jin, D. Zhang, B. Man, and B. Cheng, Phys. Rev. B **61**, 1892 (2000).
- [22] D. F. Sievenpiper and E. Yablonovitch, Phys. Rev. Lett. **80**, 2829 (1998).
- [23] W. Y. Zhang, X. Y. Lei, Z. L. Wang, D. G. Zheng, W. Y. Tam, C. T. Chan, and P. Sheng, Phys. Rev. Lett. **84**, 2853 (2000).
- [24] M. M. Sigalas, C. M. Soukoulis, R. Biswas, and K. M. Ho, Phys. Rev. B **56**, 959 (1997).
- [25] C. S. Kee, J. E. Kim, and H. Y. Park, Phys. Rev. E **57**, 2327 (1998).
- [26] B. Gates and Y. Xia, Adv. Mater **13**, 1605 (2001).

- [27] S. I. Bozhevolnyi, D. J. Erland, K. Leosson, P. M. W. Skovgaard, and J. M. Hvam, *Phys. Rev. Lett.* **86**, 3008 (2001).
- [28] S. David, A. Chelnokov, and J.-M. Lourtioz, *IEEE. J. Quant. Elect.* **37**, 1427 (2001).
- [29] K. Busch and S. John, *Phys. Rev. Lett.* **83**, 967 (1999).
- [30] S. W. Leonard, J. P. Mondia, H. M. van Driel, O. Toader, S. John, K. Busch, A. Birner, U. Gosele, and V. Lehmann, *Phys. Rev. B* **61**, R2389 (2000).
- [31] Y. K. Ha, Y. C. Yang, J. E. Kim, H. Y. Park, C. S. Kee, H. Lim, and J. C. Lee, *Appl. Phys. Lett.* **79**, 15 (2001).
- [32] P. Halevi and F. Ramos-Mendieta, *Phys. Rev. Lett.* **85**, 1875 (2000).
- [33] A. Moroz, *Phys. Rev. Lett.* **83**, 5274 (1999).
- [34] C. S. Kee and H. Lim, *Phys. Rev. B* **64**, R121103 (2001).
- [35] C. S. Kee, H. Lim, Y. K. Ha, J. E. Kim, and H. Y. Park, *Phys. Rev. B* **64**, 085114 (2001).
- [36] C. S. Kee, J. E. Kim, H. Y. Park, I. Park, and H. Lim, *Phys. Rev. B* **61**, 15523 (2000).
- [37] S. W. Kim and V. Gopalan, *Appl. Phys. Lett.* **78**, 3015 (2001).
- [38] P. Kopperschmidt, *Appl. Phys. B* **73**, 717 (2001).
- [39] Z. Z. Gu, T. Iyoda, A. Fujishima, and O. Sato, *Adv. Mater. B* **13**, 1295 (2001).
- [40] P. G. Luan and Z. Ye, E-print, cond-mat/0105428 (2001).

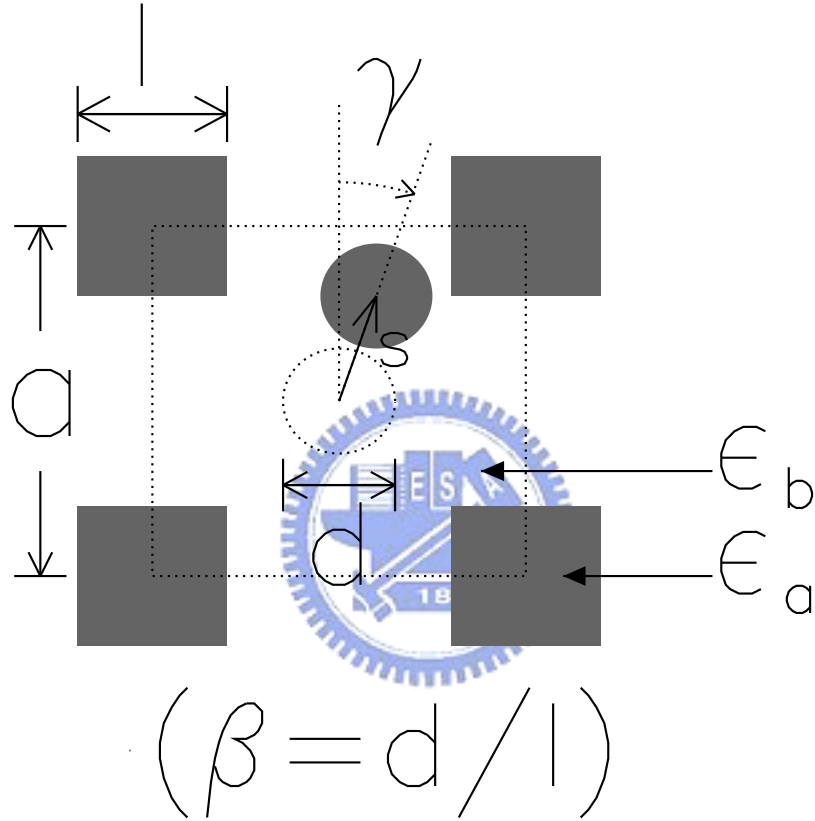


Figure 3.1: Schematic diagram of proposed tunable photonic crystals. The square dielectric cylinders with a side-length of l and dielectric ϵ_a are placed in air with $\epsilon_b = 1.0$ at the four corners of a 2D square lattice with a lattice constant, a , in the xy -plane. Another circular dielectric rod with $\epsilon = \epsilon_a$ and diameter d is inserted into each unit cell, forming composite lattices. We denote $\beta = d/l$ for convenience. This dielectric circular rod is movable. We assume that there is a shift \mathbf{s} of the inserted circular rod with respect to the center of the unit cell, that is $\mathbf{s} = s(\hat{\mathbf{x}} \sin \gamma + \hat{\mathbf{y}} \cos \gamma)$, where γ is the span angle of the displacement vector with respect to the y -axis.

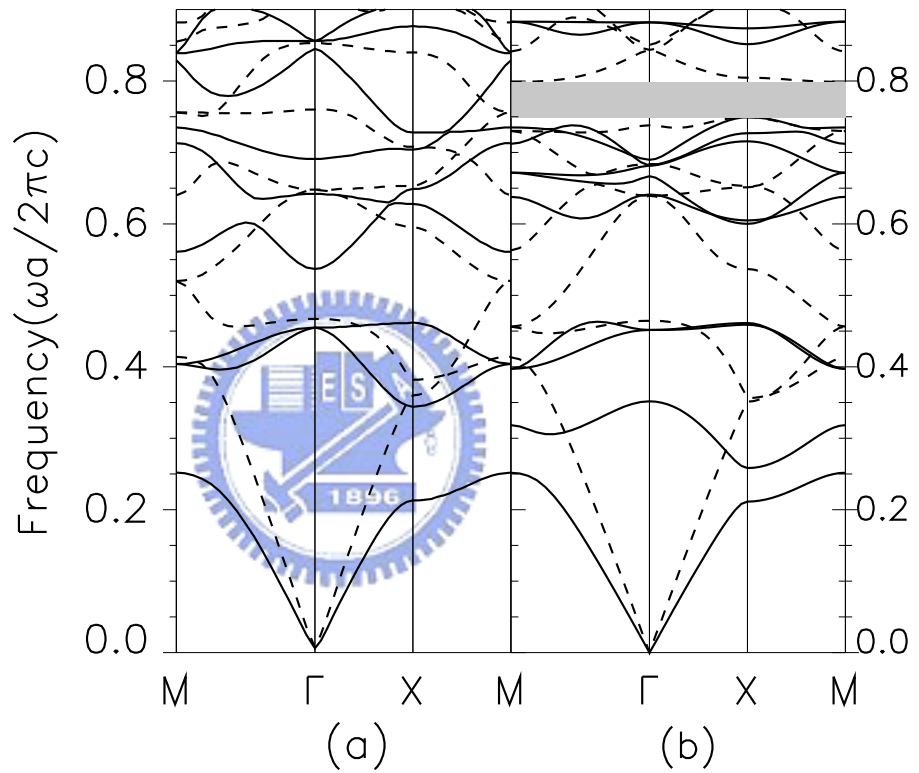


Figure 3.2: Photonic band structures for two structures : (a) the prototype structure without the inserted circular rod and (b) a TPC with a movable dielectric circular rod in internal of the unit cell. The relevant parameters are chosen as: $\epsilon_a = \epsilon = 11.4$, appropriate for GaAs material; $\epsilon_b = 1.0$ in air. (a) $f = 0.217$, $d/l = 0$ and (b) $f = 0.3$, $d/l = 0.7$, $s = 0$. The solid and dashed curves correspond to the E - and H -polarizations, respectively. The shadow area marks the complete gap region.

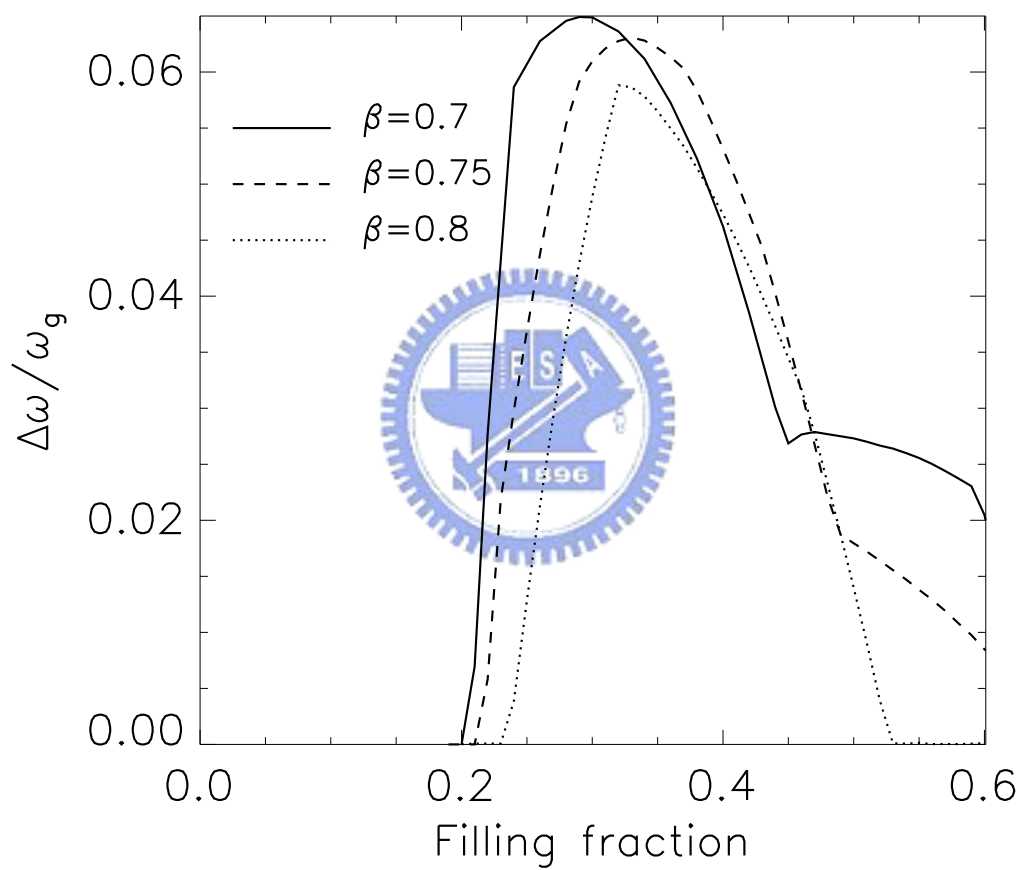


Figure 3.3: Variations of $\Delta\omega/\omega_g$ with the filling fraction f for different values of β : 0.7(solid line), 0.75(dashed line) and 0.8(dotted line). The other parameters are the same as those in Figure 2.2(b).

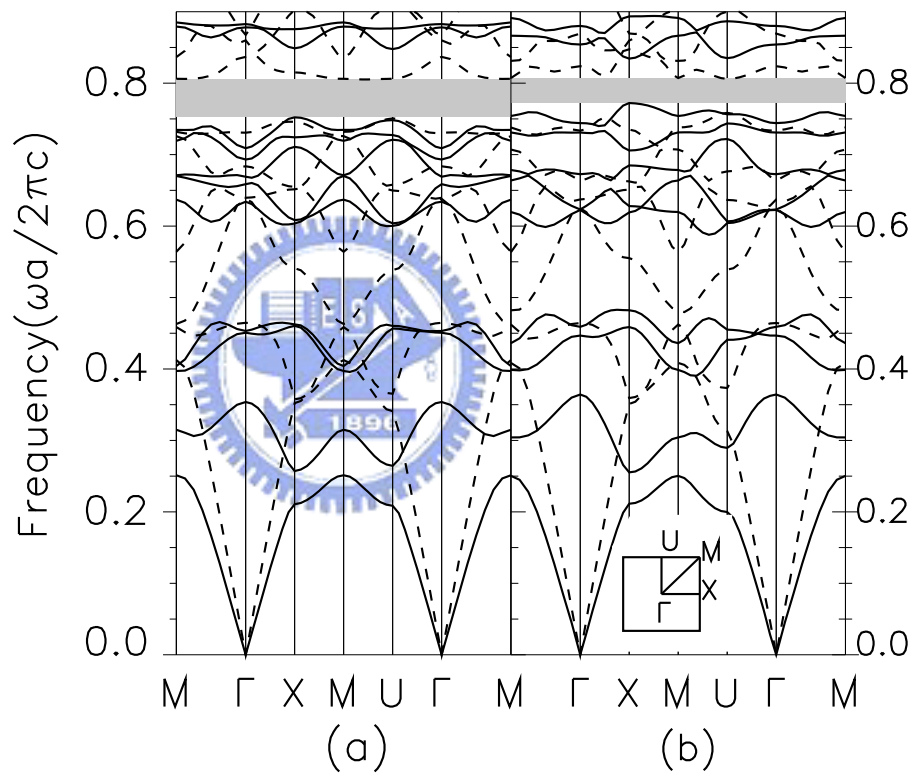


Figure 3.4: Same as Figure 2.2(b) except for different values of s : (a) $s = 0.1a$ and (b) $s = 0.25a$. The other parameters are $f = 0.3$, $\beta = 0.7$, and $\gamma = 0^\circ$.

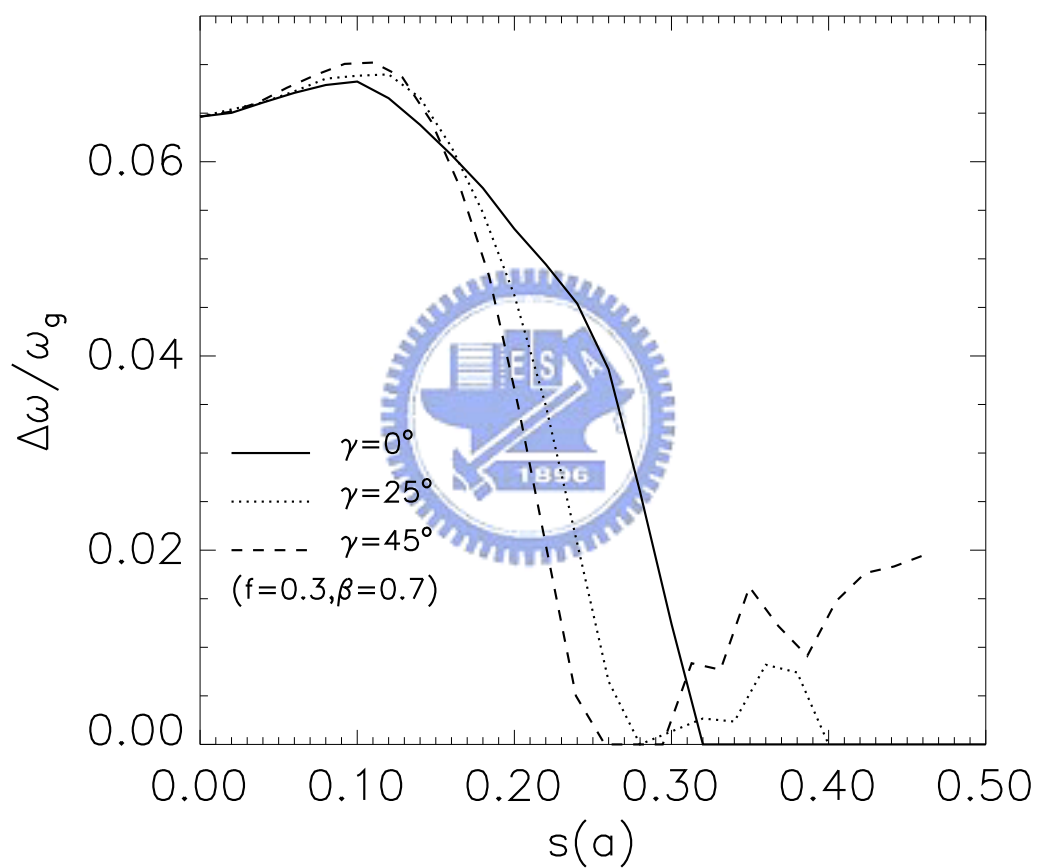


Figure 3.5: Variations of $\Delta\omega/\omega_g$ with the relative shift s for several shifting directions: $\gamma = 0^\circ$ (solid line); $\gamma = 25^\circ$ (dotted line), and $\gamma = 0.45^\circ$ (dashed line). The other parameters are the same as those in Figure 2.2(b).

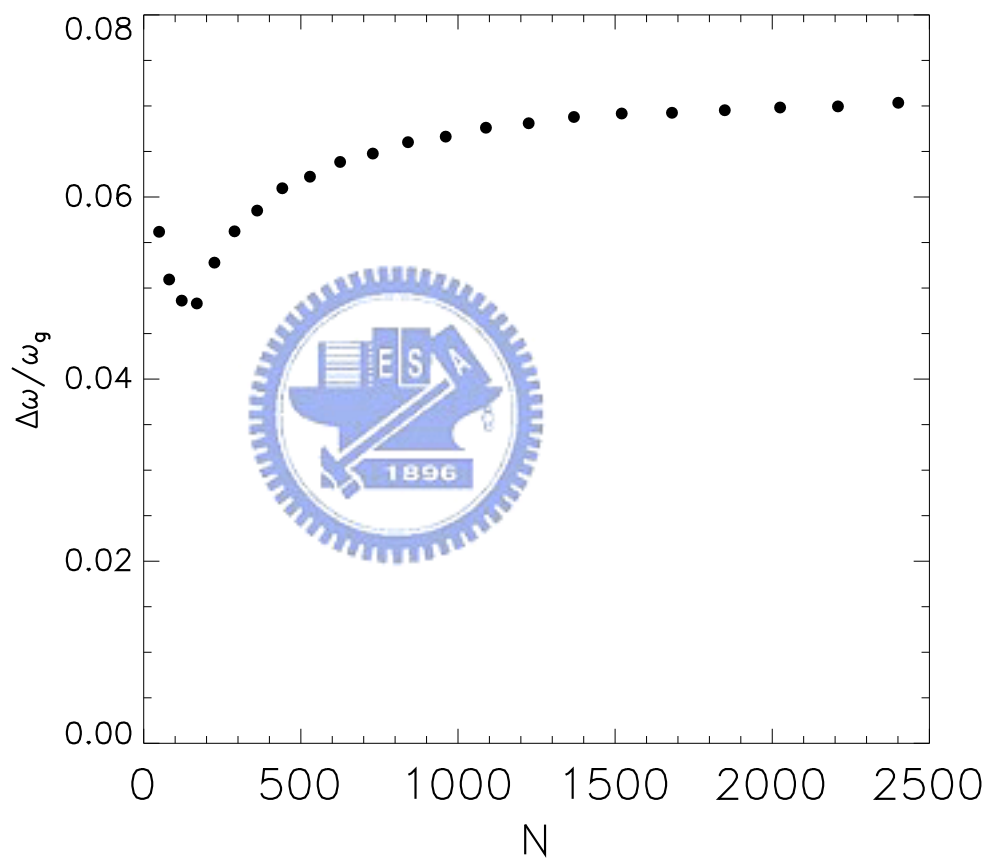


Figure 3.6: Variations of $\Delta\omega/\omega_g$ of the complete band gap versus the number N of the plane-waves in the expansion. The parameters are $f = 0.3$, $\beta = 0.7$, $s = 0.1 a$ and $\gamma = 0^\circ$.

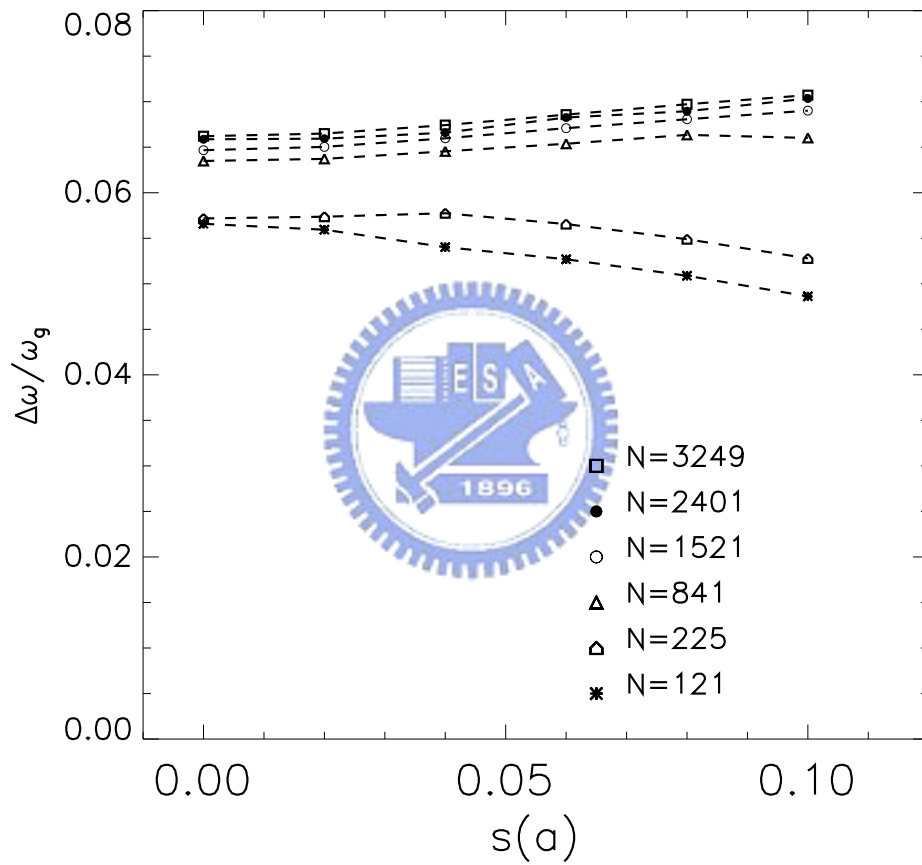


Figure 3.7: Variations of $\Delta\omega/\omega_g$ of the complete band gap with s as the number N of the plane-waves in the expansion increases for $\gamma = 0^\circ$ with $f = 0.3$, $\beta = 0.7$. The numbers of plane-waves in the expansions for the H-polarization and the E-polarization are the same.

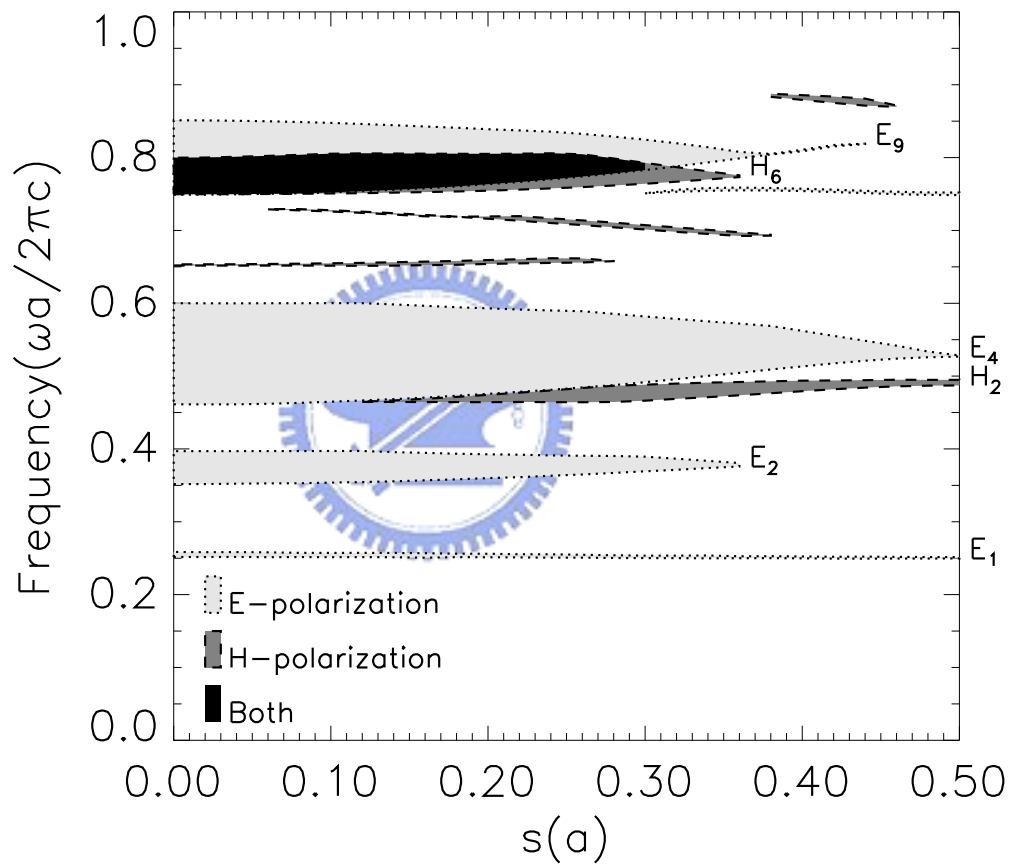


Figure 3.8: Gap map of the proposed TPC, as the relative shift s varies for both E - and H -polarizations. The parameters are $f = 0.3$, $\beta = 0.7$, and $\gamma = 0^\circ$. The black area marks the regions of the complete band gaps.



Chapter 4

Variation of group velocity and complete bandgaps in two-dimensional photonic crystals with drilling holes into the dielectric rods



A paper published in the Physica B¹

Wen-Long Liu and Tzong-Jer Yang

Two-dimensional square lattices of square cross-section dielectric rods in air, designed with an air hole drilled into each square rod, are studied theoretically. By adjusting the shift of the hole position in the square rod in each unit cell, the dielectric distribution of the square rod will be modified. A sizable complete band gap occurs for certain structural parameters and exhibits very flat photonic bands near such gap edge, which resulting in a sharp peak of density of states. In addition, the zero or small group velocities are observed in a broad region of \mathbf{k} -space. This structure can be fabricated with materials widely used today and opens a fascinating

¹Physica B **368**, 151 (2005).

area for applications in optoelectric devices.



4.1 Introduction

First introduced by Yablonovitch [1] and John [2] in 1987, photonic crystals (PCs) are now a fascinating issue of research. PCs are of artificial materials having the periodical modulation of dielectric structures in space and there exist photonic band gaps (PBGs) in which the propagation of electromagnetic (EM) waves in any propagating direction and polarization state is inhibited. In the PBG the spontaneous emission from the atoms or molecules can be rigorously forbidden [1]. The absence of normal modes of EM waves along certain directions provides the potential for application to various optical devices, such as resonant antennas [3], microscopic lasers [4], and optical switches[5], etc.

The wider a PBG is, the greater the forbidden region of the frequency spectrum. Thus, the search for photonic crystals that possess wider band gaps is an important issue. Various methods for creating large PBGs or in increasing an existing PBG by altering the dielectric constant $\epsilon(\mathbf{r})$ within a unit cell, have been proposed. These methods include rotating the lattices [7], using anisotropic dielectric materials [8], rotating the noncircular rods [9, 10, 11], and modifying the permittivity distribution in a unit cell [12, 17, 13]. In such cases, an EM wave can be decomposed into the E - and H -polarization modes for two-dimensional (2D) photonic crystal. A complete PBG exists for two-dimensional PBG crystal only when band gaps in both E - and H -polarization modes are present and they overlap each other. That is a PBG independent of the polarization of the EM waves. Many crystals generating band gaps for some light polarizations, but these may not overlap to produce a complete PBG [14]. It was reported that the symmetry reduction of atom configuration by introducing a two-point basis set in simple 2D lattice can remarkably increase complete PBG [15], quite similar to the 3D case for diamond structure [16]. In

contrast, symmetry breaking in a square lattice by changing the shape of square air rods to rectangular [17] or cylinder [18] reduces the width of complete PBGs.

In this work we study a type of square photonic lattice in two dimensions, which is formed by an air hole drilled into each square dielectric rod in air. We shift the air hole to modify dielectric distribution without changing the shape and orientation of dielectric scatterers. A sizable complete PBG occurs for certain structural parameters and exhibits very flat photonic bands near such gap edge, which resulting in a sharp peak of density of states. In addition, the zero or small group velocities are observed in a broad region of \mathbf{k} -space. These small group velocities of the eigenmode cause a long optical path in this structure [19]. It brings about the optical gain enhancement or low-threshold lasing [20, 21].

4.2 Theory

Figure 3.1 displays the schematic diagram of our proposed 2D photonic band structure. The square dielectric rods with a side-length of l and dielectric ϵ_a are placed in air background with $\epsilon_b = 1.0$ at the center of a 2D square lattice with a lattice constant, a , in the xy -plane. Another circular rod with $\epsilon_b = 1.0$ and diameter d is drilled into square rod in each unit cell. We denote $\beta = d/l$ for convenience.

The electromagnetic (EM) fields with the E/H -polarization (in-pane magnetic/electric fields) in the 2D PC are governed by the Maxwell's equations:

$$\left\{ \nabla \times \frac{1}{\epsilon(\mathbf{r})} \nabla \times \right\} \mathbf{H}(\mathbf{r}) = \frac{\omega^2}{c^2} \mathbf{H}(\mathbf{r}), \quad (4.1)$$

where $\mathbf{H}(\mathbf{r})$ denotes the magnetic fields; ω the angular frequency; c the speed of light in vacuum, and $\epsilon(\mathbf{r})$ the periodically modulated dielectric function. The magnetic fields and the dielectric function can be expanded in terms of Fourier series as

$$\mathbf{H}(\mathbf{r}) = \sum_{\mathbf{G}} \sum_{\lambda=1}^2 h_{\mathbf{G},\lambda} \hat{\mathbf{e}}_{\lambda} e^{i(\mathbf{k}+\mathbf{G})\cdot\mathbf{r}}, \quad (4.2)$$

$$\epsilon(\mathbf{r}) = \sum_{\mathbf{G}} \epsilon(\mathbf{G}) e^{i\mathbf{G}\cdot\mathbf{r}}, \quad (4.3)$$

where \mathbf{k} is the Bloch wave vector within the first Brillouin zone, and \mathbf{G} the 2D reciprocal lattice vector. The polarization unit vectors $\hat{\mathbf{e}}_\lambda$ with $\lambda = 1, 2$ are perpendicular to $(\mathbf{k}+\mathbf{G})$, and $h_{\mathbf{G},\lambda}$ is the Fourier expansion component of the magnetic fields.

The Fourier coefficient $\epsilon(\mathbf{G})$ is given by

$$\epsilon(\mathbf{G}) = \frac{1}{A_{cell}} \int_{cell} \epsilon(\mathbf{r}) e^{-i\mathbf{G}\cdot\mathbf{r}} d\mathbf{r}, \quad (4.4)$$

where the integration is performed over the unit cell. Here, the filling factor f , which is the ratio of the areas A_{scat} of dielectric scatterers in a unit cell to the area A_{cell} of a unit cell of square lattice, is

$$f = \frac{l^2}{a^2} \left(1 - \frac{\pi\beta^2}{4} \right). \quad (4.5)$$

For the proposed PC, $\epsilon(\mathbf{G})$ is evaluated by

$$\epsilon(\mathbf{G}) = \begin{cases} f\epsilon_a + (1-f)\epsilon_b & \text{for } \mathbf{G} = 0, \\ (\epsilon_a - \epsilon_b)S(\mathbf{G}) & \text{for } \mathbf{G} \neq 0, \end{cases} \quad (4.6)$$

We assume that there is a shift \mathbf{s} of the drilled circular rod with respect to the center of the unit cell, that is $\mathbf{s} = s(\hat{\mathbf{x}} \sin \gamma + \hat{\mathbf{y}} \cos \gamma)$, where γ is the span angle of the displacement vector with respect to the y -axis. The structural factor $S(\mathbf{G})$ is then given by

$$S(\mathbf{G}) = S_1(\mathbf{G}) - e^{-i\mathbf{G}\cdot\mathbf{s}} S_2(\mathbf{G}), \quad (4.7)$$

where

$$S_1(\mathbf{G}) = \left(\frac{l^2}{a^2} \right) Sinc \left(\frac{G_x l}{2} \right) Sinc \left(\frac{G_y l}{2} \right) \quad (4.8)$$

with $Sinc(x) = \sin x/x$ and

$$S_2(\mathbf{G}) = \left(\frac{l^2}{a^2} \right) \frac{\pi\beta^2}{2} \frac{J_1(Ga)}{Ga}, \quad (4.9)$$

where $J_1(x)$ is the Bessel function of the first kind, and $G = |\mathbf{G}|$.

The band structures are then determined from solving the following equation

$$\sum_{\mathbf{G}'} A(\mathbf{k} + \mathbf{G}, \mathbf{k} + \mathbf{G}') H(\mathbf{G}') = \omega^2 H(\mathbf{G}) \quad (4.10)$$

with

$$A(\mathbf{K}, \mathbf{K}') = \begin{cases} |\mathbf{K}| |\mathbf{K}'| \epsilon^{-1}(\mathbf{K} - \mathbf{K}') & \text{for the E-polarization state,} \\ \mathbf{K} \cdot \mathbf{K}' \epsilon^{-1}(\mathbf{K} - \mathbf{K}') & \text{for the H-polarization state,} \end{cases} \quad (4.11)$$

where $\mathbf{K} = \mathbf{k} + \mathbf{G}$, $\mathbf{K}' = \mathbf{k} + \mathbf{G}'$. $\epsilon^{-1}(\mathbf{K} - \mathbf{K}') = \epsilon^{-1}(\mathbf{G} - \mathbf{G}')$ can be computed from solving the following equation:

$$\sum_{\mathbf{G}''} \epsilon^{-1}(\mathbf{G} - \mathbf{G}'') \epsilon(\mathbf{G}'' - \mathbf{G}') = \delta_{\mathbf{G}\mathbf{G}'}. \quad (4.12)$$

4.3 Results and discussion

All our calculations have been performed for $\epsilon_a = \epsilon = 13.6$ appropriate for gallium arsenide (GaAs), and $\epsilon_b = 1.0$ in air. GaAs has been used because this material exhibits fascinating optical properties in the infrared region and is representative of many semiconductors. The design of this structure has many degrees of freedom which can be used to optimize the size of the gap, depending on the materials used in the fabrication. Although GaAs is used in this example, they can be replaced by other material with a different index contrast. 1521 plane waves in the Fourier expansion are used to calculate PBGs for the $E(H)$ -polarization. First, the PBG structures and the corresponding density of states (DOS) of an air hole drilled into the center of each square dielectric rod in each unit cell are calculated, as shown in Figure 3.2(a). The parameters in this figure are chosen as $a/l=1.63$,

$\beta=0.35$ (corresponding to filling factor $f = 0.34017$) and $s = 0$. The solid (dotted) curves correspond to the $E(H)$ -polarization. It is shown that there are four PBGs for the E -polarization and two PBGs for the H -polarization. However, overlap of PBG for E - and H -polarization does not exist. Along the left-hand and right-hand margin of this figure the density of photonic states in arbitrary units were plotted. The eigenfrequencies for 6400 uniformly spaced values of \mathbf{k} vectors inside the first Brillouin zone were calculated. In Figure 3.2(b), the calculated result for $s = 0.11a$ and $\gamma = 45^\circ$ is illustrated. The other parameters are the same as those quoted in Figure 3.2(a). A complete PBG with a gapwidth of $\Delta\omega = 0.0415(2\pi c/a)$, and a central value, $\omega_g = 0.66335(2\pi c/a)$, which is in the region of overlap of E_8 and H_6 band gaps, is found. E_i and H_i denotes the gaps that appear between the i th and $(i + 1)$ th bands, for the corresponding polarization. In the spectral range of this complete bandgap neither E -polarized nor H -polarized photonic states exist (DOS=0). Notably, modifying the position of circular hole in the square dielectric rod in air seems to lower the frequency of the ninth E -polarization band and the fifth and sixth H -polarization bands at the \mathbf{M} (\mathbf{M}') point of the Brillouin zone that depicted in Figure 3.2(a), then the overlap of E_8 and H_6 band gaps occurs. This result can be understood to be due to the fact that reducing the symmetry of the dielectric distribution in the square rod. Apparently, the band structure in Figure 3.2(b) also exhibits very gently sloped bands near the complete PBG's edge. Thus, a sharp peak of density of states can be observed due to the flat band. Since the group velocity v_g of the modes given by the slope of the dispersion curves, $\partial\omega/\partial k$, is expected to be zero or very small and correspondingly, the optical path is expected to be long. Comparison between Figure 3.2(a) and 3.2(b) shows that the zero or small group velocities are observed in a broad region of \mathbf{k} -space as the increase of s . The fifth, sixth H -polarization bands and the ninth E -polarization band become

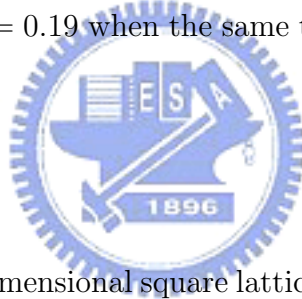
more restricted to a narrow spectral region, thus, light waves become more localized as s increased. There are \mathbf{k} points between the M–U direction at which the sixth H -polarization and the eighth E -polarization bands are almost flat. That is to say, group velocities of both mode approach to zero. Generally, the zero group velocity appears near photonic band edge only for E - or H -polarization. In this case, the zero group velocity is allowed for both E - and H -polarization simultaneously.

An additional plot in Figure 3.3 provides more information on PCs. The PBG map as the relative shift s of the drilled rod for three different directions of (a) $\gamma = 0^\circ$, (b) $\gamma = 22.5^\circ$ and (c) $\gamma = 45^\circ$. The other parameters are as those in Figure 3.2(a). Only the first ten-bands are involved in this map for both E - and H -polarizations. Notably, for a given γ , the varying region of s is limited, i.e., only from zero to a certain value at which the outermost edge of the internal air circular rod just touches the outermost edge of the square dielectric rod at the lattice. The gap map for E -polarization shown in Figure 3.3(a) exhibits six large gaps. We note that E_1 and E_3 gaps occur over the range of the shift s within $[0, 0.199]a$. Moreover, a remarkable gaps H_6 occur in the same range for H -polarization. Some other gaps only lie in the intermediate range of s . There are three complete PBG's in this configuration due to the overlap of E_8 with H_5 ; E_7 with H_5 , and E_8 with H_6 gaps. Comparison among Figure 3.3(a), 3.3(b) and 3.3(c) shows that gap widths strongly depend on the shift of the air hole position. The most important result is the appearance of the overlap of E_8 with H_6 gap, which occurs for s in the region $[0.015, 0.18]a$ for $\gamma = 0^\circ$, $[0.016, 0.215]a$ for $\gamma = 22.5^\circ$ and $[0.014, 0.253]a$ for $\gamma = 45^\circ$, in turn. One would see this complete PBG to get larger width as the γ is increased. This complete PBG is always bounded at the top by the upper boundary of the E_8 gap. The lower boundary switches from H_6 to E_8 gap both in Figure 3.3(a) and 3.3(b). Furthermore, its bottom side shown in Figure 3.3(c) is wholly bounded by

the lower boundary of the E_8 gap. In fact, since E and H polarized modes are decoupled and are governed by different equations for a right choice of s and γ .

We have also examined the case of an air hole drilled at the center of each square dielectric rod in air. Figure 3.4 shows the PBG map as a function of the parameter β for filling factor $f=0.34017$. Several gaps in both E - and H -polarization appear and disappear as β is varied. We should note here that one H -polarization and four E -polarization gaps exhibit near $\beta = 0$ when air hole is absent. One large complete PBG occurs due to the overlap of H_6 and E_8 gaps. This complete PBG starts near $\beta = 0$ and ends at about 0.34. The gap size $\Delta\omega$ reaches the maximum value $0.0427(2\pi c/a)$ at about $\beta = 0.19$ when the same total filling factor $f = 0.34017$ and $a/l = 1.69$.

4.4 Conclusion



This study proposes two-dimensional square lattices of square cross-section dielectric rods in air, designed with an air hole drilled into each square rod. By adjusting the shift of the hole position in the square rod in each unit cell, the dielectric distribution of the square rod will be modified. The calculations show that the photonic crystal structure proposed here has a sizable complete band gap and exhibits very gently sloped bands near such gap edge, which resulting in a sharp peak of density of state. In addition, the zero or small group velocities are observed in a broad region of \mathbf{k} -space. This property can be utilized for optical gain enhancement or low-threshold lasing.

Acknowledgements

The authors would like to thank the National Science Council of the Republic of China, Taiwan (Contract No. NSC 93-2112-M-009-010) and the Electrophysics De-

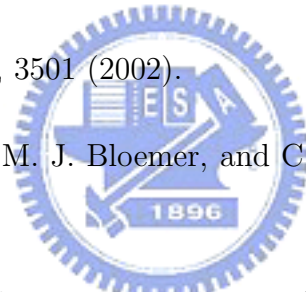
partment, National Chiao Tung University, Taiwan, for their support. We acknowledge Ben-Yuan Gu for discussions.



Bibliography

- [1] E. Yablonovitch, Phys. Rev. Lett. **58**, 2059 (1987).
- [2] S. John, Phys. Rev. Lett. **58**, 2486 (1987).
- [3] B. Temelkuran, M. Bayindir, E. Ozbay, R. Biswas, M. M. Sigalas, G. Tuttle, and K. M. Ho, J. Appl. Phys. **87**, 603 (2000).
- [4] O. Painter, R. K. Lee, A. Scherer, A. Yariv, J. D. O'Brien, P. D. Dapkus, and I. Kim, Science **284**, 1819 (1999).
- [5] K. Busch and S. John, Phys. Rev. Lett. **83**, 967 (1999).
- [6] C. M. Anderson and K. P. Giapis, Phys. Rev. B **56**, 7313 (1997).
- [7] Z. Y. Li, B. Y. Gu, and G. Z. Yang, Phys. Rev. Lett. **81**, 2574 (1998); Eur. Phys. J. B **11**, 65 (1999).
- [8] X. H. Wang, B.Y. Gu, Z. Y. Li, and G. Z. Yang, Phys. Rev. B **60**, 11417 (1999).
- [9] C. Goffaux and J. P. Vigneron, Phys. Rev. B **64**, 075118 (2001).
- [10] N. Susa, J. Appl. Phys. **91**, 3501 (2002).
- [11] R. D. Meade, A. M. Rappe, K. D. Brommer, and J. D. Joannopoulos, J. Opt. Soc. Am. B **10**, 328 (1993).

- [12] Min Qiu and Sailing He, *J. Opt. Soc. Am. B* **17**, 1027 (2000).
- [13] X. D. Zhang, Z. Q. Zhang, L. M. Li, C. Jin, D. Zhang, B. Man, and B. Cheng, *Phys. Rev. B* **61**, 1892 (2000).
- [14] Z. Sun and T. Stirner, *Physica B* **322**, 323 (2002).
- [15] C. M. Anderson and K. P. Giapis, *Phys. Rev. Lett.* **77**, 2949 (1996).
- [16] K. M. Ho, C. T. Chan and C. M. Soukoulis, *Phys. Rev. Lett.* **65**, 3152 (1990)
- [17] Pierr R. Villeneuve and Michel Pich'e, *Phys. Rev. B* **46**, 4696 (1992).
- [18] N. Susa, *J. Appl. Phys.* **91**, 3501 (2002).
- [19] J. P. Dowling, M. Scalora, M. J. Bloemer, and C. M. Bowden, *J. Appl. Phys.* **75**, 1896 (1994).
- [20] S. Nojima, *Jpn. J. Appl. Phys., Part 2* **37**, L565 (1998).
- [21] K. Sakoda, K. Ohtaka, and T. Ueta, *J. Appl. Phys.* **4**, 481 (1999).



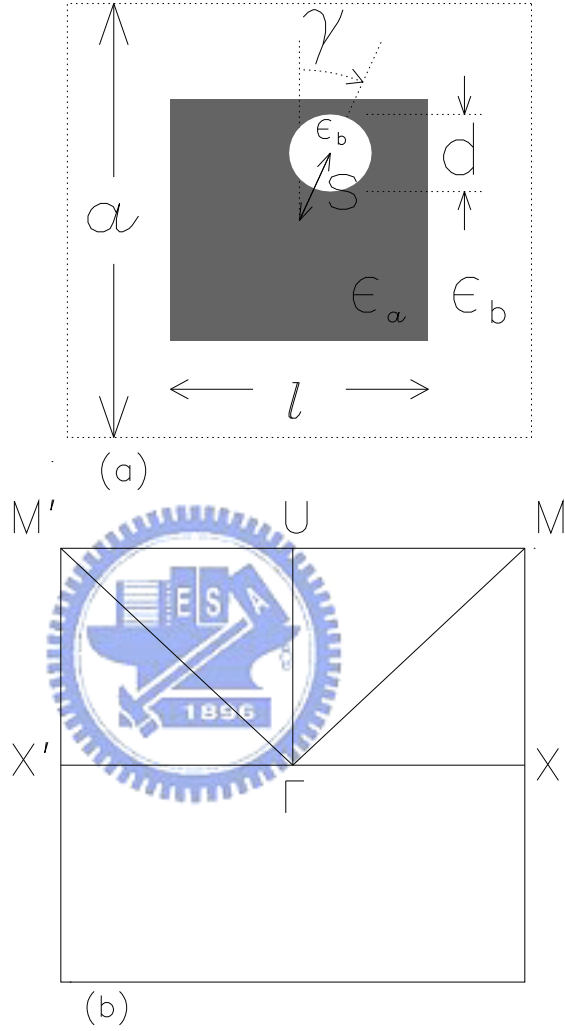
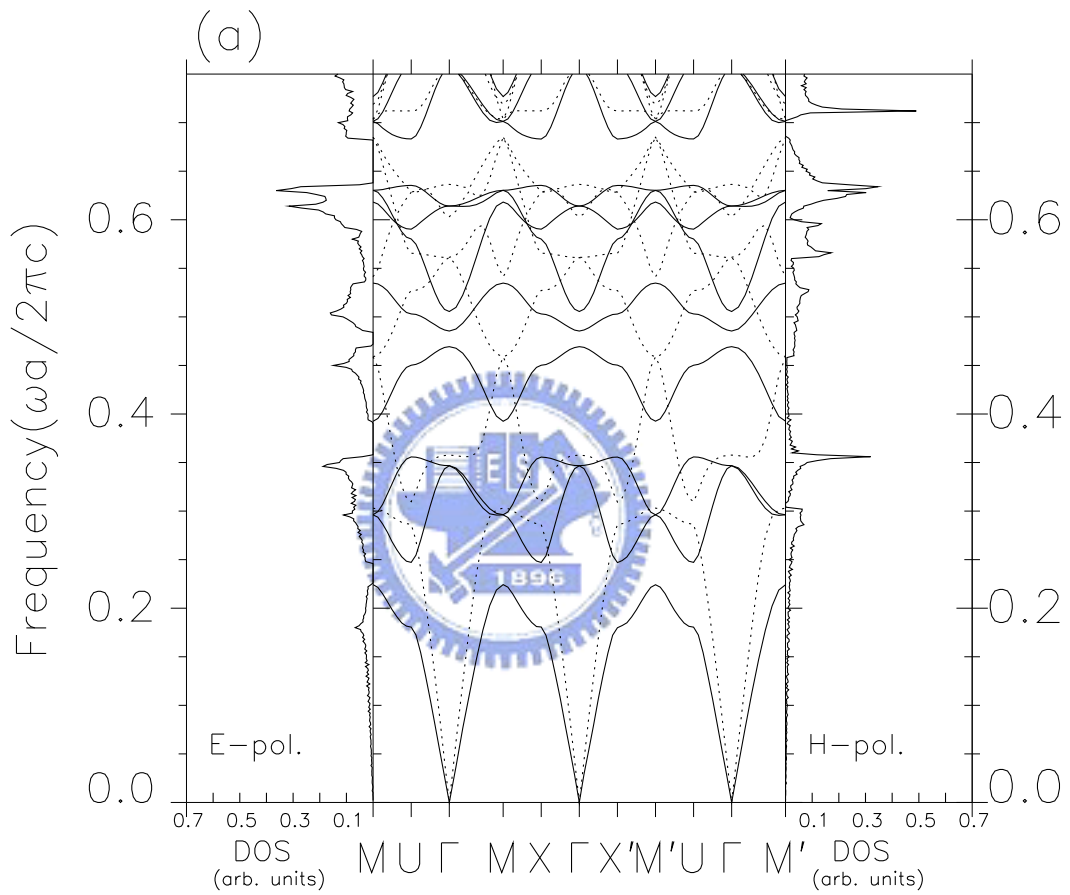
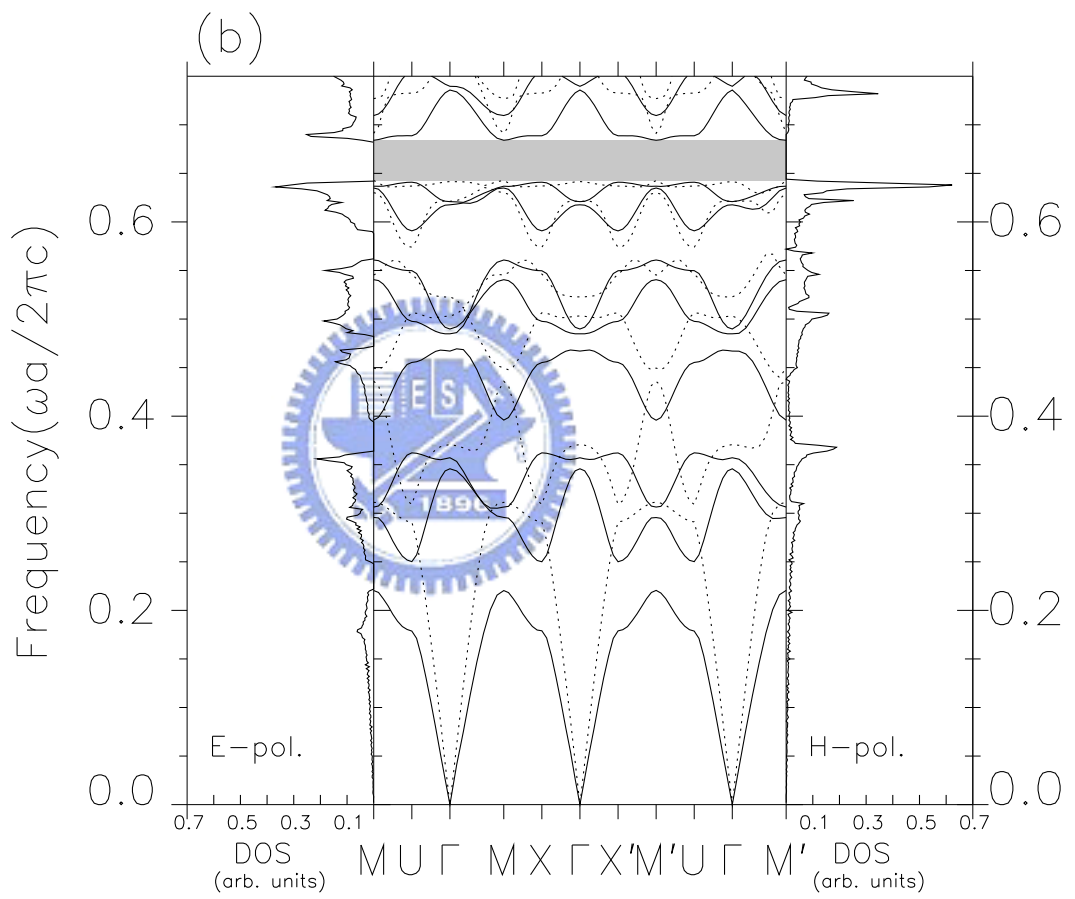


Figure 4.1: (a) Schematic diagram of proposed photonic crystals. The square dielectric rods with a side-length of l and dielectric ϵ_a are placed in air background with $\epsilon_b = 1.0$ at the center of a 2D square lattice with a lattice constant, a , in the xy -plane. Another circular rod with $\epsilon_b = 1.0$ and diameter d is drilled into square rod in each unit cell. We denote $\beta = d/l$ for convenience. We assume that there is a shift \mathbf{s} of the drilled circular rod with respect to the center of the unit cell, that is $\mathbf{s} = s(\hat{\mathbf{x}} \sin \gamma + \hat{\mathbf{y}} \cos \gamma)$, where γ is the span angle of the displacement vector with respect to the y -axis. (b) the Brillouin zone with symmetry points, Γ , \mathbf{X} , \mathbf{M} , \mathbf{U} , \mathbf{M}' and \mathbf{X}' .



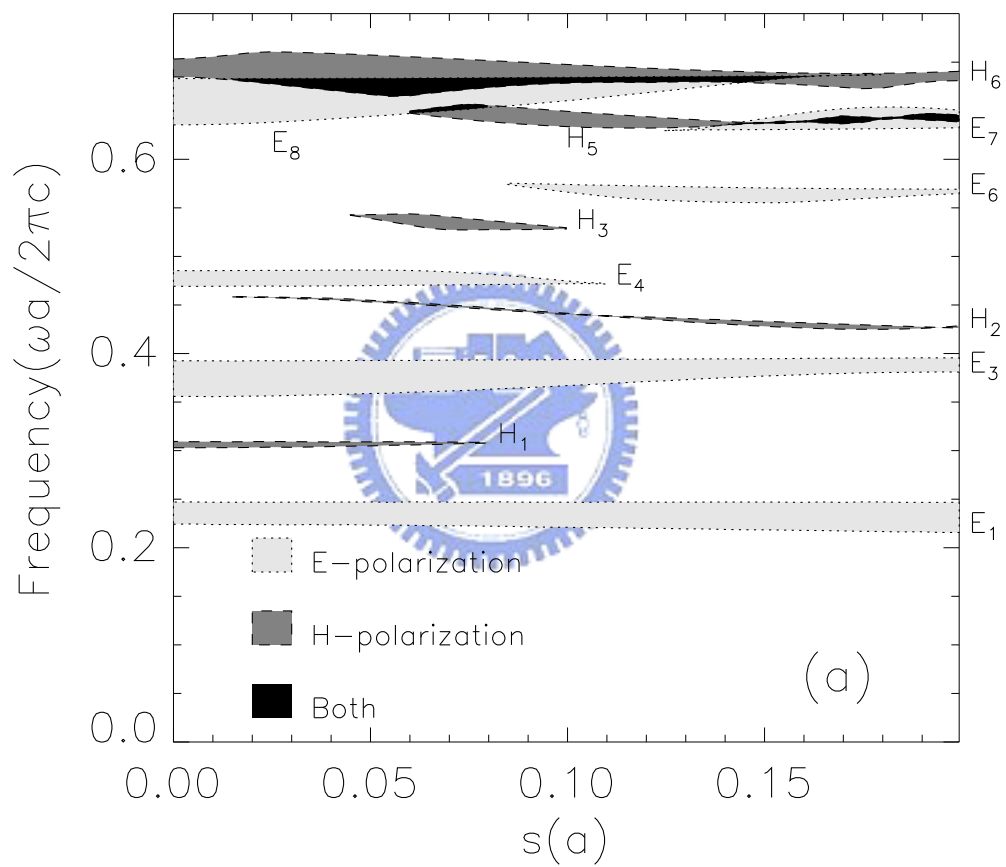
(a) $s=0, \gamma = 45^\circ$

Figure 4.2: Photonic band structures and the corresponding density of states (DOS) for two structures. The parameters in this figure are chosen as $a/l=1.63$, $\beta=0.35$ (corresponding to filling factor $f = 0.34017$). The solid and dotted curves correspond to the E - and H -polarizations, respectively. The shadow area marks the complete gap region.



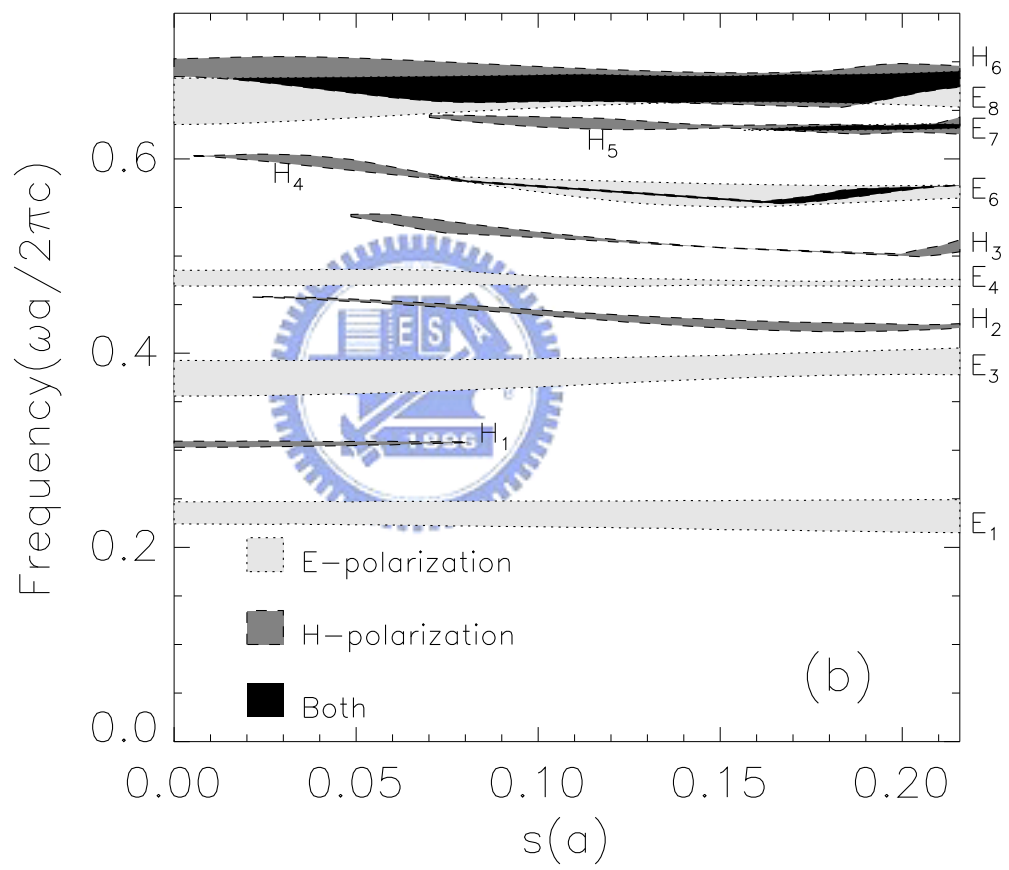
(b) $s=0.11, \gamma = 45^\circ$

Figure 4.2: (con't)



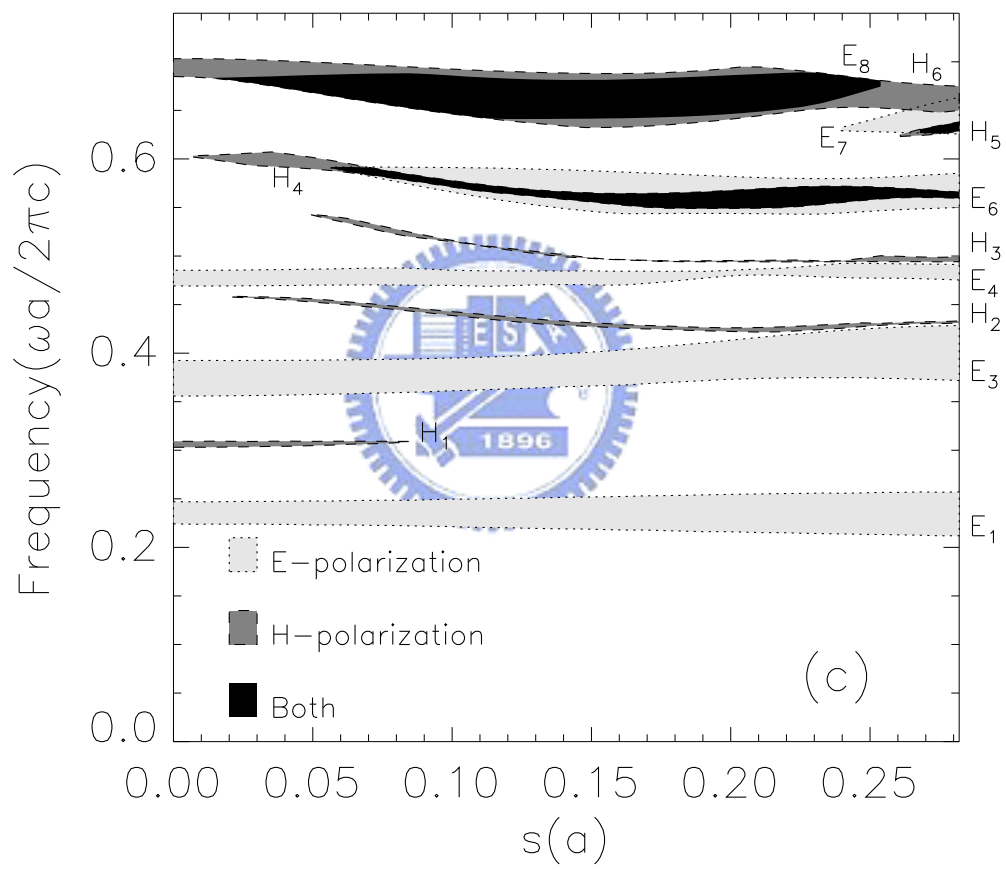
(a) $\gamma = 0^\circ$

Figure 4.3: The PBG map as the the relative shift s of the drilled rod for three different directions($\gamma = 0^\circ, 22.5^\circ$, and 45°). The other parameters are as those quoted in Figure 4.2(a). The black area denotes the complete band gaps.



(b) $\gamma = 22.5^\circ$

Figure 4.3: (con't)



(b) $\gamma = 45^\circ$

Figure 4.3: (con't)

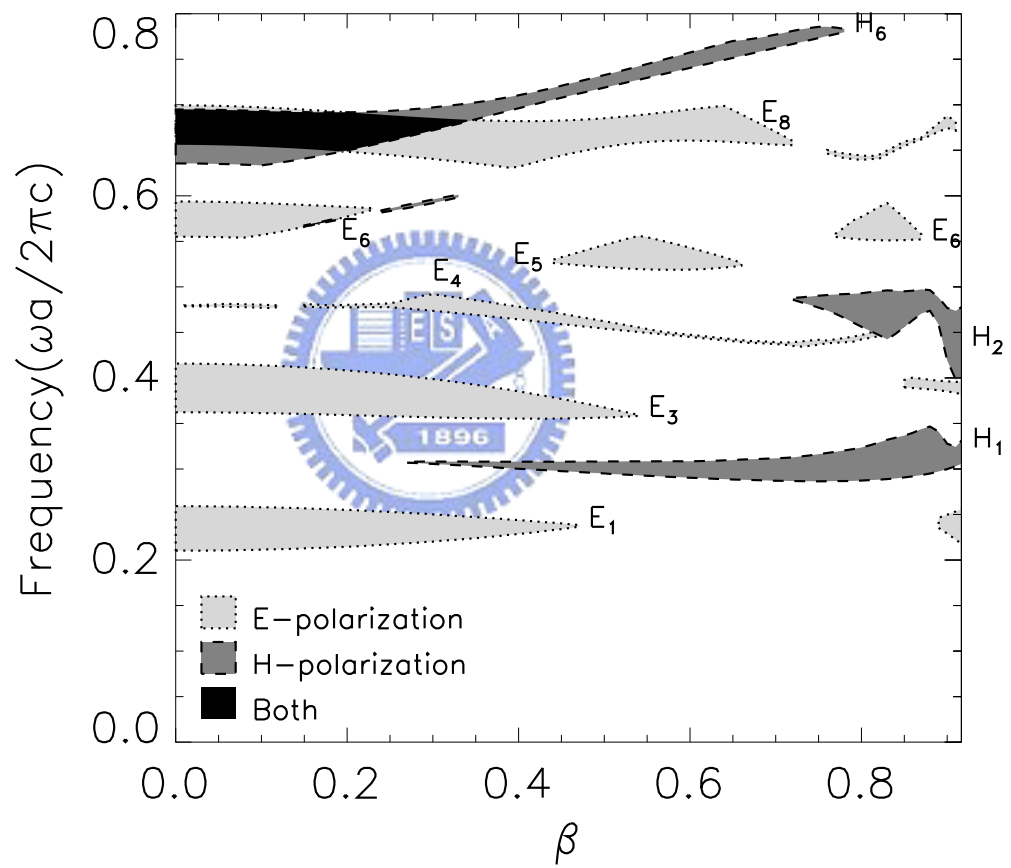
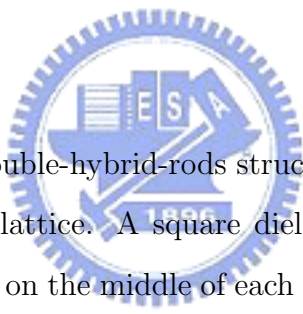


Figure 4.4: The PBG map as a function of the parameter β for filling factor $f=0.34017$, $s=0$.



Chapter 5

Photonic band gaps in a two-dimensional photonic crystal with veins



This study proposes the double-hybrid-rods structure of two-dimensional (2D) photonic crystals of a square lattice. A square dielectric rod connected with slender rectangular dielectric veins on the middle of each side of dielectric square rod. Some specific modes are found to be sensitive to certain structural parameters, such as the length, width the dielectric constant and the shift of the position of the veins, etc., and giving rise to a new complete PBG at lower index bands. These results could be understood by the use of band structure point of view. In particular, by carefully adjusting the structural parameters, the band structure of the photonic crystal can be substantially engineered to achieve large bandgaps.

5.1 Introduction

Since the pioneering works of Yablonovitch and John in 1987 [1, 2], photonic crystals (PCs) are now a fascinating issue of research. PCs are of artificial materials having the periodical modulation of dielectric structures in space and there exist photonic

band gaps (PBGs) in which the propagation of electromagnetic (EM) waves in any propagating direction and polarization state is inhibited. A PBG can lead to various peculiar physical phenomena [3] and providing potential applications [4, 5, 6]. The wider a PBG is, the greater the forbidden region of the frequency spectrum. Thus, the search for photonic crystals that possess wider band gaps is an important issue. Various methods for creating large PBGs or in increasing an existing PBG by altering the dielectric constant $\epsilon(\mathbf{r})$ within a unit cell, have been proposed. These methods include rotating the lattices [7], using anisotropic dielectric materials [8], rotating the noncircular rods [9, 10, 11], and modifying the permittivity distribution in a unit cell [12, 13]. Some research groups have successfully fabricated PCs by holographic lithography [14] that can yield two- and three-dimensional (3D) complete PBGs [15, 16]. Several PC structures consisting of rods, spheres or cubes linked by dielectric veins as a completely closed 2D or 3D structures would give a large complete band gap [17, 18, 19]. In addition, the search for 3D PBG structures based on a non-close-packed face-centered cubic lattice of spherical shells connected by thin cylindrical tubes was proposed [20].

This study proposes the double-hybrid-rods structure of 2D PCs by placing slender rectangular dielectric veins on the middle of each side of square rod in each unit cell. There exists one complete photonic band gap (PBG) in higher frequency band of the prototype square lattices with only square rods [21]. When extending the dielectric veins, some specific modes are found to be sensitive to certain structural parameters, such as the length, the dielectric constant and the shift of the position of the veins, etc. Then, this PBG disappears and for a proper value of vein length another complete PBG at lower index bands opens. The variation of bands near the PBG's boundaries can be interpreted by considering the effects of Mie scattering and interference of EM waves to be significantly modified and enhanced when

introducing the extra dielectric veins into each unit cell. In this study, we want to understand these effects by the use of band structure point of view. When the length of veins increases, the wavelength of resonance mode would increase too. That is the resonance frequency would decrease. Generally, the EM-field distributions bear strong resemblances to electronic orbitals and, like their electronic counterparts, could lead to bonding and anti-bonding interactions between neighboring rods [22]. The relevance (the strength) of the interactions among scattering rods is attributed to the field distribution characteristics. In terms of band structure terminology, the band center of the band reflects the resonance frequency and the band width reflects the relevance (the strength) of the interactions or the EM-field distribution characteristics among scattering rods. In this PC, the structural parameters (the length, width, dielectric constant and the shift of the position of the veins) are properly chosen so that the photonic band structure can be optimized. Thus, it will prove useful in designing PBGs of a variety of photonic crystals.

5.2 Theory

Figure 5.1 displays the schematic diagram of the proposed PC structure. The square dielectric rod with a side-length of l and dielectric ϵ_a is placed in air background with $\epsilon_b = 1.0$ at the center of a 2D square lattice with a lattice constant, a , in the xy -plane. Another dielectric vein with $\epsilon = \epsilon_v$, length h and width d is placed in each unit cell on the middle of each side of the dielectric square rod, forming composite lattices. The term δ is the crevice between the edges of square rod and vein. The shift length s is thus given by $s = \delta + h$.

In our calculations, the band structures of the PCs were calculated using the plane-wave expansion method, described in detail in the literature [23, 24, 25]. The electromagnetic (EM) fields with the E/H -polarization (in-pane magnetic/electric

fields) in the 2D PC are governed by Maxwell's equations

$$\left\{ \nabla \times \frac{1}{\epsilon(\mathbf{r})} \nabla \times \right\} \mathbf{H}(\mathbf{r}) = \frac{\omega^2}{c^2} \mathbf{H}(\mathbf{r}), \quad (5.1)$$

where $\mathbf{H}(\mathbf{r})$ denotes the magnetic fields; ω the angular frequency; c the speed of light in vacuum, and $\epsilon(\mathbf{r})$ the periodically modulated dielectric function. The magnetic fields and the dielectric function can be expanded in terms of Fourier series as

$$\mathbf{H}(\mathbf{r}) = \sum_{\mathbf{G}} \sum_{\lambda=1}^2 h_{\mathbf{G},\lambda} \hat{\mathbf{e}}_{\lambda} e^{i(\mathbf{k}+\mathbf{G})\cdot\mathbf{r}}, \quad (5.2)$$

$$\epsilon(\mathbf{r}) = \sum_{\mathbf{G}} \epsilon(\mathbf{G}) e^{i\mathbf{G}\cdot\mathbf{r}}, \quad (5.3)$$

where \mathbf{k} is the Bloch wave vector in the first Brillouin zone (FBZ), and \mathbf{G} is the 2D reciprocal lattice vector. The polarization unit vectors $\hat{\mathbf{e}}_{\lambda}$ with $\lambda = 1, 2$ are perpendicular to $(\mathbf{k}+\mathbf{G})$ and $h_{\mathbf{G},\lambda}$ is the Fourier expansion component of the magnetic fields. The Fourier coefficient $\epsilon(\mathbf{G})$ is given by

$$\epsilon(\mathbf{G}) = \frac{1}{A_{cell}} \int_{cell} \epsilon(\mathbf{r}) e^{-i\mathbf{G}\cdot\mathbf{r}} d\mathbf{r}, \quad (5.4)$$

where the integration is performed over the unit cell. For structures with a unit cell including veins centered at \mathbf{u}_i , the corresponding dielectric constant is expressed as

$$\epsilon^{-1}(\mathbf{r}) = \epsilon_b^{-1} + (\epsilon_a^{-1} - \epsilon_b^{-1}) \sum_{\mathbf{R}} P_{sq}(\mathbf{r} - \mathbf{R}) + (\epsilon_v^{-1} - \epsilon_b^{-1}) \sum_i \sum_{\mathbf{R}} P_v^{(i)}(\mathbf{r} - \mathbf{u}_i - \mathbf{R}), \quad (5.5)$$

where P_{sq} and P_v describe the probability of the square rod and veins, respectively, and \mathbf{R} denotes the translation vector of the Bravais lattice, and

$$P_{sq}(\mathbf{r}) = \begin{cases} 1 & \text{for } \mathbf{r} \in \mathbf{R}_{sq}, \\ 0 & \text{for } \mathbf{r} \notin \mathbf{R}_{sq}, \end{cases} \quad (5.6)$$

$$P_v^{(i)}(\mathbf{r}) = \begin{cases} 1 & \text{for } \mathbf{r} - \mathbf{u}_i \in \mathbf{R}_v^{(i)}, \\ 0 & \text{for } \mathbf{r} - \mathbf{u}_i \notin \mathbf{R}_v^{(i)}, \end{cases} \quad (5.7)$$

where \mathbf{R}_{sq} and $\mathbf{R}_v^{(i)}$ are the region in the xy -plane defined by the cross-section of the square rod and the i th vein, respectively. The Fourier transforms of $\epsilon^{-1}(\mathbf{r})$ are given by

$$\epsilon^{-1}(\mathbf{G}) = \epsilon_b^{-1} \delta_{\mathbf{G}0} + (\epsilon_a^{-1} - \epsilon_b^{-1}) S_1(\mathbf{G}) + (\epsilon_v^{-1} - \epsilon_b^{-1}) \sum_i S_2^{(i)}(\mathbf{G}) \cdot e^{-i\mathbf{G} \cdot \mathbf{u}_i} \quad (5.8)$$

The structural factor $S_1(\mathbf{G})$ and $S_2^{(i)}(\mathbf{G})$ are then given by

$$S_1(\mathbf{G}) = \left(\frac{l^2}{a^2} \right) \text{Sinc} \left(\frac{G_x l}{2} \right) \text{Sinc} \left(\frac{G_y l}{2} \right) \quad (5.9)$$

with $\text{Sinc}(x) = \sin x/x$, and

$$S_2^{(i)}(\mathbf{G}) = \left(\frac{l_x^{(i)} l_y^{(i)}}{a^2} \right) \text{Sinc} \left(\frac{G_x l_x^{(i)}}{2} \right) \text{Sinc} \left(\frac{G_y l_y^{(i)}}{2} \right), \quad (5.10)$$

where $l_x^{(i)}$ and $l_y^{(i)}$ are the side-lengths of the i th vein in the x - and y -axes respectively.

The band structures are then determined from solving the following equation

$$\sum_{\mathbf{G}'} A(\mathbf{k} + \mathbf{G}, \mathbf{k} + \mathbf{G}') H(\mathbf{G}') = \omega^2 H(\mathbf{G}) \quad (5.11)$$

with

$$A(\mathbf{K}, \mathbf{K}') = \begin{cases} |\mathbf{K}| |\mathbf{K}'| \epsilon^{-1}(\mathbf{K} - \mathbf{K}') & \text{for the E-polarization state,} \\ \mathbf{K} \cdot \mathbf{K}' \epsilon^{-1}(\mathbf{K} - \mathbf{K}') & \text{for the H-polarization state,} \end{cases} \quad (5.12)$$

where $\mathbf{K} = \mathbf{k} + \mathbf{G}$, $\mathbf{K}' = \mathbf{k} + \mathbf{G}'$. $\epsilon^{-1}(\mathbf{K} - \mathbf{K}') = \epsilon^{-1}(\mathbf{G} - \mathbf{G}')$ can be computed by solving the following equation

$$\sum_{\mathbf{G}''} \epsilon^{-1}(\mathbf{G} - \mathbf{G}'') \epsilon(\mathbf{G}'' - \mathbf{G}') = \delta_{\mathbf{G}\mathbf{G}'}. \quad (5.13)$$

5.3 Results and discussion

The following parameters were used in the calculations: $\epsilon_a = 11.4$ appropriate for gallium arsenide (GaAs) at wavelength $\lambda \approx 1.5\mu m$ and $\epsilon_b = 1.0$ in air. The Fourier expansion with 625 plane waves was used to calculate the PBGs for the E/H -polarization (in-plane magnetic/electric fields) and the convergence accuracy for the several lowest photonic bands was better than 1%. This study explored the influence of the slender dielectric veins on the 2D complete PBG. As an example, three cases of the dielectric constant of veins ϵ_v were considered, with $\epsilon_v = 6, 11.4$ and 16. First, the PBG structures of the prototype square lattices with only square rods were calculated, as shown in Fig. 5.2(a), the side-length of square rod fixed at $l = 0.57a$. The solid (dotted) curves correspond to the $E(H)$ -polarization. The diagram clearly shows that a complete PBG exists at higher index bands resulting from the superposition of the $E8 - 9$ and $H6 - 7$ gaps. If the square rods are linked with dielectric veins at each middle side of the square rods, the influences of the length h of the dielectric vein on the PBGs is now investigated. The calculated band structures for three choices of the dielectric constant of veins are demonstrated in Fig. 5.2(b) as $\epsilon_v = 6$, (c) $\epsilon_v = 11.4$ and (d) $\epsilon_v = 16$, respectively. The dielectric vein has a width of $d = 0.08a$, and a crevice of $\delta=0$ between the edges of vein and square rod.

We find that the higher complete PBG shown in Fig. 5.2(a) disappears in Figs. 5.2(b)–(d) and another complete PBG at lower index bands opens while the length of veins continues to increase. For $\epsilon_v=6$ the overlap of the $H2 - 3$ band gap and the far wider $E3-4$ band gaps creates a complete PBG, with the band edges lying at the \mathbf{M} symmetry point. On increasing the vein length substantially lowers the frequency of \mathbf{M} symmetry point of $H2$ band. The same happens when ϵ_v increases from 6 to

16. Consequently, the \mathbf{M} point is lower than the $\mathbf{\Gamma}$ point somewhere for the case of $\epsilon_v = 11.4$ and $\epsilon_v = 16$, and then this complete PBG is bounded on the lower side by the $\mathbf{\Gamma}$ point of $H2$ band. On the other hand, the top edge of this complete PBG remains unchanged and lies at \mathbf{M} point of $H3$ band. When it reaches $\epsilon_v=16$ and $h = 0.19a$, the $\mathbf{\Gamma}$ point of $E4$ band is below than the \mathbf{M} point of $H3$ band; thus the complete PBG is bounded on the upper side by the $\mathbf{\Gamma}$ point of $E4$ band. Comparison with the variation of complete PBG boundaries of Figs. 5.2 (b)–(d) shows that the lower boundary first shifts downwards, then remains unmodified. While the upper boundary first remains unchanged, then moves downwards. It is clearly seen that the largest complete PBG occurs at $h = 0.215a$, namely, the veins are fully connected at the lattice unit cell boundary for the case $\epsilon_v = 6$. However the complete PBG reaches its maximum width with midgap frequency $\omega_g = 0.42385(2\pi c/a)$ and the gap size $\Delta\omega = 0.0557(2\pi c/a)$ at the intermediate value of $h = 0.19a$ for the case $\epsilon_v=11.4$, and then remains unchanged where $h = 0.215a$. Here c is the light speed in vacuum. In particular, for $\epsilon_v = 16$ increasing h from $0.155a$ to $0.19a$, we find that both the lower and upper boundaries shift towards lower frequencies. The lower boundary of this complete PBG (i.e., the lower band edge of the H -polarized gap) moves a bit faster than the upper boundary (i.e., the upper band edge of the E -polarized gap); therefore, this complete PBG becomes wider. If h continues to increase and reaches $0.215a$, the complete PBG shrinks again.

What is the the key factor that leads to lower band edges at certain symmetry points and hence create a gap when the square dielectric rod is connected with slender dielectric veins? In order to clarify this issue, we calculate the spatial energy distribution for the corresponding states. Figures 5.3 (a)–(c) plot the spatial distributions of the electric field intensity $|E^2|$ within a unit cell of the PC at the \mathbf{M} point of (a) $H2$ band (or denoted by $H^{(2,M)}$) for $h=0$, (b) $H4$ band ($H^{(4,M)}$)

for $h = 0$, and (c) $H2$ band ($H^{(4,M)}$) for $\epsilon_v = 6$ and $h = 0.215a$. Here we mark the states in accordance with their ordering in frequency for the prophase, namely, the initial mode $H^{(n,M)}$ denotes the n th band for the H -polarization mode at \mathbf{M} point. When $h = 0$ it is apparent that the spatial $|E^2|$ distributions of the $H^{(2,M)}$ mode always concentrates inside the square rod, exhibiting a single parallelogram-like spot; on the contrary, the high index mode ($H^{(4,M)}$) possesses four spots close to the edges of square rod. While the square dielectric rod is connected with slender dielectric veins, the $|E^2|$ distribution of $H^{(4,M)}$ mode in the unit cell will spread out from square rod and concentrate inside the dielectric veins, then leads to the shift of frequencies of $H^{(4,M)}$ mode; consequently, the $H^{(4,M)}$ mode is below the $H^{(2,M)}$ and $H^{(3,M)}$ modes. Figure 5.3(c) plots the spatial $|E^2|$ distribution of $H^{(4,M)}$ mode (corresponding to the \mathbf{M} point of $H2$ band shown in the right panel of Fig. 5.2(b)). The energy distributions for other modes of certain symmetry points at band edges are also investigated, and the same phenomenon is observed. It is worth pointing out that field is more spreading out from the square rod owing to extending the vein length.

Figures 5.3(d) and 5.3(e) plot the band center (BC) and band width (BW) versus vein length for $H2$ band with $\epsilon_v=6, 11.4, 16$ and $E4$ band with $\epsilon_v=6$; the other parameters are as those in Fig. 5.2. The curves of BC for $H2$ band in Fig. 5.3(d) exhibit a plateau profile with slightly sloping at the beginning of curves, and then decline rapidly to their minimum values with $0.372, 0.356$ and $0.354(2\pi c/a)$ in turn at a certain h , depending on ϵ_v . The BC of $H2$ band falls off and so the complete PBG occurs (owing to $H^{(4,M)} < H^{(2,M)}$ (or $H^{(3,M)}$)). It can be understood here that the resonance frequency would decrease. Clearly, it is also seen that the curves exhibit another plateau profile at the end of curves (owing to $H^{(4,M)} < H^{(2,\Gamma)}$), except for the solid one with $\epsilon_v = 6$. In the same figure, the BC curves of $E4$ band

for $\epsilon_v = 16$ is shown. Notably, the BC curve of $E4$ band decline monotonically to its minimum value around $0.456(2\pi c/a)$ when dielectric veins are fully connected ($h = 0.215a$). The curves of BW for $H2$ band of $\epsilon_v=6, 11.4$ and 16 versus h are shown in Fig. 5.3(e). Apparently, all of the BW curves of $H2$ band exhibit a similar profile to the corresponding BC curves. However, they have same value of BW in the flat region at around $0.135(2\pi c/a)$ and $0.08(2\pi c/a)$, respectively. Its existence shows that the BW is insensitive to the extension of dielectric veins. However, the curves of BW with a sharp slant because the $H^{(4,M)}$ mode (i.e., the mode of top band edge of $H2$ band lying at \mathbf{M} point) is sensitive to the extension of dielectric veins. Besides, this means that field energy is more spreading out from the square rod. The BW curves of $E4$ band ($\epsilon_v = 16$) is also shown in this figure. Here, we have mostly paid attention to the curve of $E4$ band for which the complete PBG is bounded when $h > 0.155a$. It is clearly seen that the BW curve mount up soon from 0.046 to $0.076(2\pi c/a)$ in this region ($h > 0.155a$) because the $E^{(6,\Gamma)}$ mode (i.e., the mode of bottom band edge of $E4$ band lying at Γ point) downshifts to the lower frequency, and thus the field energy is more spreading out from the square rod.

The complete PBG is interesting issue for the extra veins formed on rods. An additional plot in Fig. 5.4 presents the PBG map as a function of length of veins, h . The parameters were chosen as: $\epsilon_a = 11.4, l = 0.57a, d = 0.08a, \delta=0$. Three cases of the dielectric constant of veins were demonstrated in (a) $\epsilon_v = 6.0$, (b) $\epsilon_v = 11.4$ and (c) $\epsilon_v = 16.0$, respectively. The gap map for E -polarization showing in Fig. 5.4(a) exhibits four large gaps. Significantly, the higher gap gradually shrinks as h increase; nevertheless, three other gaps remain almost unchanged. For H -polarization, two remarkable gaps in this structure. The first gap varies significantly as the vein length h increases toward $0.19a$, while the higher frequency gap width remains almost unchanged. As ϵ_v increases, in Fig. 5.4(b) and (c) the higher frequency gaps for E -

and H -polarized mode shrink. Figures 5.4(a), (b) and (c) each shows two complete PBGs. The complete PBGs for three different dielectric constants of veins found in the higher index bands are in the range $h = [0, 0.155]a$ for $\epsilon_v=6$; $h = [0, 0.079]a$ for $\epsilon_v=11.4$, and $h = [0, 0.059]a$ for $\epsilon_v=16$. Notably, the complete PBG spans a wider range of h for $\epsilon_v=6$, while the lower complete PBG results from the overlap between the first gap for H -polarized mode and the second gap for E -polarized mode. The figure shows that the lower complete PBGs are opened near: $h > 0.19a$ for $\epsilon_v=6.0$; $h > 0.155a$ for $\epsilon_v=11.4$, and $h > 0.145a$ for $\epsilon_v=16.0$. In these cases the complete PBG spans a wider range of h for $\epsilon_v=16$ than for $\epsilon_v = 6$, while the larger size of the complete PBG occurs for $\epsilon_v=11.4$ as shown in Fig. 5.4(b). When the vein lengthens up to about $h = 0.155a$, the bottom edge band of gap drops dramatically, but the top edge band remains almost unmodified, and consequently overlaps with the gap formed by E -polarization. Hence, the complete PBG increases in size rapidly and reaches its maximum value at $h = 0.19a$, and then remains almost unaltered until the vein is completely closed. Notably, for extending the length of veins substantially shrinks the complete PBG located at higher index bands, and for an appropriate vein length generates the new complete PBG at lower index bands. These results were dominated at higher index bands by E -polarization and at lower index bands by H -polarization through extending veins.

To get better insight into superior features of the hybrid structure, we investigate in detail the edge states of the complete PBGs. Here we will address the lower complete PBG that form the structure described above. In our case slender dielectric veins play a crucial role in opening the lower complete PBG, therefore we have performed two kind of evolutions. First, we have calculated the positions of edge states of the lower complete PBG for a fixed value of dielectric constant of veins. We examined the PBG structures with only square rods (i.e., $h=0$) to start with and

then varied the value of vein length, h . Second, we have investigated the positions of edge states of the lower complete PBG for three different h values as functions of the index of refraction of the slender dielectric veins. Figure 5.5(a) plots the evolution of edge states of the lower complete PBG as functions of the vein length, h , for $\epsilon_a = \epsilon_v = 11.4$. The other parameters are as those quoted in Fig. 5.2(c) (i.e., $\delta = 0$, $l = 0.57a$, $d = 0.08a$). According to the calculation of the photonic band structures, the edge states of the lower complete PBG are $H^{(2,M)}$, $H^{(3,M)}$, $H^{(4,M)}$ and $H^{(2,\Gamma)}$ modes. While, the $H^{(2,M)}$ and $H^{(3,M)}$ modes are degenerate in the region given by $h = [0, 0.215]a$. The frequencies of these two modes and $H^{(2,\Gamma)}$ remain almost unmodified at around 0.452 and $0.396(2\pi c/a)$ in turn. The frequencies of $H^{(4,M)}$ decrease significantly for increasing h . As the $H^{(4,M)}$ mode is below $H^{(2,M)}$ and $H^{(3,M)}$ modes for $h > 0.155a$, the lower complete PBG is opened, and its width increases quite sharply. In the region $h > 0.155a$, the complete PBG is bounded on the lower side by the $H^{(4,M)}$ boundary, and on its upper side by the $H^{(2,M)}$ or $H^{(3,M)}$ boundary. Furthermore, the vein length increases up to about $h = 0.19a$, the $H^{(4,M)}$ mode is again lower than $H^{(2,\Gamma)}$ mode. The complete PBG is thus bounded on the lower side by the $H^{(2,\Gamma)}$ boundary, and on its upper side by the $H^{(2,M)}$ ($H^{(3,M)}$) boundary in the region $h = [0.19, 0.215]a$. Notably, this complete PBG tends to increase in size dramatically in the region $h = [0.155, 0.19]a$, and reaches its maximum value at $h = 0.19a$. Then, the width of this complete PBG remain unmodified.

Figure 5.5(b) shows the positions of edge states of the complete PBGs as functions of the vein refractive index (in the range of $2.0 \leq n \leq 4.5$) for three different length of veins ($h = 0.155a$, $0.19a$, and $0.215a$). Apparently, the appearance of the complete PBGs exhibits a triangle-like outline for $h = 0.155a$ (indicated by the dark gray region) and two parallelogram-like outlines for $h = 0.19a$ (shaded by vertical

solid lines) and $h = 0.215a$ (indicated by light gray region). It is seen that the curves of $H^{(2,M)}$ (or $H^{(3,M)}$) and $H^{(2,\Gamma)}$ modes are flat in the region given by $n = [2.0, 4.5]$. However, The $H^{(4,M)}$, $E^{(4,\Gamma)}$ and $E^{(6,\Gamma)}$ modes decrease monotonously for increasing n . For $h = 0.155a$ the bottom edge state is always $H^{(4,M)}$ as $n = [3.43, 4.4]$, while the top edge states of this complete PBG are $H^{(2,M)}$ (or $H^{(3,M)}$) and $E^{(6,\Gamma)}$ modes as $n = [3.43, 4.03]$ and $n = [4.03, 4.4]$ in turn. The maximum width of this gap occurs at $n = 4.03$. For $h = 0.19a$ the complete PBG opens for $n = 2.4$ and closes above $n = 4.5$. When n is increased from 2.4, the top edge states are $H^{(2,M)}$ (or $H^{(3,M)}$) modes, while the bottom edge state is $H^{(4,M)}$ mode. As $n > 3.33$ the $H^{(4,M)}$ mode is below the $H^{(2,\Gamma)}$ mode, thus the complete PBG is bounded on the lower side by the $H^{(2,\Gamma)}$ mode. Meanwhile, the $E^{(6,\Gamma)}$ mode is below the $H^{(2,M)}$ ($H^{(3,M)}$) mode for $n > 3.65$, and hence the complete PBG is bounded on the upper side by the $E^{(6,\Gamma)}$ mode. For $h = 0.215a$, the edge states are the same as those for $h = 0.19a$. However, both left- and right-hand ends of the parallelogram-like outline are shifted toward lower n regime. In this case the complete PBG starts near $n = 2.13$ and ends at about $n = 4.29$. Notably, in the range of $n = [3.33, 3.65]$ for $h = 0.19a$ and $n = [2.78, 3.43]$ for $h = 0.215a$ the complete PBGs remain unchanged or vary a little. Moreover, there exists the equal maximum size of the complete PBG in the overlap region of $n = [3.33, 3.43]$ for $h = 0.19a$ and $0.215a$. This broad profile with large gap size manifests the large freedom in the choice of the structural parameters, which provide the benefit of the facilitated construction of the PCs with a large allowance of tolerance.

The effect of the veins width while veins are completely connected (i.e., $h = h_{max} = 0.215a$) is presented here. Figure 5.6 shows the PBG map as a function of the vein width, d , for (a) $\epsilon_v = 6.0$, (b) $\epsilon_v = 11.4$ and (c) $\epsilon_v = 16.0$. The other parameters are: $\epsilon_a = 11.4$, $l = 0.57a$, $\delta = 0$ and $d = 0.08a$. In these cases,

the 2D photonic structure exhibits two complete PBGs, the first at higher index bands around $d = 0$ and the second in the intermediate range of d . Comparing Fig. 5.6 (a), (b) and (c), both complete PBGs appear to span a shorter region of d as ϵ_v increases. Furthermore, in each case, the complete PBG closing at the higher index bands and opening again at lower index bands are almost at the same time. The complete PBGs exist when the vein width is in the region $d = [0, 0.04]a$ and $[0.01, 0.4]a$ for $\epsilon_v = 6.0$; $d = [0, 0.02]a$ and $[0.01, 0.155]a$ for $\epsilon_v = 11.4$, and $d = [0, 0.015]a$ and $[0.02, 0.098]a$ for $\epsilon_v = 16$. In each case, the complete PBGs reach their maximum value at $d = 0.11a$ for $\epsilon_v = 6.0$; $0.08a$ for $\epsilon_v = 11.4$, and $0.05a$ for $\epsilon_v = 16.0$, respectively. As ϵ_v increases, the position of the largest gap, $(\Delta\omega)_{max}$, shifts towards the smaller d region.

The influence of the shift s outward of the veins on dispersion spectrum is demonstrated by the plot of the dependence of $\Delta\omega/\omega_g$ (the gap width to midgap frequency ratio) as a function of s for different h values ($0.17a$, $0.18a$ and $0.2a$) as shown in Fig. 5.7 for (a) $\epsilon_v = 6.0$, (b) $\epsilon_v = 11.4$ and (c) $\epsilon_v = 16.0$, respectively. The other parameters were also chosen as $\epsilon_a = 11.4$, $\epsilon_b = 1$, $l = 0.57a$ and $d = 0.08a$. The shift length s , is given as the sum of δ and h . The varying region of s is limited, i.e., only from $s = h$ to $s = (a - l)/2$. All $\Delta\omega/\omega_g$ versus s curves appear to exhibit an asymmetric profile in a finite s range. Moreover, the right-hand end of the curve in a larger ϵ_v extends to a wider region of s . For each value of s , $(\Delta\omega/\omega_g)_{h=0.2a} > (\Delta\omega/\omega_g)_{h=0.18a} > (\Delta\omega/\omega_g)_{h=0.17a}$ when $\epsilon_v=6$; by contrast, $(\Delta\omega/\omega_g)_{h=0.17a} > (\Delta\omega/\omega_g)_{h=0.18a} > (\Delta\omega/\omega_g)_{h=0.2a}$ when $\epsilon_v=16$. In the lower- ϵ_v , the vein length of $h = 0.2a$ widens the PBG while shifting the vein towards the lattice unit cell boundary (see Fig. 5.7(a)). All the curves in Fig. 5.7(b) exhibit a plateau profile at the right-hand end of the curves spanning a finite region of s in which $\Delta\omega/\omega_g$ is insensitive to changes of s . However, the right-hand end of the curves in

Fig. 5.7(c) declines gradually. These results can be understood to be related to the effective dielectric constant of veins in the region of s . In fact, the complete PBGs can be optimized for a right choice of h and s for a given ϵ_v , since the complete PBGs are always governed by the vein dielectric constant and the vein length.

5.4 Conclusion

We have investigated in detail the photonic band structures of 2D square lattices of a square dielectric rod connected with slender rectangular dielectric veins on the middle of each side of dielectric square rod. Properly adjusting the length, width, dielectric constant and the shift of the position of veins in the unit cell enables the large complete PBG generated from the composite structure to be achieved. Additionally, the large freedom in the choice of the structural parameters which provide the benefit of the facilitated construction of the PCs with a large allowance of tolerance. The PCs can be easily fabricated and operated in the micro-wave region because a is in the order of microwave wavelengths — several mm or cm, and hence it is anticipated to be encouraged in applications to new microwave devices.

Acknowledgements

The authors would like to thank the National Science Council of the Republic of China, Taiwan (Contract No. NSC94-2112-M-009-001 and No. NSC 95-2119-M-009-029) and the Electrophysics Department, National Chiao Tung University, Taiwan, for their support and to Young-Chung Hsue for his useful discussions.

Bibliography

- [1] E. Yablonovitch, Phys. Rev. Lett. **58**, 2059 (1987).
- [2] S. John, Phys. Rev. Lett. **58**, 2486 (1987).
- [3] S. John, Nature **390**, 661 (1997).
- [4] K. Sakoda, *Optical Properties of Photonic Crystals* (Springer-Verlag, 2001).
- [5] J. D. Joannopoulos, R. D. Meade, and J. N. Winn, *Photonic Crystals– Molding the Flow of Light* (Princeton University Press, 1995).
- [6] *Photonic Band Gaps and Localization*, edited by C. M. Soukoulis (Plenum, New York, 1993).
- [7] C. M. Anderson and K. P. Giapis, Phys. Rev. B **56**, 7313 (1997).
- [8] Z. Y. Li, B. Y. Gu, and G. Z. Yang, Phys. Rev. Lett. **81**, 2574 (1998); Eur. Phys. J. B **11**, 65 (1999).
- [9] X. H. Wang, B.Y. Gu, Z. Y. Li, and G. Z. Yang, Phys. Rev. B **60**, 11417 (1999).
- [10] C. Goffaux and J. P. Vigneron, Phys. Rev. B **64**, 075118 (2001).
- [11] N. Susa, J. Appl. Phys. **91**, 3501 (2002).
- [12] R. D. Meade, A. M. Rappe, K. D. Brommer, and J. D. Joannopoulos, J. Opt. Soc. Am. B **10**, 328 (1993).

- [13] X. D. Zhang, Z. Q. Zhang, L. M. Li, C. Jin, D. Zhang, B. Man, and B. Cheng, Phys. Rev. B **61**, 1892 (2000).
- [14] M. Campbell, D. N. Sharp, M. T. Harrison, R. G. Denning and A. J. Turberfield, Nature **404**, 53 (2000).
- [15] L. Z. Cai, G. Y. Dong, C. S. Feng, X. L. Yang, X. X. Shen, and X. F. Meng, J. Opt. Soc. Am. B **23**, 1708 (2006).
- [16] D. N. Sharp, A. J. Turberfield, and R. G. Denning, Phys. Rev. B **68**, 205102 (2003).
- [17] M. Qiu and S. He, J. Opt. Soc. Am. B **17**, 1027 (2000).
- [18] M. Maldovan and E. L. Thomas, J. Opt. Soc. Am. B **22**, 466 (2005).
- [19] R. Biswas, M. M. Sigalas, K. M. Ho, and S. Y. Lin, Phys. Rev. B **65**, 205121 (2002).
- [20] H. B. Chen, Y. Z. Zhu, Y. L. Cao, Y. P. Wang, and Y. B. Chi, Phys. Rev. B **72**, 113113 (2005).
- [21] C. S. Kee, J. E. Kim, and H. Y. Park, Phys. Rev. E **56**, R6291 (1997).
- [22] M. I. Antonoyiannakis and J. B. Pendry, Phys. Rev. B **60**, 2363 (1999).
- [23] K. M. Ho, C. T. Chan, and C. M. Soukoulis, Phys. Rev. Lett. **65**, 3152 (1990).
- [24] Z. Zhang and S. Satpathy, Phys. Rev. Lett. **65**, 2650 (1990).
- [25] K. M. Leung and Y. F. Liu, Phys. Rev. Lett. **65**, 2646 (1990).



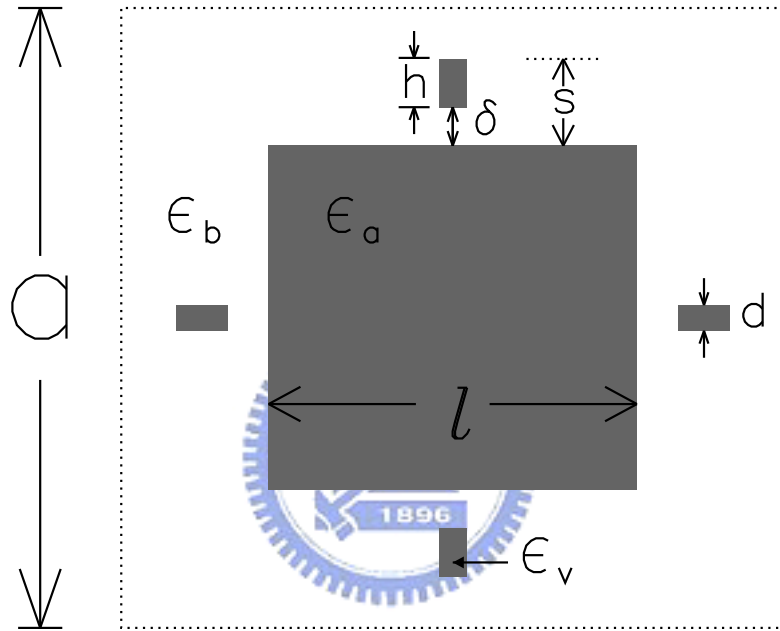


Figure 5.1: Schematic diagram of the proposed photonic crystals. The square dielectric rod with a side-length l and dielectric ϵ_a is placed in air with $\epsilon_b = 1.0$ at the center of a 2D square lattice with a lattice constant, a , in the xy -plane. Another dielectric veins with $\epsilon = \epsilon_v$ and length h and width d is inserted in each unit cell on the middle of each side of dielectric square rod, forming composite lattices. The shift length s of the inserted vein is defined with respect to the edge of the square rod, where δ is the crevice between the edges of the square rod and the vein, thus s is denoted by $s = \delta + h$.

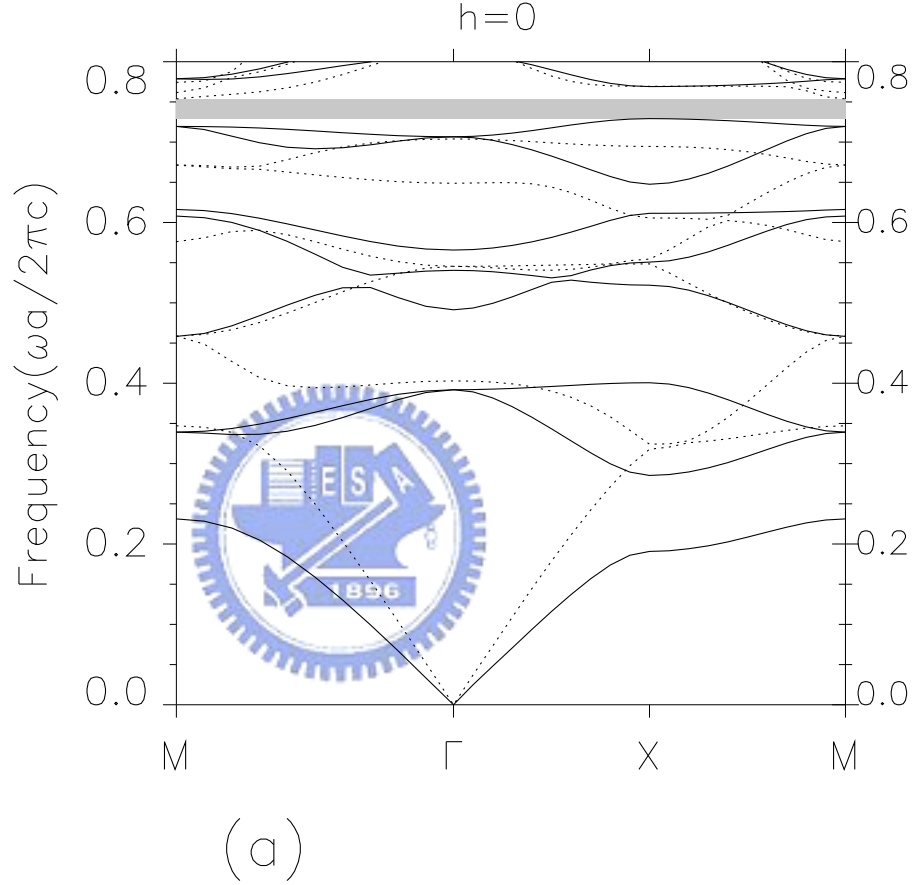
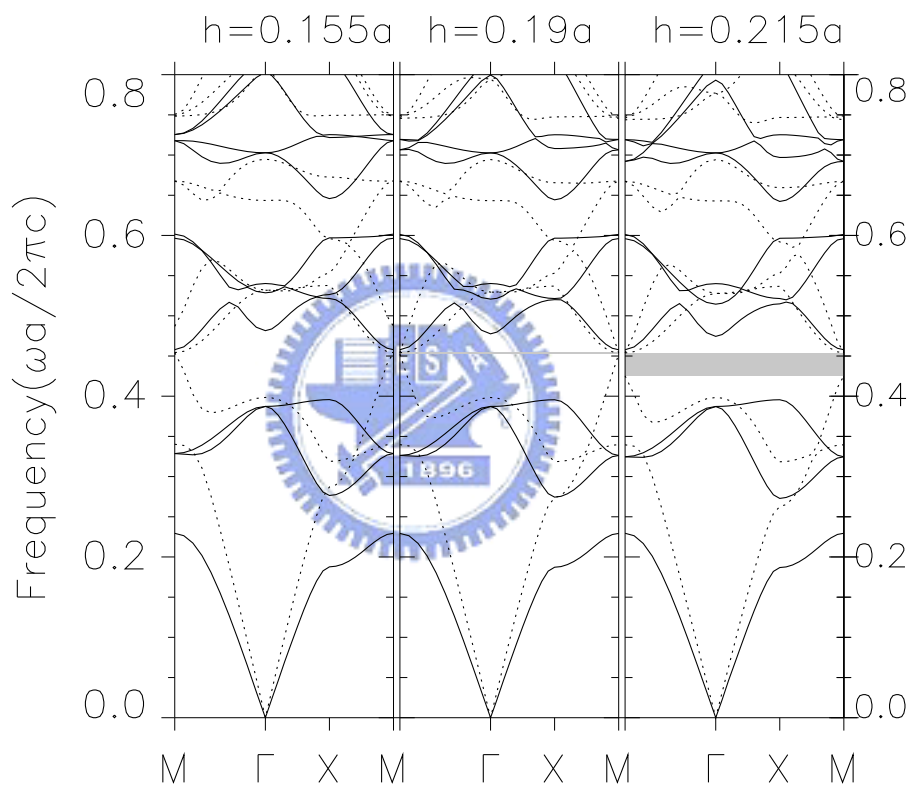
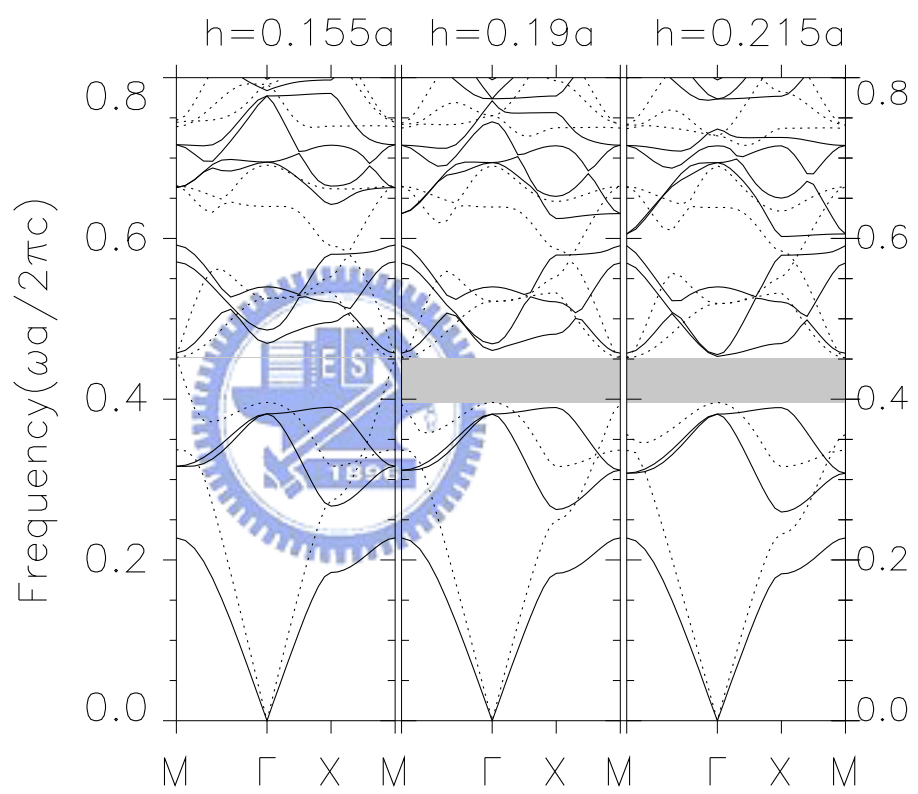


Figure 5.2: Photonic band structures for two structures: the prototype structure without the inserted veins for fixing the side-length of square rod at $l = 0.57a$, $\epsilon_a = 11.4$, appropriate for GaAs material; $\epsilon_b = 1.0$ in air as shown in (a) and three choices of the dielectric constant of veins are demonstrated in (b) $\epsilon_v = 6.0$, (c) $\epsilon_v = 11.4$, (d) $\epsilon_v = 16.0$. The other parameters are the same as those in (a) except for parameters of veins: $\delta=0$, $d = 0.08a$ and h : $0.155a$ (left panel), $0.19a$ (middle panel), $0.215a$ (right panel). The solid and dotted curves correspond to the E - and H -polarizations, respectively. The gray area marks the complete gap region.



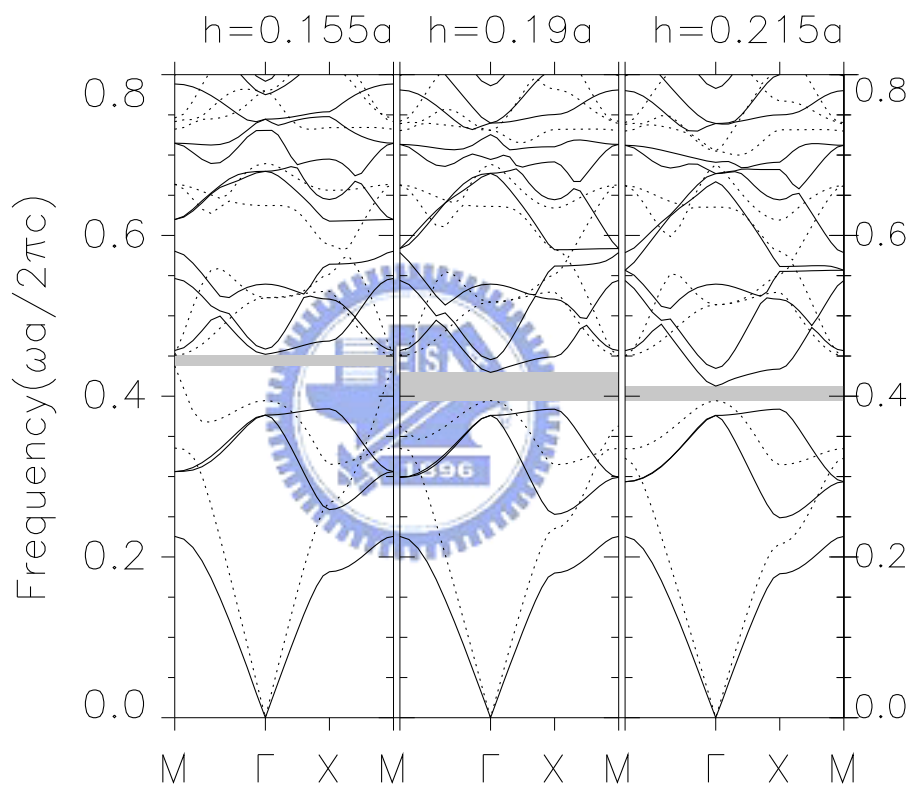
(b)

Figure 5.2: (con't)



(c)

Figure 5.2: (con't)



(d)

Figure 5.2: (con't)

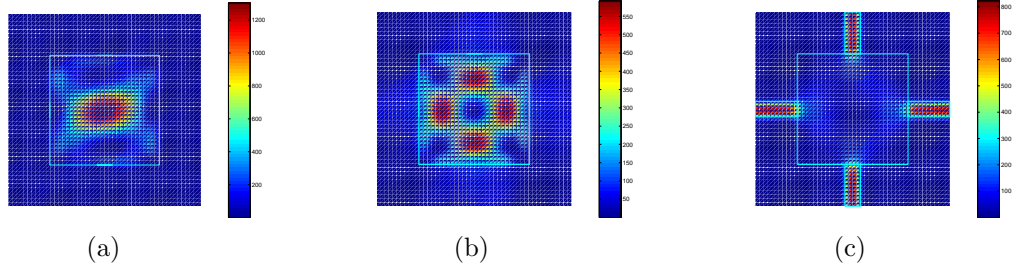
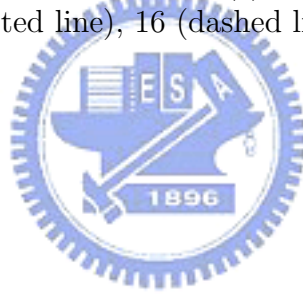
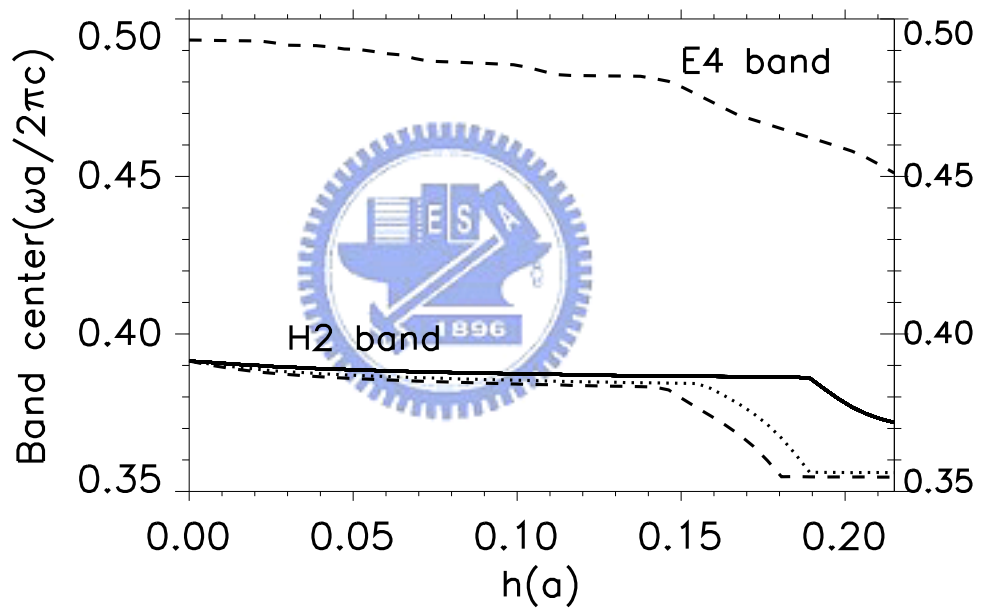


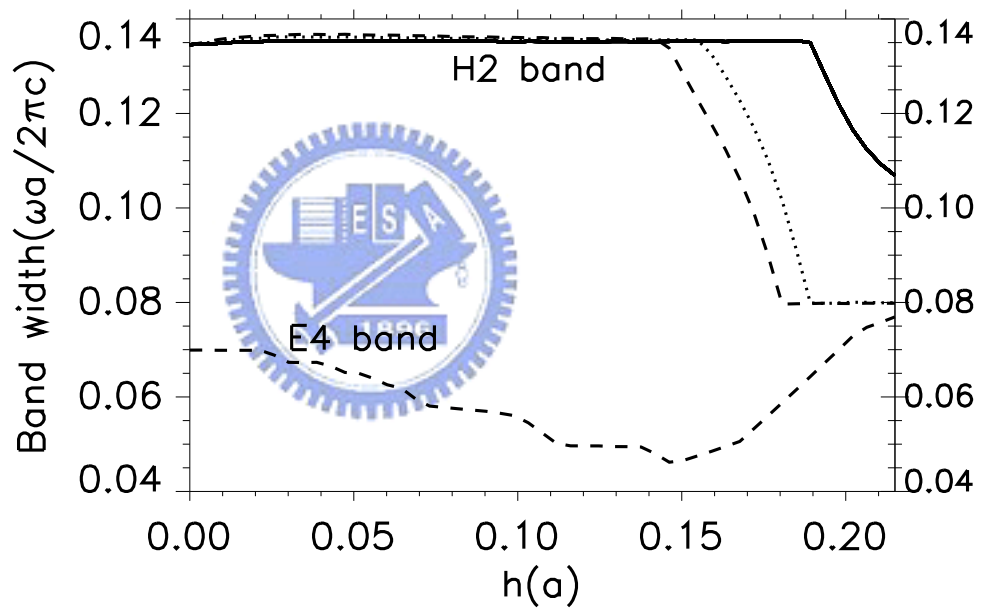
Figure 5.3: The spatial distributions of the electric field intensity $|E^2|$ at the \mathbf{M} point of (a) $H2$ band (or denoted by $H^{(2,M)}$) for $h=0$, (b) $H4$ band ($H^{(4,M)}$) for $h = 0$, and (c) $H2$ band ($H^{(4,M)}$) for $\epsilon_v = 6$ and $h = 0.215a$. Here we mark the states in accordance with their ordering in frequency for the prophase, namely, the initial mode $H^{(n,M)}$ denotes the n th band for the H -polarization mode at \mathbf{M} point. The band center (d) and the band width (e) as functions of h for $H2$ band with $\epsilon_v=6$ (solid line), 11.4 (dotted line), 16 (dashed line) and $E4$ band with $\epsilon_v=16$.





(d)

Figure 5.3: (con't)



(e)

Figure 5.3: (con't)

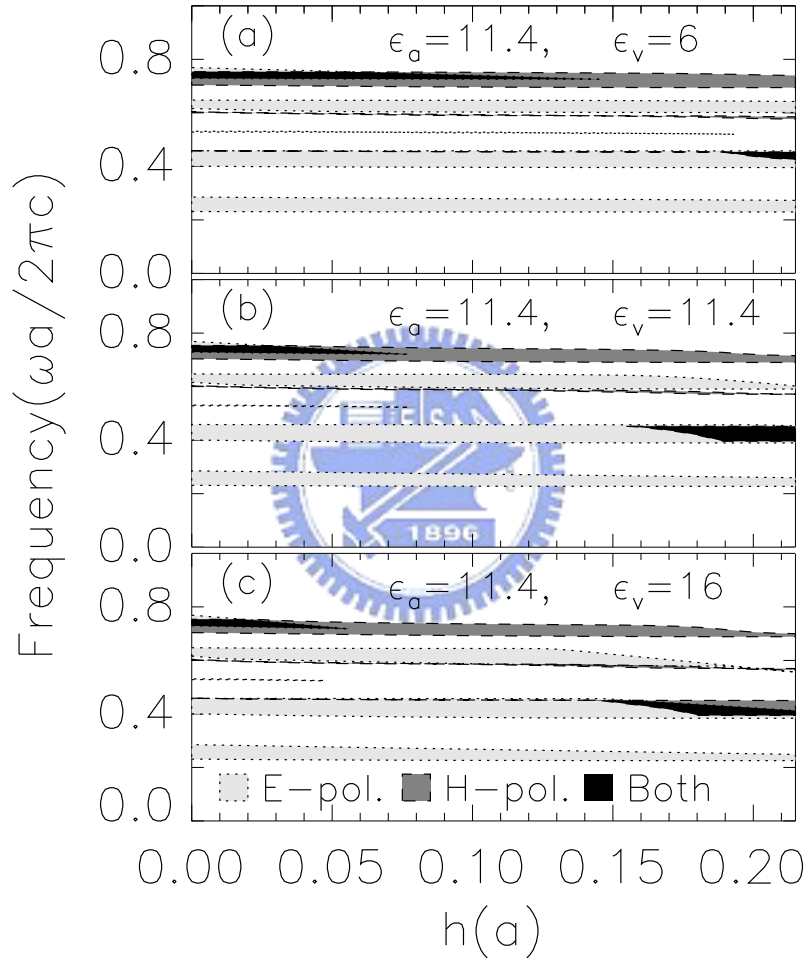
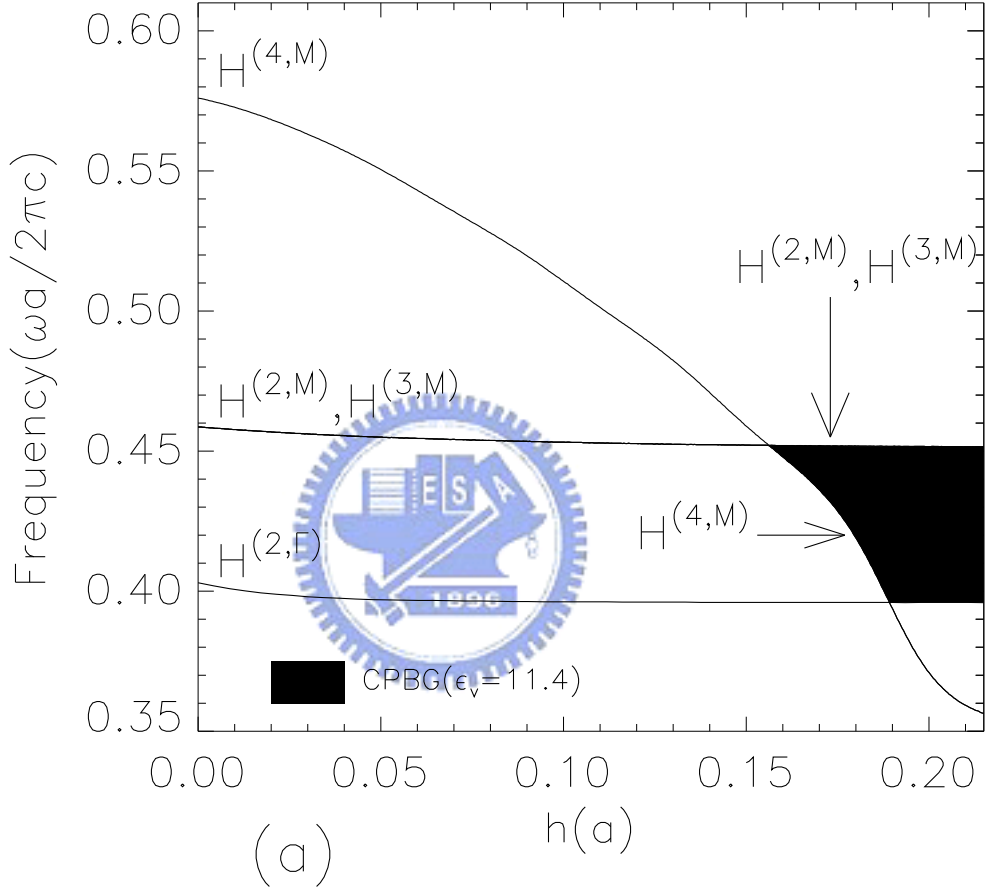
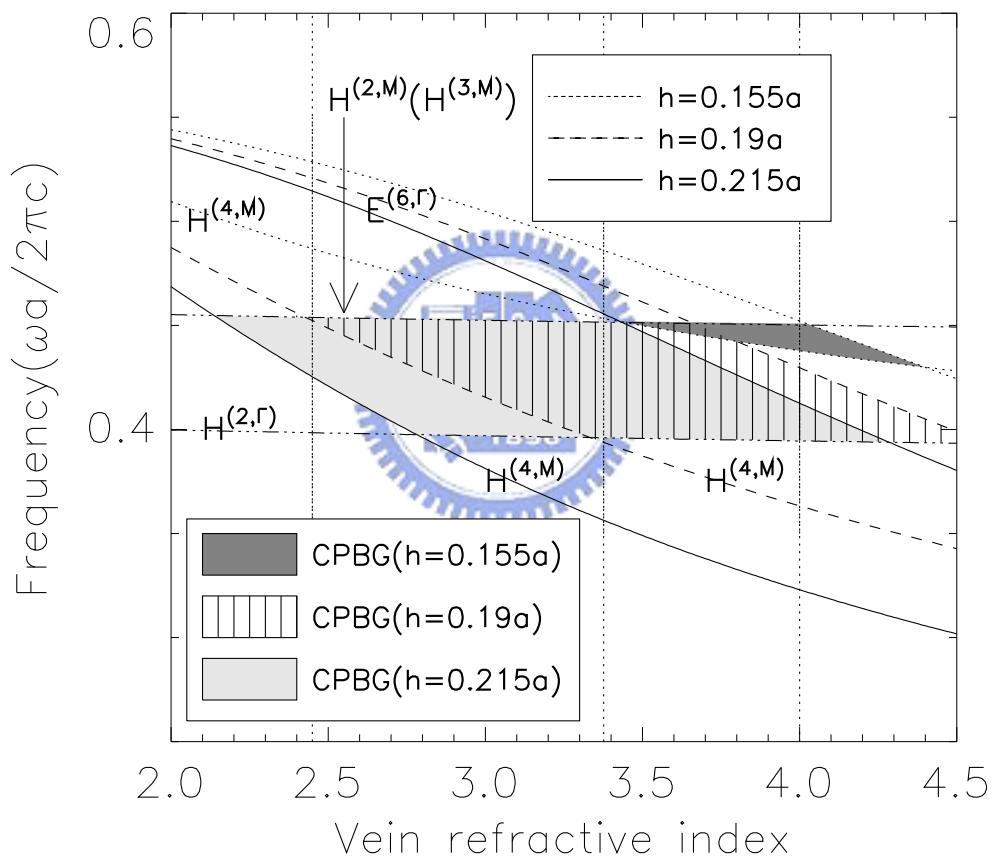


Figure 5.4: Gap map of the proposed PC, as the vein length h varies for both E - and H -polarizations for (a) $\epsilon_v = 6.0$, (b) $\epsilon_v = 11.4$ and (c) $\epsilon_v = 16.0$, respectively. The parameters are $\epsilon_a = 11.4$, $l = 0.57a$, $\delta=0$ and $d = 0.08a$. The black area denotes the complete band gaps.



(a)

Figure 5.5: The positions of the edge states of the lower complete PBG (CPBG): (a) the evolution of the edge states of the lower complete PBG as a function of vein length, h , for $\epsilon_v = \epsilon_a = 11.4$. The other parameters are: $\epsilon_a = 11.4$, $l = 0.57a$, $\delta=0$ and $d = 0.08a$. The dark region indicates the complete PBG. $H^{(n,\Gamma)}$ ($E^{(n,\Gamma)}$) denote the n th band for the $H(E)$ -polarization modes at Γ point. (b) the evolution of the edge states of the lower complete PBG as functions of the vein refractive index for three different vein lengths ($h = 0.155a$, $0.19a$, and $0.215a$). The vein refractive index of $n=2.45$, 3.376 and 4.0 (i.e., $\epsilon_v=6.0$, 11.4 and 16.0) are indicated by the vertical dotted lines. The dashed-dotted lines represent the curves of $H^{2,M}$ ($H^{3,M}$) or $E^{2,\Gamma}$ modes for different h values



(b)

Figure 5.5: (con't)

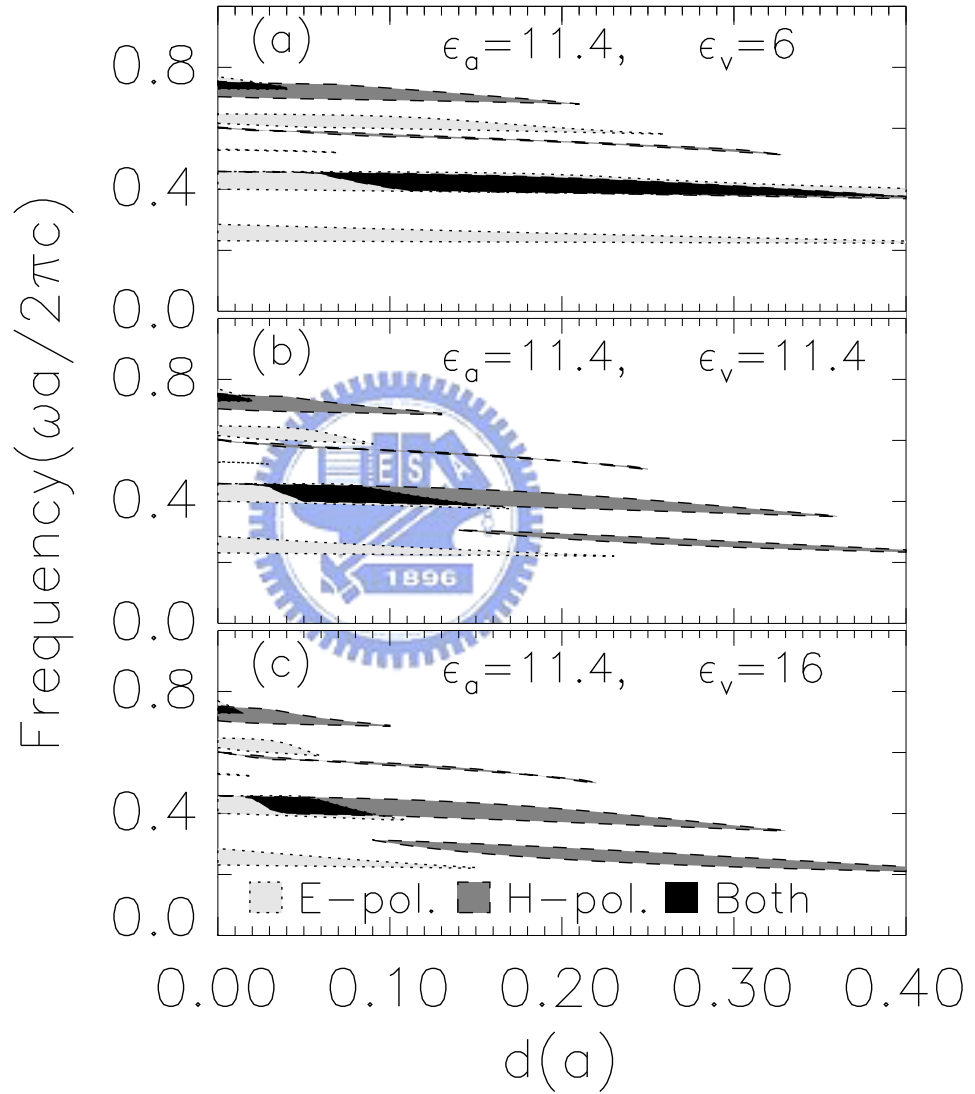


Figure 5.6: Gap map of the proposed PC, as the vein width d varies for both E - and H -polarizations for (a) $\epsilon_v = 6.0$, (b) $\epsilon_v = 11.4$ and (c) $\epsilon_v = 16.0$, respectively. The parameters are $\epsilon_a = 11.4$, $l = 0.57a$, $\delta = 0$ and $h = h_{max} = 0.215a$.

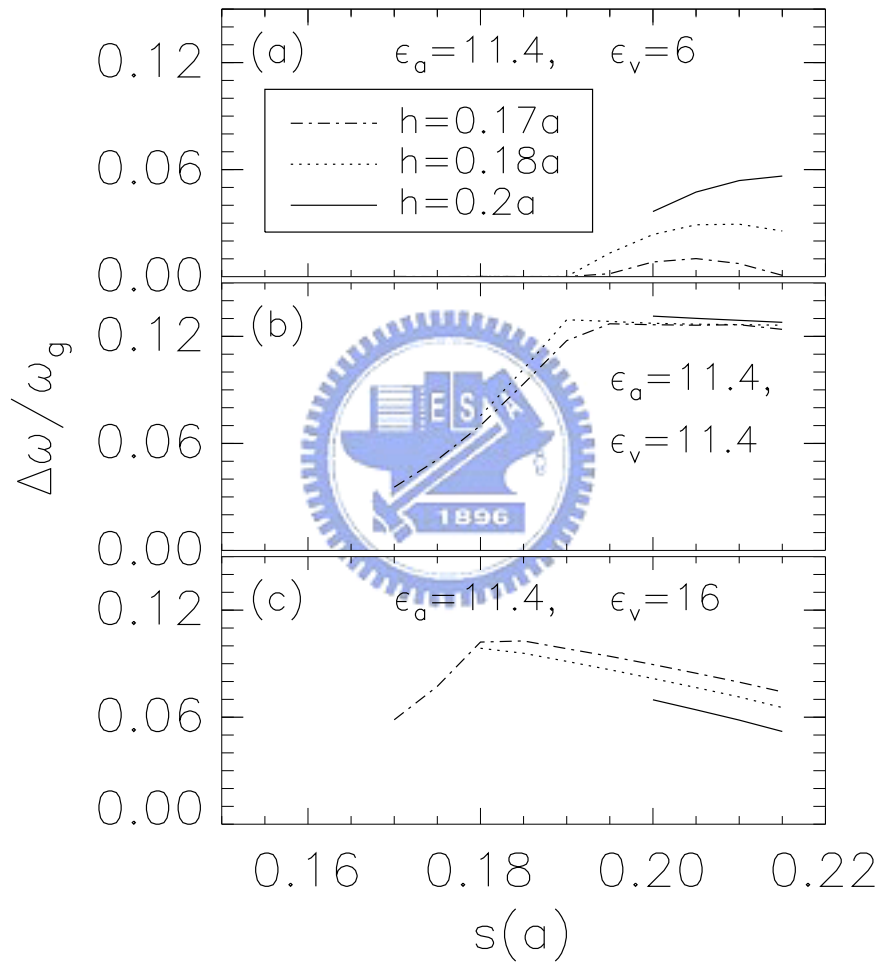


Figure 5.7: Variations of $\Delta\omega/\omega_g$ with the shift length s for different vein lengths h : $0.17a$, $0.18a$ and $0.2a$ for (a) $\epsilon_v = 6.0$, (b) $\epsilon_v = 11.4$ and (c) $\epsilon_v = 16.0$. The other parameters are $\epsilon_a = 11.4$, $l = 0.57a$ and $d = 0.08a$.

Chapter 6

Conclusion

Photonic crystals are now a fascinating issue of research, due to their potential for applications in optics technology. In this work, we have engineering the band gap of a 2D PC with some hybrid-rods structures. Band gap structures are calculated with the use of plane-wave expansion method.

In Chapter 3 we studied the PC system in the presence of a movable dielectric circular rod in each unit cell. Such TPCs can be fabricated by separately building two 2D PCs, one PC consists of dielectric circular rods located at internal of a square lattice, and the other PC consists of dielectric square cylinders located at four corners of a square lattice with the identical lattice constant, a . They are then combined into a final interpenetrating structure. Properly adjusting the position of the dielectric circular rod in the unit cell enables the tunable *complete* PBG generated from the composite structure to be opened and closed. Additionally, when the relative shift s of the circular rod is under $0.1a$, the ratio of the gap-width to the midgap almost remains unchanged or varies a little. This property provides the large benefit of relaxing the fabrication tolerance of the TPCs. The TPCs can be easily fabricated and operated in the micro-wave region because a is in the order of microwave wavelengths — several mm or cm.

In Chapter 4 we propose two-dimensional square lattices of square cross-section

dielectric rods in air, designed with an air hole drilled into each square rod. By adjusting the shift of the hole position in the square rod in each unit cell, the dielectric distribution of the square rod will be modified. The calculations show that the photonic crystal structure proposed here has a sizable complete band gap and exhibits very gently sloped bands near such gap edge, which resulting in a sharp peak of density of state. In addition, the zero or small group velocities are observed in a broad region of \mathbf{k} -space. This property can be utilized for optical gain enhancement or low-threshold lasing.

In Chapter 5 we have investigated in detail the photonic band structures of 2D square lattices of a square dielectric rod connected with slender rectangular dielectric veins on the middle of each side of dielectric square rod. Properly adjusting the length, width, position and dielectric constant of veins in the unit cell enables the tunable *complete* PBG generated from the composite structure to be opened and closed. Moreover, it is not necessary for veins to be fully connected to yield the greatest improvement in complete gap size depending on a relative dielectric constant of veins in comparison with those of square rods. These mechanisms may open up a new way for designing photonic band gaps in 2D photonic crystals.

VITA

- 基本資料

姓名: 劉文龍(Wen-Long Liu)

出生年月日: 西元 1958 年 12 月 1 日

出生地: 台灣省台中市

- 學歷:

1981 國立台灣師範大學物理系地球科學組畢業

1994 國立清華大學暑期 40 學分班結業

1996 國立中興大學物理系碩士

2007 國立交通大學電子物理系博士班

- 期刊論文

(1.) W.-L. Liu, T.-J. Yang and B.-Y. Gu, “*Sensitivity of complete bandgaps to the shift of movable dielectric rod in two-dimensional photonic crystals with complex lattices*”, Journal of Physics: Condensed Matter, **16**, 4557-4566 (2004).

(2.) W.-L. Liu and T.-J. Yang, “*Variation of group velocity and complete bandgaps in two-dimensional photonic crystals with drilling holes into the dielectric rods*”, Physica B, **368**, 151-156 (2005).

(3.) W.-L. Liu and T.-J. Yang, “*Photonic band gaps in a two-dimensional photonic crystal with open veins*”, Solid State Communications, **40**, 144-148 (2006).

(4.) W.-L. Liu and T.-J. Yang, “*Engineering the bandgap of a two-dimensional photonic crystal with slender dielectric veins*”, Physics Letters A, accepted for publication (2007).